Heart attack prediction via fluid-structure interaction simulation

Ištvanović, Josip

UNIVERSITY OF ZAGREB
FACULTY OF MECHANICAL ENGINEERING AND NAVAL ARCHITECTURE

MASTER'S THESIS

Josip Ištvanović

Zagreb, 2022

UNIVERSITY OF ZAGREB
FACULTY OF MECHANICAL ENGINEERING AND NAVAL ARCHITECTURE

MASTER'S THESIS

Mentor:

Prof. dr. sc. Željko Tuković, dipl. ing.

Student:

Josip Ištvanović

Zagreb, 2022

I hereby declare that this thesis is entirely the result of my own work except where otherwise indicated. I have fully cited all used sources and I have only used the ones given in the list of references.

I would like to express my sincere appreciation to my mentor, professor Željko Tuković for this opportunity and for helping me through this project.

Furthermore, I would like to thank Anja Horvat for her constructive criticism, patience and guidance through the project.

Finally, I would like to thank my family for all the support and understanding they have provided me.

Josip Ištvanović

SVEUČILIŠTE U ZAGREBU
FAKULTET STROJARSTVA I BRODOGRADNJE
Središnje povjerenstvo za završne i diplomske ispite
Povjerenstvo za diplomske ispite studija strojarstva za smjerove:
Procesno-energetski, konstrukcijski, inženjersko modeliranje i računalne simulacije i brodostrojarski

Sveučilište u Zagrebu Fakultet strojarstva i brodogradnje	
Datum	Prilog
Klasa: **602 - 04 / 22 - 6 / 1**	
Ur.broj: **15 - 1703 - 22 -**	

DIPLOMSKI ZADATAK

Student: **Josip Ištvanović** JMBAG: 0035208526

Naslov rada na hrvatskom jeziku: **Predviđanje srčanog udara primjenom simulacije međudjelovanja između fluida i deformabilnog tijela**

Naslov rada na engleskom jeziku: **Heart attack prediction via fluid-structure interaction simulation**

Opis zadatka:

Coronary artery disease (CAD) is the build-up of plaque in coronary arteries (CA). Plaque is made up of fats, cholesterol, calcium and other substances in the blood. It can develop over time, locally reducing the diameter in a CA branch. This is called CA stenosis and restricts the flow of oxygen-rich blood to the myocardium. If this happens slowly over time, the vascular network can adapt by creating additional arterioles. Another possible compensation is widening of the pressure-regulating arterioles, which results in increased blood velocity in the stenosis upstream. However, this results in additional load to the plaque which may burst, triggering a blood clot that can cause a heart attack (sudden blockage of oxygen-rich blood supply to the myocardium downstream a CA branch). The therapies for CAD are medication, Percutaneous Coronary Intervention or stenting and Coronary Artery Bypass Graft surgery.
Modern computerized tomography (CT) imaging technologies can visualize the coronary artery lumen and the plaque volumes in detail. It is possible to segment both lumen and plaque geometries from these scans. Geometries from patients suffering from CAD will be made available to the student. The aims of this thesis are as follows:

1. Perform a literature survey and describe the applied models and methods.
2. Reconstruct a simplified geometrical model of the coronary artery lumen with the accumulated plaque from the provided CT scans.
3. Perform a numerical fluid-structure interaction analysis of the blood flow through the coronary artery with the accumulated plaque, assuming a rigid artery wall and an incompressible hyperelastic plaque body.
4. Estimate the risk of heart attack based on the numerically determined stress state in the plaque body during cardiac cycle.

This thesis is supported by AZ Delta hospital from Belgium, which will provide the CT scans and feedback from physicians. The aim is to provide better care for patients, by introducing non-invasive analysis of the patient-specific situation.
It is necessary to list the references used in this work, and to acknowledge any help or support possibly received during the course of this study.

Zadatak zadan:	Datum predaje rada:	Predviđeni datumi obrane:
5. svibnja 2022.	7. srpnja 2022.	18. – 22. srpnja 2022.

Zadatak zadao:

Prof.dr.sc. Željko Tuković

Izv.prof.dr.sc. Peter De Jaeger
AZ Delta, Belgium

DocuSigned by:
Peter De Jaeger
F007A5C59B4D4BE...

Predsjednik Povjerenstva:

Prof. dr. sc. Tanja Jurčević Lulić

TABLE OF CONTENTS

LIST OF FIGURES

LIST OF TABLES

NOMENCLATURE

Latin Characters

Symbol	Description	Unit of Measure
$\mathbf{b}$	Left Cauchy-Green tensor	[-]
E	Young's modulus	[Pa]
c_1	Strain energy constant	[-]
$\mathbf{F}$	Deformation gradient tensor	[-]
$\mathbf{f}$	External force vector	[N]
$\mathbf{f}_b$	Body force vector	[N]
$\mathbf{I}$	Second-order identity tensor	[-]
I_1	Strain invariant 1	[-]
I_2	Strain invariant 2	[-]
I_3	Strain invariant 3	[-]
m	Mass	[kg]
$\mathbf{n}$	Surface normal vector	[-]
$\mathbf{n}_i$	Surface normal vector	[-]
p	Pressure	[Pa; mm Hg]
p_{av}	Aortic valve pressure	[Pa; mm Hg]
Q	Volume flow rate	[m^3/s ; mL/s]
Q_{av}	Aortic valve volume flow rate	[m^3/s ; mL/s]
Q_{cor}	Coronary volume flow rate	[m^3/s ; mL/s]
t	Time	[s]
$\mathbf{t}_{F,i}$	Traction at fluid interface	[N/m^2]
$\mathbf{u}$	Displacement	[m]
$\mathbf{u}_{F,i}$	Displacement at fluid interface	[m]
$\mathbf{u}_{S,i}$	Displacement at solid interface	[m]
$\mathbf{v}$	Velocity	[m/s]
$\mathbf{v}_{F,i}$	Velocity at fluid interface	[m/s]
$\mathbf{v}_n$	Normal velocity component	[m/s]
$\mathbf{v}_{S,i}$	Velocity at solid interface	[m/s]
$\mathbf{v}_t$	Tangential velocity component	[m/s]
W	Strain energy	[J]

Greek Characters

Γ	Diffusion coefficient	$[\mathrm{m}^2/\mathrm{s}]$
λ_p	Under-relaxation pressure factor	[-]
λ_U	Under-relaxation velocity factor	[-]
λ_ϕ	Under-relaxation physical property factor	[-]
μ	Dynamic viscosity	$[\mathrm{Pa}\cdot\mathrm{s}]$
μ_1	Neo-Hookean constant	[-]
ν_f	Kinematic viscosity	$[\mathrm{m}^2/\mathrm{s}]$
ν_s	Poisson's ratio	[-]
ρ_f	Blood density	$[\mathrm{kg}/\mathrm{m}^3]$
ρ_s	Solid material density	$[\mathrm{kg}/\mathrm{m}^3]$
$\boldsymbol{\sigma}$	Cauchy stress tensor	$[\mathrm{N}/\mathrm{m}^2]$
$\boldsymbol{\sigma}_{F,i}$	Cauchy stress tensor at fluid interface	$[\mathrm{N}/\mathrm{m}^2]$
$\boldsymbol{\sigma}_{S,\mathrm{i}}$	Cauchy stress tensor at solid interface	$[\mathrm{N}/\mathrm{m}^2]$
σ_VM	von Mises stress	$[\mathrm{N}/\mathrm{m}^2]$
$\boldsymbol{\tau}$	Wall shear stress	$[\mathrm{N}/\mathrm{m}^2]$
ϕ	Physical property	[-]

Superscripts

T	Transpose
ϕ	Physical property

Subscripts

av	Aortic valve
b	Body
cor	Coronary
D/U	Displacement/velocity
F,i	Fluid interface
f	fluid
i	Index
n	Normal component

S, i	Solid interface
s	solid
t	Tangential component

Abbreviations

CAD	Coronary Artery Disease
CFD	Computational Fluid Dynamics
CT	Computerized tomography
CV	Control Volume
FE	Finite Element
FMS	File Management System
FSI	Fluid-Structure Interaction
FV	Finite Volume
FVM	Finite Volume Method
GAMG	Geometric Agglomerated Algebraic Multigrid
GGI	General Grid Interface
GPL	General Public License
LAD	Left Anterior Descending
LCx	Left Circumflex
LDL	Low Density Lipoprotein
LM	Left Main
MPI	Message Passing Interface
MV	Material Volume
PISO	Pressure Implicit with Splitting of Operator
RCA	Right Coronary Artery
RDF	Računalna Dinamika Fluida
RI	Ramus Intermedius
SIMPLE	Semi-Implicit Method for Pressure-Linked Equations
STL	Stereo Lithography
SMP	Shared Memory Parallelization
WSS	Wall Shear Stress
3D	3-Dimensional

ABSTRACT

Cardiovascular diseases are the leading cause of death in modern civilization, which result from insufficient coronary blood flow. The majority of them can be attributed to atherosclerosis, which causes the development of plaques that protrude into the vessel lumens and either block or partially block blood flow. The partial blockage leads to the development of collateral coronary circulation that can eliminate any symptoms of cardiac dysfunction to some degree. When the collateral circulation is insufficient, the heart muscle becomes severely limited in its work output, resulting in a heart attack.

The main focus of this thesis is to simulate the nonlinear dynamics of the atherosclerotic coronary artery as a tool to predict the occurrence of a heart attack. A three-dimensional fluid-structure interaction (FSI) model is reconstructed based on the patient-specific computerized tomography (CT) scans and simulated via the finite volume method using OpenFOAM® for the determination of regions with the highest von Misses and shear stresses. The arterial wall is assumed to be rigid, while the accumulated plaque is modeled as a hyperelastic incompressible body. The fluid model incorporates transient isothermal and laminar blood flow with simplified geometry and realistic hemodynamic conditions, where blood is modeled as a Newtonian and incompressible fluid. The atherosclerotic plaque is modeled as a homogeneous solid body with mixed material properties such as smooth muscle cells, collagen, and lipids. These are the main constituents of the plaque body, all significantly different in their stiffness level, which may be the main cause of plaque rupture and initiation of myocardial infarction.

In the future, the study of arterial blood flow will lead to the prediction of individual hemodynamic flows in any patient, the development of diagnostic tools to quantify the disease, and the design of devices that mimic or alter blood flow. This field is rich in challenging problems in fluid mechanics involving three-dimensional, pulsating flows at the edge of turbulence.

Keywords: coronary artery, atherosclerosis, fluid-structure interaction, FSI, OpenFOAM

SAŽETAK

Bolesti krvožilnog sustava predstavljaju glavni uzrok smrti u suvremeno dobra, a posljedica su nedostatnog koronarnog protoka krvi. Većina ih se može pripisati aterosklerozi koja uzrokuje stvaranje aterosklerotskog plaka, koji strši u lumen krvnih žila i djelomično ili posve priječi protok krvi. Djelomično začepljenje dovodi do razvoja kolateralne koronarne cirkulacije koja u određenoj mjeri može ukloniti simptome srčane disfunkcije. Kada i kolateralna cirkulacija nije dovoljna, sposobnost srčanog mišića za obavljanje rada se značajno smanjuje, što s vremenom dovodi do srčanog udara.

Glavni cilj ovo rada je simulacija nelinearnog ponašanja aterosklerotične koronarne arterije koja može poslužiti kao alat za predviđanje srčanog udara. Trodimenzionalni model međudjelovanja fluida i čvrstog tijela (FSI) rekonstruiran je na temelju CT skenova, specifičnog za pojedinog pacijenta, i simuliran metodom kontrolnih volumena koristeći programski paket OpenFOAM® za određivanje područja s najvećim normalnim i posmičnim naprezanjima. Pretpostavljena je kruta arterijska stijenka, dok je nakupljeni plak modeliran kao hiperelastično nestlačivo tijelo. Model fluida uključuje nestacionarni izotermni i laminarni protok krvi s pojednostavljenom geometrijom i realnim hemodinamičkim uvjetima, dok je krv modelirana kao nestlaičivi i newtonski fluid. Aterosklerotski plak je modeliran kao homogeno čvrsto tijelo s miješanim svojstvima materijala kao što su glatke mišićne stanice, kolagen i lipidi. Oni predstavljaju glavne slojeve plaka, a njihova značajna razlika u krutosti može biti jedan od glavnih uzroka njegova puknuća, a samim time i infarkta miokarda.

U budućnosti će proučavanje arterijskog krvotoka dovesti do predviđanja pojedinačnih hemodinamičkih tokova kod pacijenata, razvoja dijagnostičkih alata za kvantificiranje bolesti i dizajna uređaja koji oponašaju ili mijenjaju protok krvi. Ovo polje je bogato izazovnim problemima u mehanici fluida koji uključuju trodimenzionalne, pulsirajuće tokove na rubu turbulencije.

Ključne riječi: koronarne arterije, ateroskleroza, međudjelovanje fluida i deformabilnog tijela, FSI, OpenFOAM

PROŠIRENI SAŽETAK

Uvod

Ishemijske bolesti srca i moždani udari su prema podacima Svjetske zdravstvene organizacije glavni uzroci smrti u cijelom svijetu. Većina krvožilnih bolesti uzrokovana je aterosklerozom koja predstavlja razvoj plaka na unutarnjoj stijenki arterije, poznatog kao aterom. Početna faza ateroskleroze je asimptomatska, dok postupno nakupljanje plaka tijekom duljeg vremenskog perioda uzrokuje značajno smanjenje promjera lumena koje se naziva stenoza. Razvoj aterosklerotskog plaka povezan je s prisutnošću niskog posmičnog naprezanja stijenke arterije. Zone niskog posmičnog naprezanja povezane su s trajnom upalom endotela, stvarajući povoljne uvjete za stvaranje plaka. Plak predstavlja tkivo bogato kolesterolom koje uzrokuje suženje lumena, puknuće ili eroziju arterijske stijenke, otvrdnuće arterija i gubitak njihove elastičnosti, što dovodi do djelomičnog ili potpunog smanjenja protoka krvi.

Hemodinamika, grana fizike koja proučava protok krvi, je ključna za razumijevanje mehanizama koji utječu na razvoj krvožilnih bolesti. *In vivo* istraživanja, koja uključuju protok krvi, obično je teško izvesti zbog etičkih problema, visokih troškova i tehničkih komplikacija. Stoga, numeričke simulacije zajedno s medicinskim snimkama mogu pružiti vrijedne informacije o hemodinamičkim uvjetima i anatomskim promjenama zbog prisutnosti stenoze koja može uzrokovati značajne padove tlaka, povećano posmično naprezanje stijenke, odvajanje i puknuće plaka. Prevencija bolesti koronarnih arterija je važna jer se njezina pojava danas smatra jednim od najvećih ekonomskih tereta za globalno društvo. To je razlog zašto identificiranje ranjivog plaka, s visokim rizikom od puknuća, predstavlja najvažniji zadatak na području hemodinamike. U ovom radu primarna ideja je razviti pojednostavljeni dinamički model lijeve koronarne arterije, kojim se želi predvidjeti ranjivi aterosklerotski plak i na taj način identificirati pacijente koji su pod visokim rizikom od srčanog udara. Ovaj model bi omogućio neinvazivnu analizu pojedinog pacijenta, a time i intervencije za stabilizaciju plaka i prevenciju infarkta miokarda.

Cilj ovog rada je rekonstruirati pojednostavljeni geometrijski model lumena koronarne arterije s nakupljenim plakom na temelju CT skenova i provesti numeričku simulaciju međudjelovanja fluida i čvrstog tijela (FSI) uz pretpostavku krute arterijske stijenke i nestlačivog hiperelastičnog tijela plaka.

Matematički model

U ovom radu koristi se model nestacionarnog nestlačivog izotermnog i laminarnog strujanja, dok se krv promatra kao newtonski fluid. Model aterosklerotskog plaka smatra se homogenim nestlačivim i hiperelastičnim, dok se stijenka arterije smatra krutom.

Model međudjelovanja fluida i čvrstog tijela (FSI) opisan je sljedećim zakonima u kojima kose veličine predstavljaju skalare, a podebljane i uspravne veličine vektore i tenzore drugog reda. Osnovne jednadžbe numeričkog modela vezane za fluid temelje se na zakonima očuvanja:

- Zakon očuvanja mase:

$$\nabla \cdot \mathbf{v} = 0\,. \tag{0.1}$$

- Zakon očuvanja količine gibanja:

$$\underbrace{\frac{\partial \mathbf{v}}{\partial t}}_{\text{lokalna promjena}} + \underbrace{\nabla \cdot (\mathbf{v}\mathbf{v})}_{\text{konvekcija}} = \underbrace{\underbrace{\nu \nabla^2 \mathbf{v}}_{\text{difuzija}} - \underbrace{\frac{1}{\rho}\nabla p}_{\text{gradijent tlaka}}}_{\text{površinske sile}} + \underbrace{\mathbf{f}_b}_{\text{masene sile}}\,. \tag{0.2}$$

U jednadžbama (0.1) i (0.2), $\mathbf{v}$ predstavlja brzinu, ν kinematičku viskoznost i ρ gustoću fluida. Model čvrstog tijela opisan je:

- Zakonom očuvanja količine gibanja:

$$\rho \frac{\partial^2 \mathbf{u}}{\partial t^2} = \nabla \cdot \boldsymbol{\sigma} + \rho \mathbf{f}_b, \tag{0.3}$$

gdje $\mathbf{u}$ predstavlja pomak, $\boldsymbol{\sigma}$ Cauchyjev tenzor naprezanja i $\mathbf{f}_b$ masene sile. Cauchy-ev tenzor naprezanja računa se prema hiperelastičnom neo-Hookovom materijalnom modelu:

$$\boldsymbol{\sigma} = -p\mathbf{I} + \mu \mathbf{b}, \tag{0.4}$$

gdje $\mathbf{b}$ predstavlja lijevi Cauchy-Greenov tenzor, a $\mathbf{I}$ jediničnu matricu.

FSI model rješava se odvojenim pristupom u kojem se fluid i solid domena rješavaju zasebno. Na fluid-solid granici (eng. FSI interface) ih povezuje algoritam sprezanja koji osigurava kontinuirani prijelaz sile i pomaka s jedne domene na drugu. Jedan od takvih algoritama koristi Dirichlet-Neumannov pristup koji pri rješavanju domene fluida koristi Dirichletov rubni uvjet za brzinu, dok pri rješavanju solid domene Neumannov rubni uvjet za trakciju (silu).

Korišten je Gauss-Seidelov algoritam sprezanja s Dirichlet-Neumannovom dekompozicijom koji za sve vremenske korake:

- Riješi model strujanja fluida;
- Prenese sile fluida na čvrsto tijelo preko fluid-solid granice
- Riješi model čvrstog tijela;
- Prenese izračunate pomake na čvrstom tijelu na fluid preko zajedničke granice;
- Ažurira mrežu;
- Izračuna reziduale između fluid-solid domene i ponovi postupak do konvergencije.

Također postoji monolitički pristup u kojem se jednadžbe vezane za fluid i solid rješavaju istovremeno, ali trenutno nije implementiran u *solids4foam* rješavač.

Valja naglasiti da je vremenski profil koronarnog protoka bitno različit od profila ulaznog protoka aorte te ostalih sistemnih arterija. To se može objasniti činjenicom da se koronarne arterije nalaze u mišićnoj stijenki srca. Tijekom faze kontrakcije srca dolazi do stezanja koronarnih arterija, čiji rezultat je velik otpor strujanju krvi, a u fazi dijastole, kada je srčani mišić relaksiran, otpor se smanjuje i protok raste. Dolazi do paradoksa, pri visokom tlaku u korijenu aorte (za vrijeme kontrakcije srca) je koronarni protok nizak, a tijekom relaksacije srca, koronarni protok raste. To znači da se otpor koronarnih arterija mijenja tijekom srčanog ciklusa (moguće da im se značajnije mijenja i promjer), što nije slučaj kod sistemnih arterija, gdje se može računati s konstantnim perifernim otporom. Stoga je i model strujanja u koronarnim arterijama složeniji od modela strujanja u sistemnim arterijama.

Stoga je u ovom radu prvo provedena RDF (eng. Computational fluid dynamics, CFD) simulacija s ciljem određivanja rubnih uvjeta na izlazu. Poznati su eksperimentalni podaci za tlak u korijenu aorte i koronarni protok, dok njihova kombinacija predstavlja realne hemodinamičke uvjete strujanja. Pomoću njih je izračanut profil tlaka na izlazima koji su kasnije korišteni kao rubni uvjeti u FSI simulaciji.

CFD simulacija provedena je s geometrijom zdrave arterije tj. arterije bez plaka. Ova pretpostavka je posljedica razvoja kolateralne cirkulacije, koja nastaje paralelno s rastom i razvojem aterosklerotičnog plaka tijekom dužeg vremenskog perioda. Kolateralna cirkulacija može u određenoj mjeri ukloniti simptome srčane disfunkcije. Kolateralni tok predstavlja nepromijenjene nizvodne uvjete, dok se uzvodni tok mijenja zbog rasta plaka.

Geometrija i rezultati CFD simulacije

Pojednostavljena geometrija napravljena je u programu SolidWorks, a izrađena je na temelju realne geometrije koja je dobivena iz CT skenova koronarnih arterija pojedinih pacijenata. Geometrija je prikazana na slici 1. Sastoji se od ulaza, zida i tri izlaza, pri čemu je oznakom LAD prikazana prednja lijeva silazna grana, s oznakom RI srednja grana te s oznakom LCx lijeva cirkumfleksna grana.

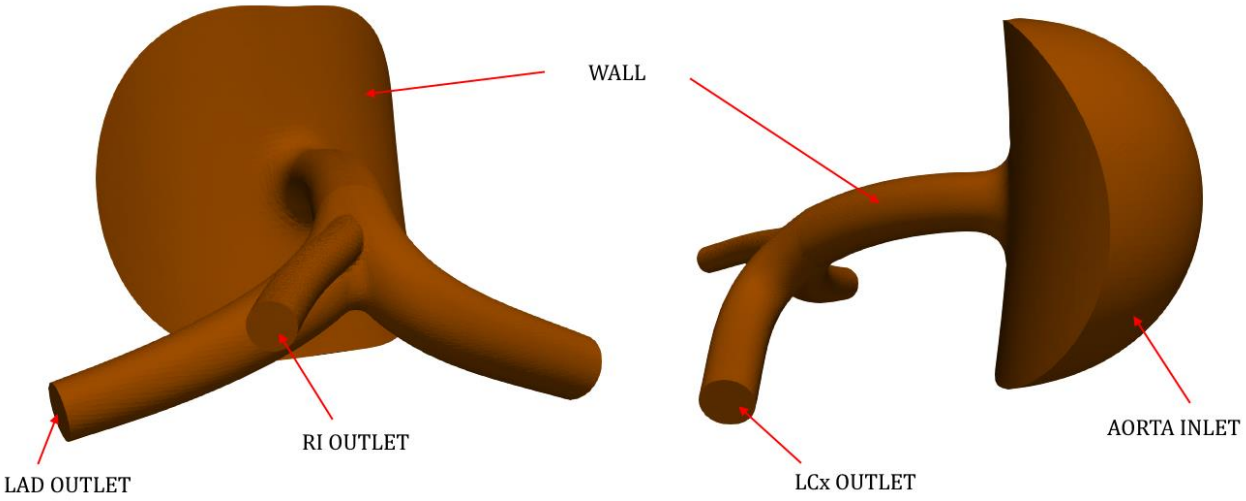

Slika 1. Geometrija

Laminarni protok nestlačivog newonovskog fluida modeliran je pomoću jednadžbe očuvanja mase (0.1) i jednadžbe očuvanje količine gibanja (0.2). Prostorna domena diskretizirana je metodom kontrolnih volumena shemama drugog reda točnosti, dok je vremenska domena diskretizirana implicitnom shemom, također drugog reda točnosti.

Numerička mreža napravljena je pomoću višeplatformske biblioteke otvorenog koda za automatsko generiranje mreže cfMesh® koja se nalazi u sklopu novijih verzija OpenFOAM paketa. Mreža se sastoji od 133 998, uglavnom heksaedarskih volumena. Dio mreže prikazan je na slici 2.

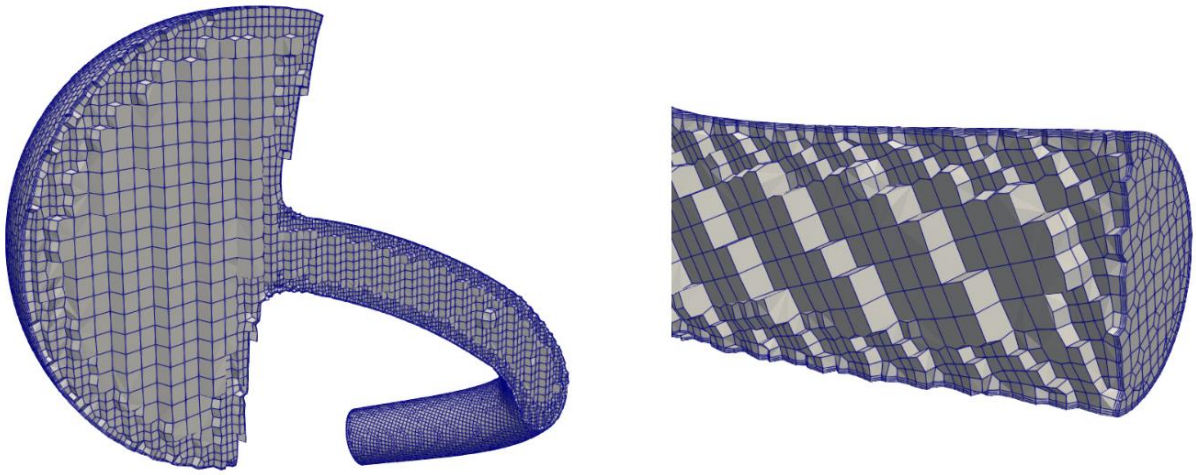

Slika 2. Numerička mreža u poprečnom presjeku lijeve koronarne arterije

Proračuni su provedeni u računalnom programu za rješavanje strujanja otvorenog koda OpenFOAM. Rezultati su dobiveni za 4 vremenska ciklusa kako bi se sa sigurnošću postigla periodičnost tj. kako bi iščeznuo utjecaj početnih uvjeta.

Jedine relevantne rezultate predstavljaju volumni protoci, čija usporedba će se naknadno analizirati s protocima iz FSI simulacije, i tlakovi na izlazima, koji će se koristiti kao rubni uvjeti u FSI simulaciji. Rezultati su dani na sljedećim slikama:

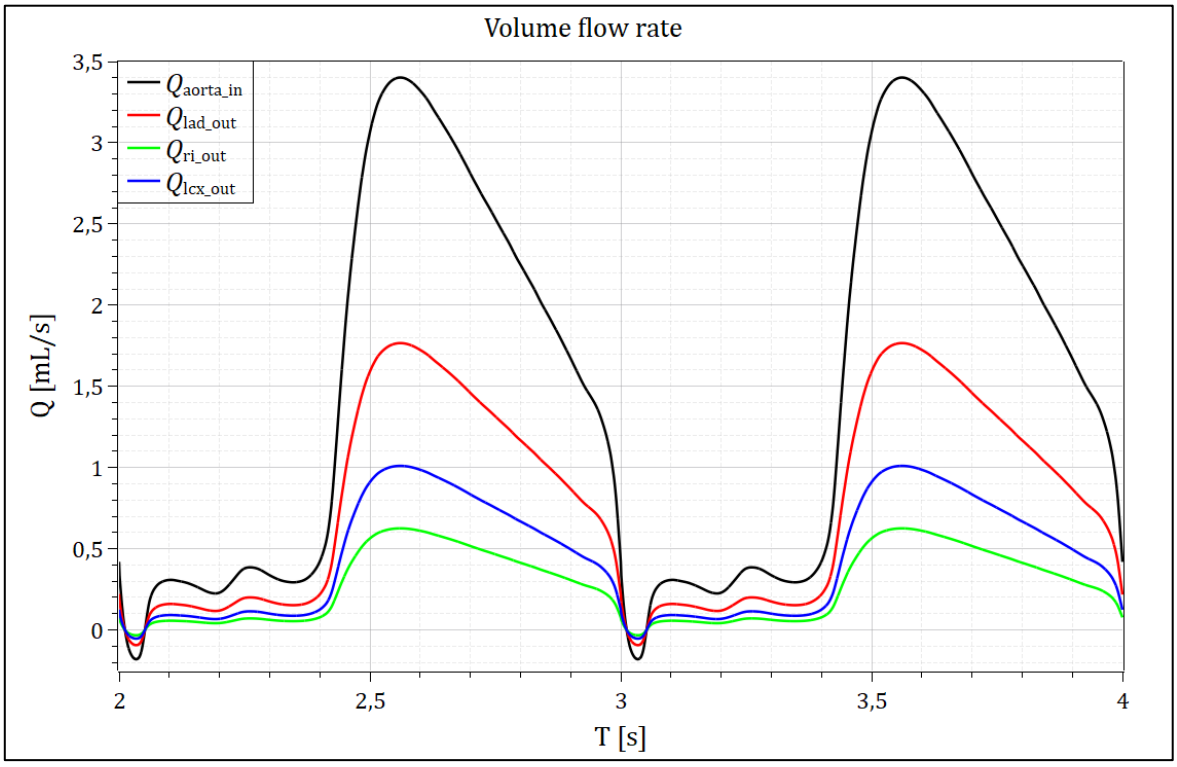

Slika 3. Volumni protoci na ulazu i izlazima koronarnih grana

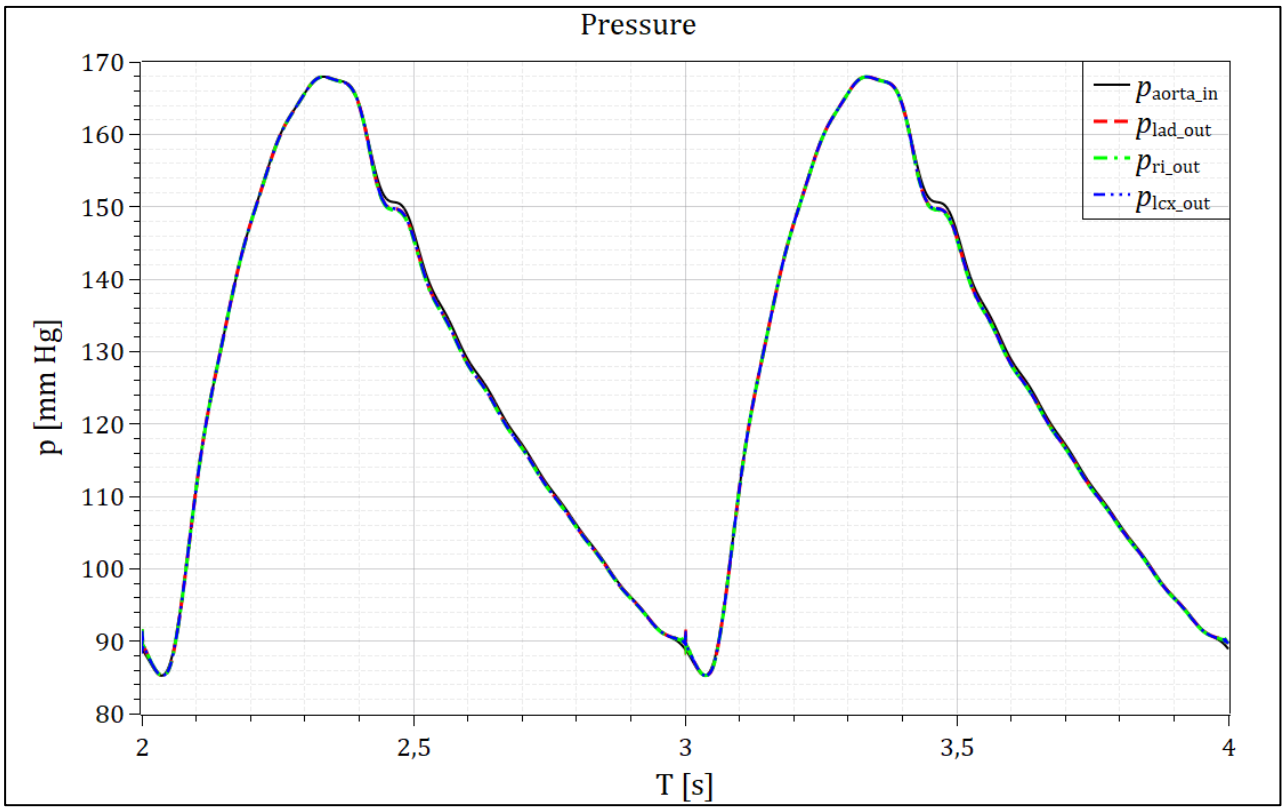

Slika 4. Tlak na ulazu i izlazima koronarnih grana

Numerička mreža i postavke FSI simulacije

Napravljena su dva usporedna geometrijska modela pomoću kojih će se analizirati učinak različitog postotka stenoze na koronarnu arteriju. Indeks 1 označuje model s 30 % stenoze, dok indeks 2 s 50 % stenoze.

Numerička mreža, za oba modela, rađena je pomoću biblioteke cfMesh kojim je dobivena pretežno heksaedarska mreža s poliedarskim volumenima u prijelaznom području volumena različitih veličina. Imena granica i detalji mreža dani su na slici 5 i tablici 1.

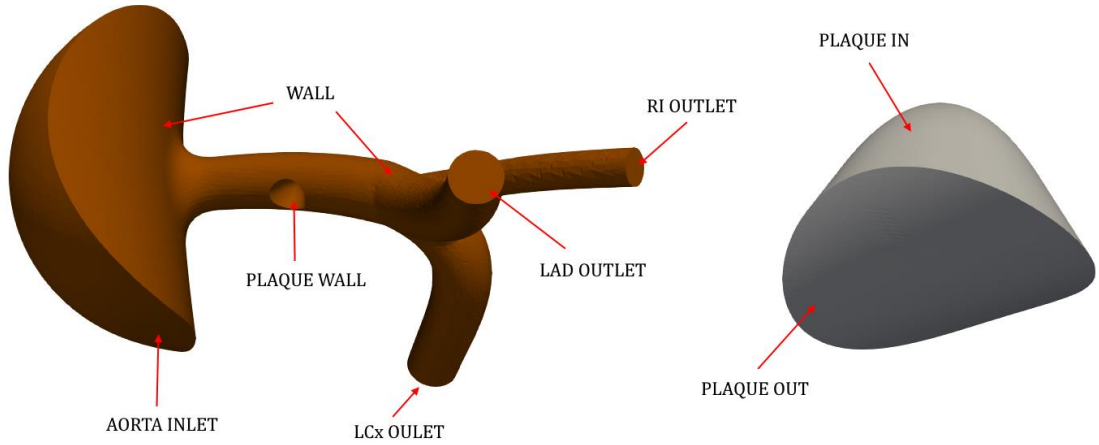

Slika 5. Rubne granice geometrijskih modela

Regija fluida opisana je s jednakim granicama, kao u prethodnoj simulaciji, s dodatkom granice *plaque wall*, koja zajedno s granicom *plaque in* na solid regiji čini zajedničku granicu međudjelovanja fluida i čvrstog tijela (eng. FSI interface). Granice se moraju dobro poklapati jer je simulacija osjetljiva na numeričku mrežu. Granica *plaque out* predstavlja vanjsku dodirnu površinu između plaka i koronarne arterije.

Tablica 0.1: Detalji numeričke mreže

Regija	Broj volumena
Fluid 1	141 366
Solid 1	4858
Fluid 2	145 229
Solid 2	8845

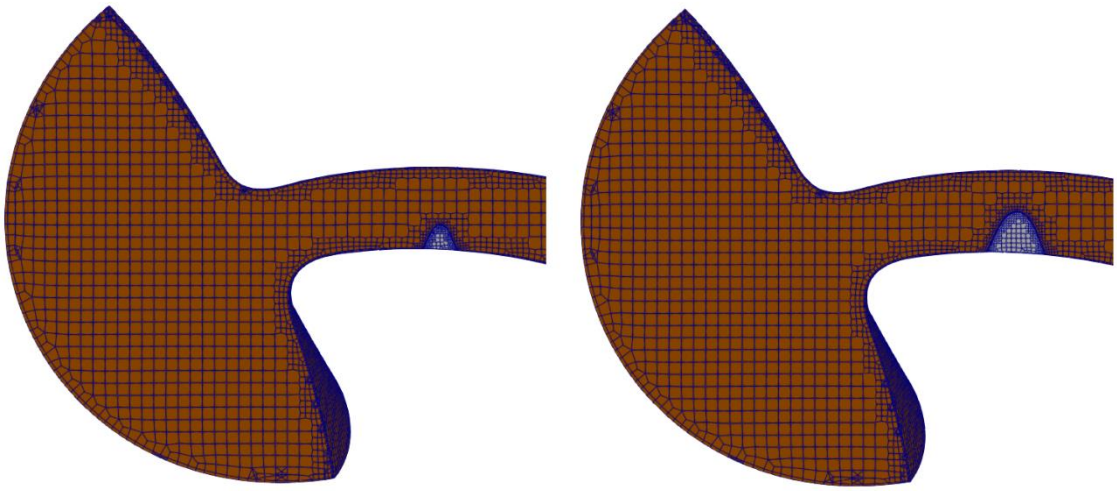

Slika 6. Numerička mreža

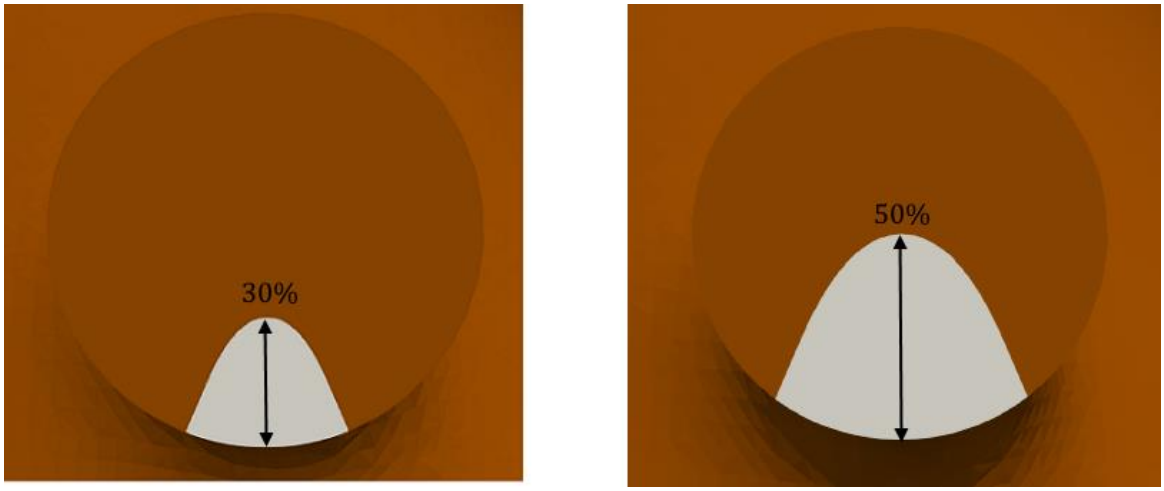

Slika 7. Poprečni presjek modela 1 i modela 2

Simulacije su provedene u računalnom programu OpenFOAM, tj. njegovoj inačici foam-extend 4.1. Rubni uvjet na ulazu fluida zadan je vremenski promjenjivim volumnim protokom, dok na izlazu vremenski promjenjivim tlakom. Na granici čvrstog tijela zadan je Dirichlet-Neumannov rubni uvjet koji prenosi izračunate sile fluida na površinu čvrstog tijela i samim time postiže međusobnu interakciju dvaju regija.

Prostorna domena obje regije diskretizirana je metodom kontrolnih volumena shemama drugog reda točnosti, dok je vremenska domena diskretizirana implicitom shemom prvog reda točnosti. Sheme prvog reda točnosti koriste se radi poboljšanja stabilnosti simulacije jer je osjetljiva na numeričku mrežu.

Rezultati simulacija

U ovom dijelu bit će prikazana usporedni analiza najbitnijih rezultata dvaju modela. Model 1 označuje model s 30 % stenoze, dok model 2 s 50 % stenoze.

Sljedeće slike prikazuju raspodjelu tangencijalnog naprezanja na stijenki aterosklerotskog plaka. Valja napomenuti da je tangencijalno naprezanje računato s kinematičkom viskoznosti, te je tako i prikazano. Stoga je potrebno pomnožiti cijelo polje s gustoćom kako bi se došlo do pravih vrijednosti naprezanja.

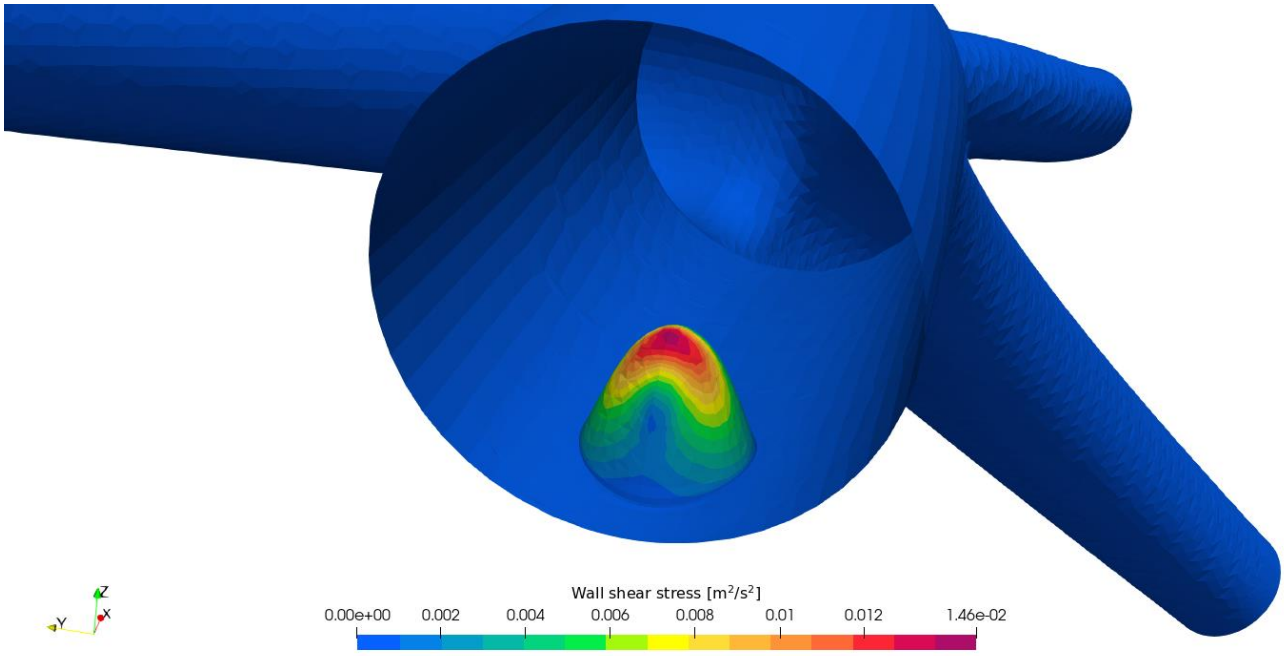

Slika 8. Raspodjela tangencijalnog naprezanja, model 1

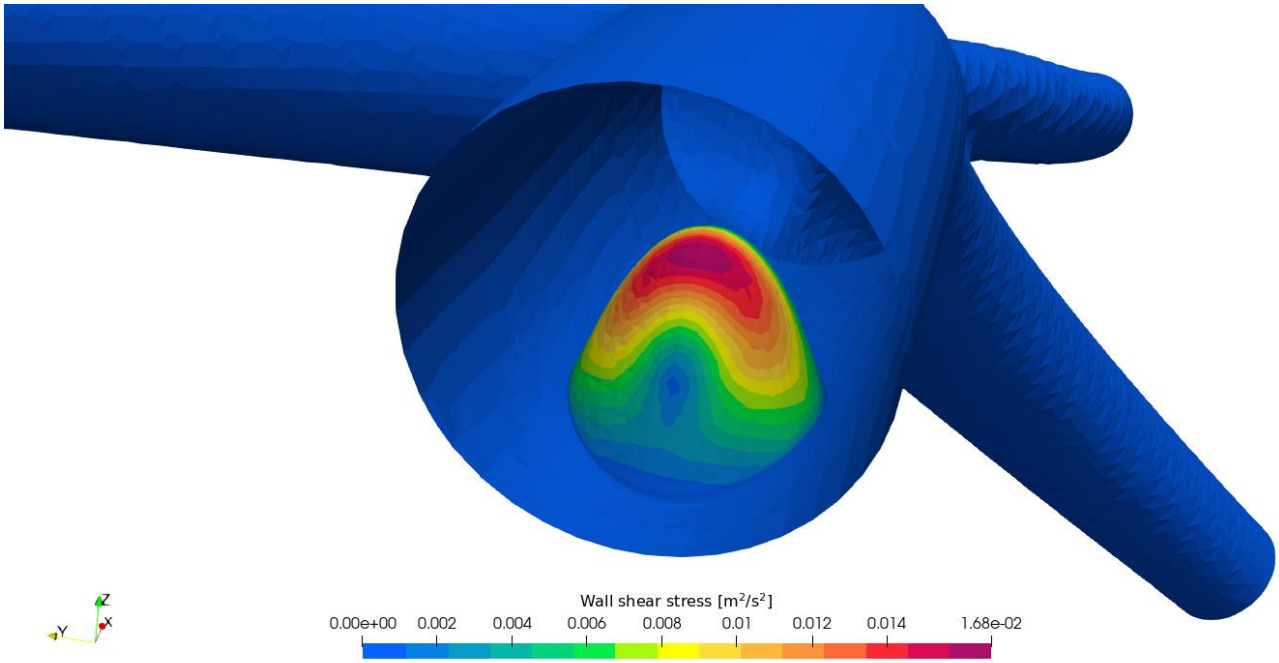

Slika 9. Raspodjela tangencijalnog naprezanja, model 2

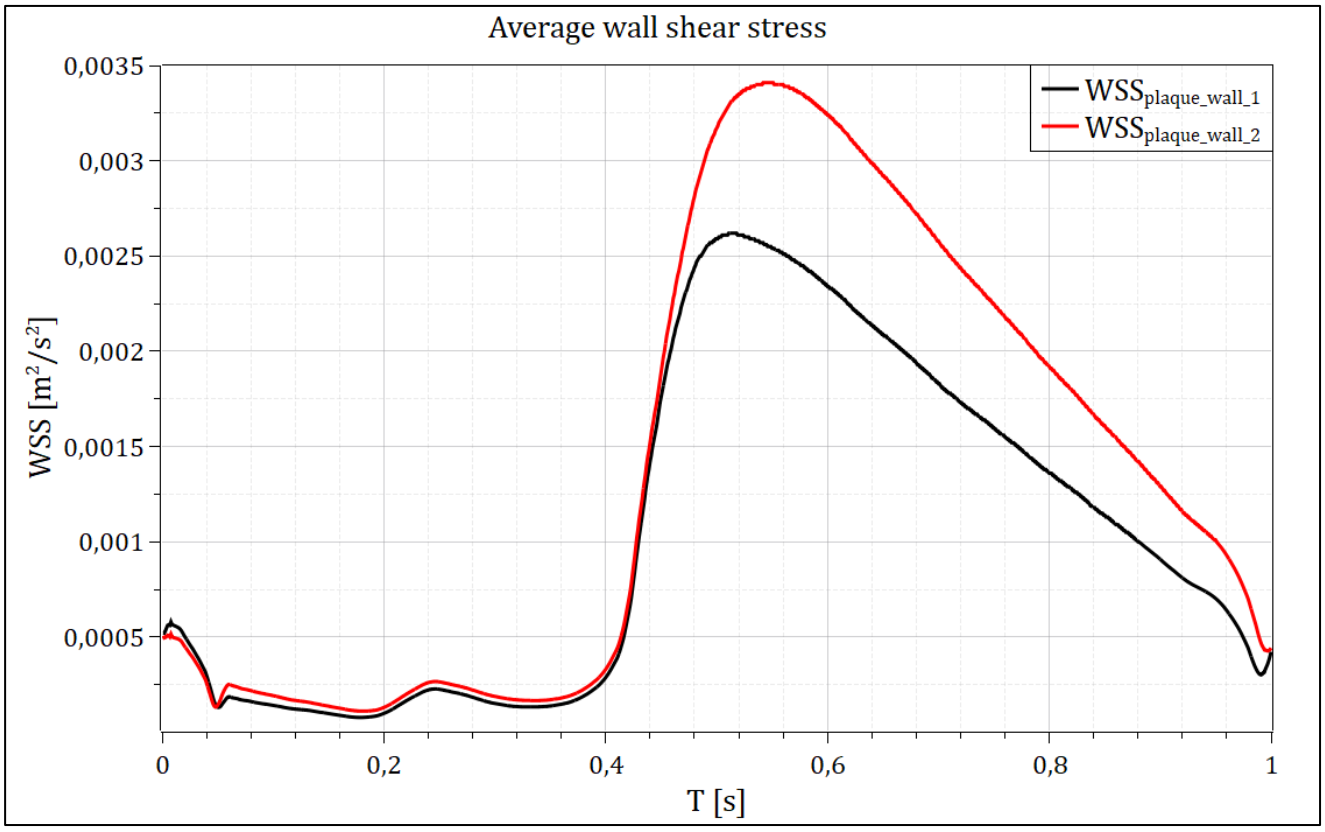

Slika 10. Vremenska promjena prosječnog tangencijalnog naprezanja

Sljedeće slike prikazuju pomake i ekvivalentna naprezanja pri maksimalnom tlaku u trenutku $t = 0.34$ s.

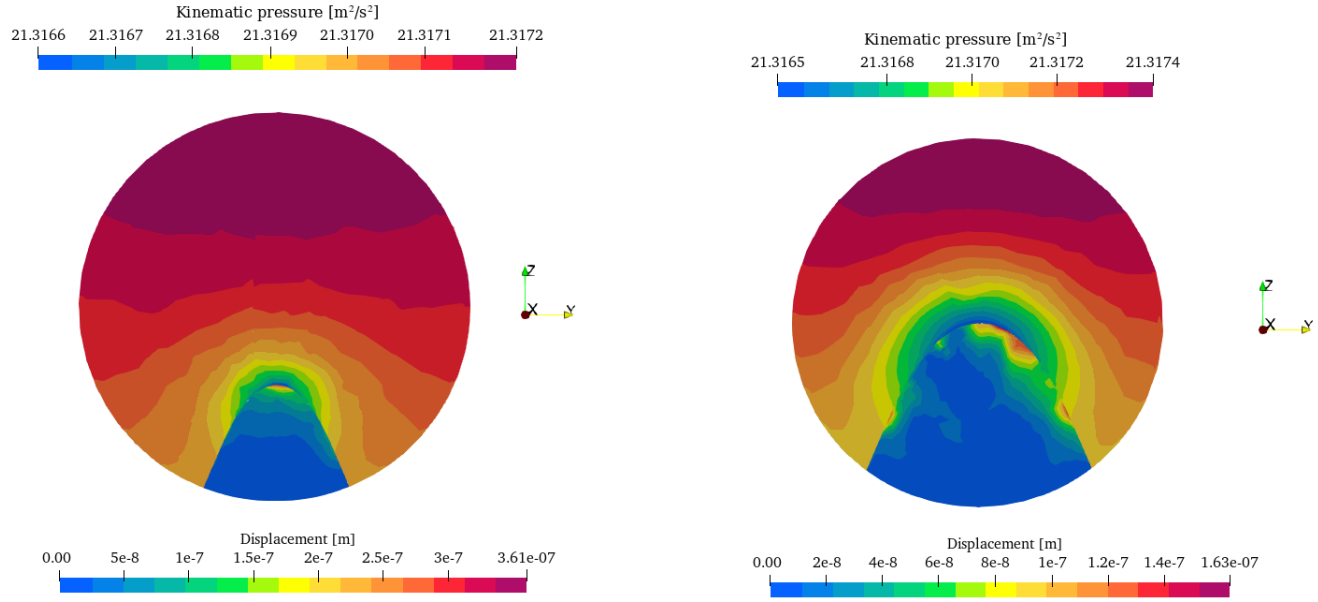

Slika 11. Usporedba tlak-pomak I

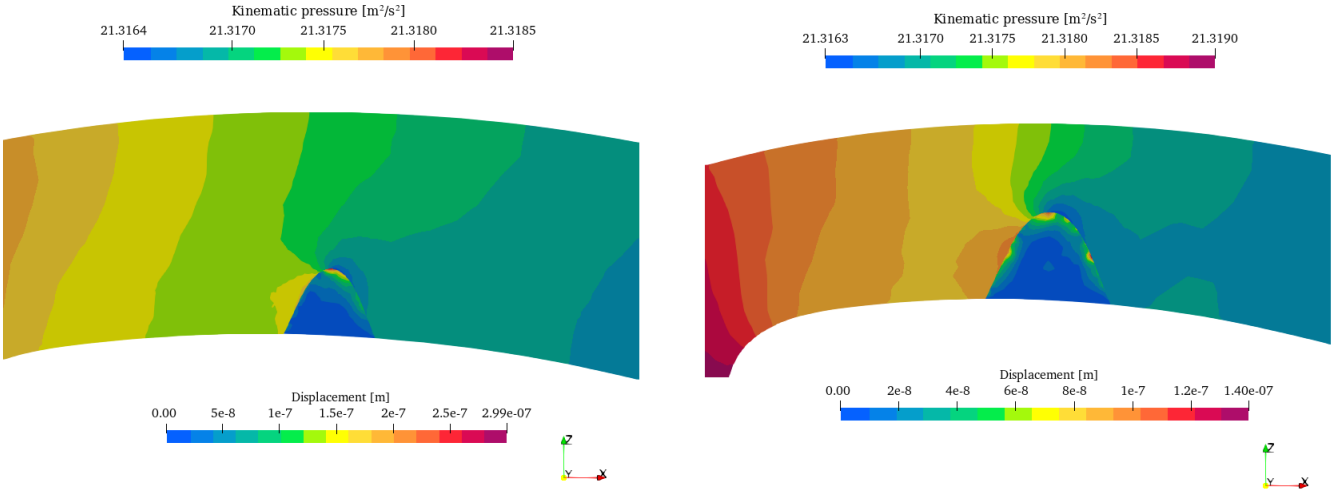

Slika 12. Usporedba tlak-pomak II

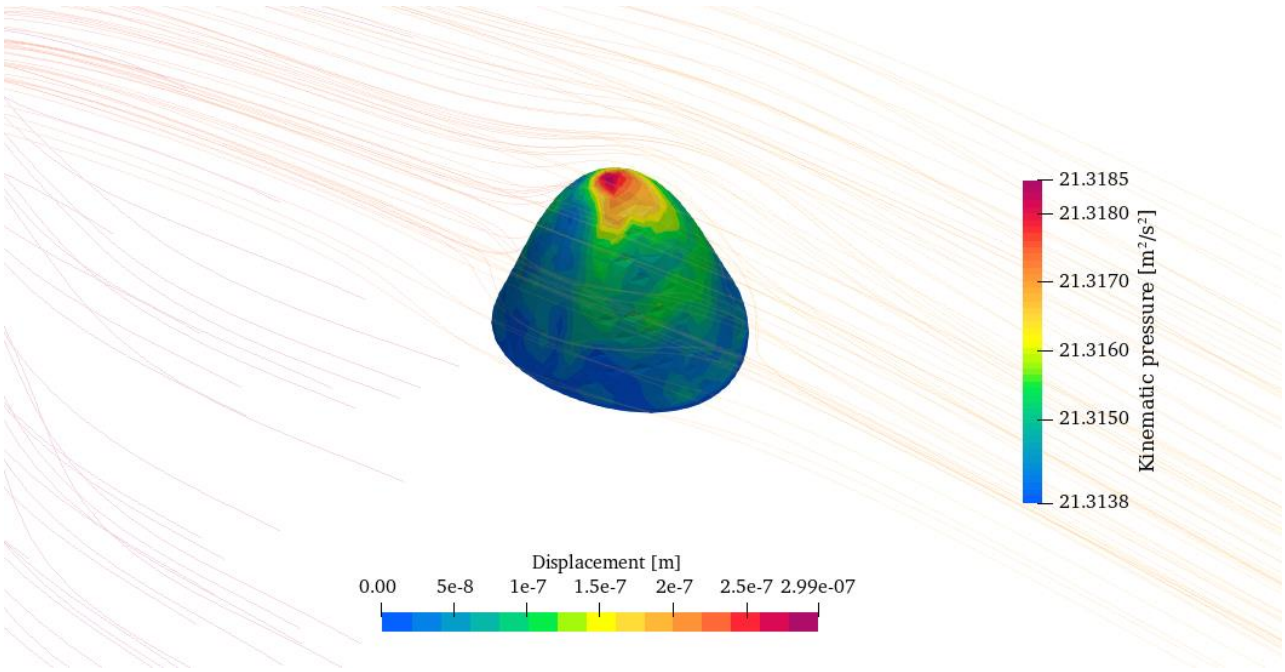

Slika 13. Usporedba polja tlak-pomak, model 1

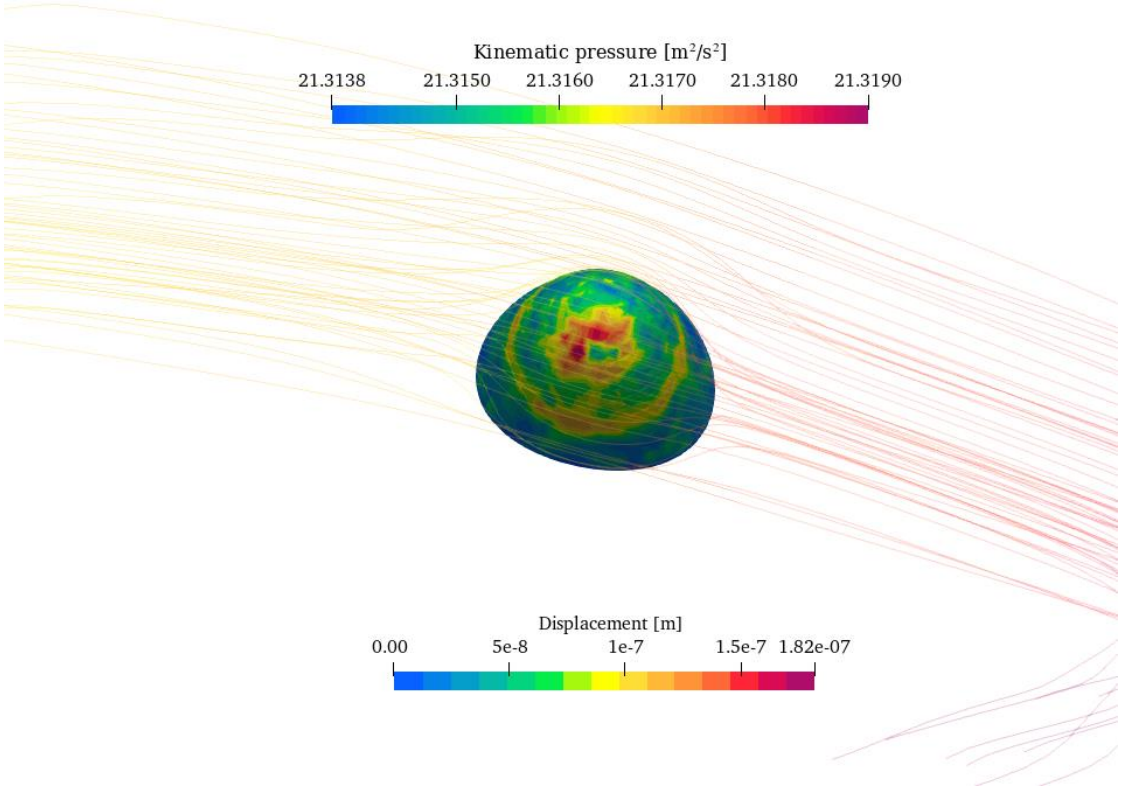

Slika 14. Usporedba polja tlak-pomak, model 2

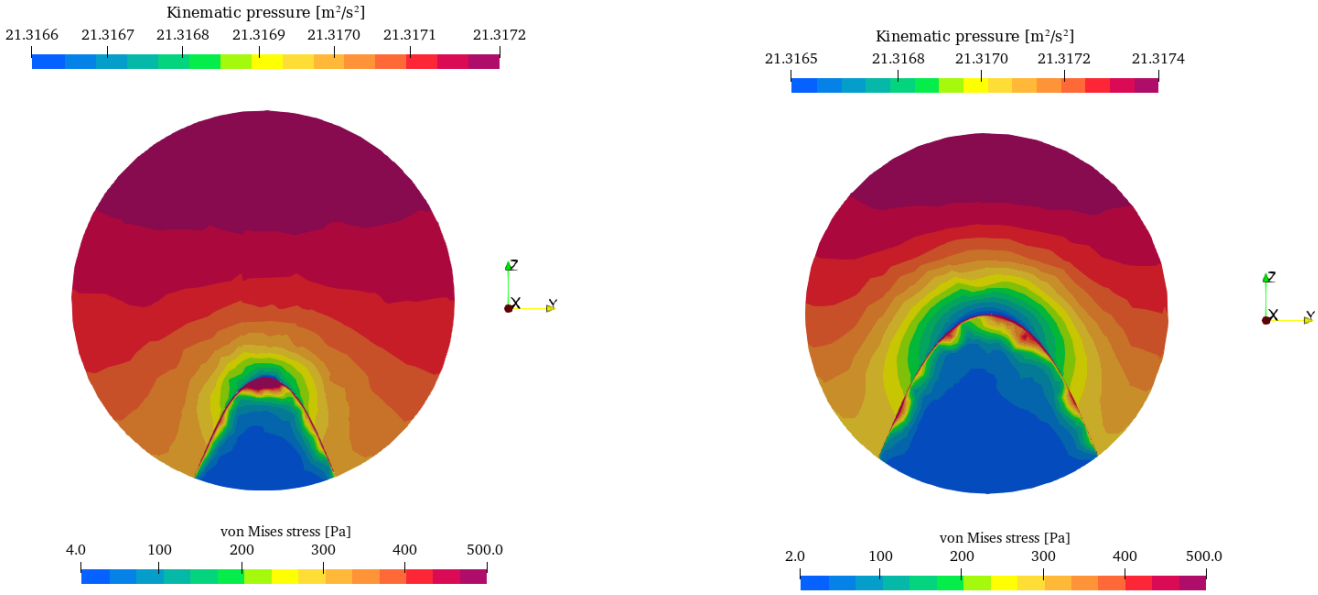

Slika 15. Usporedba tlak-naprezanje I

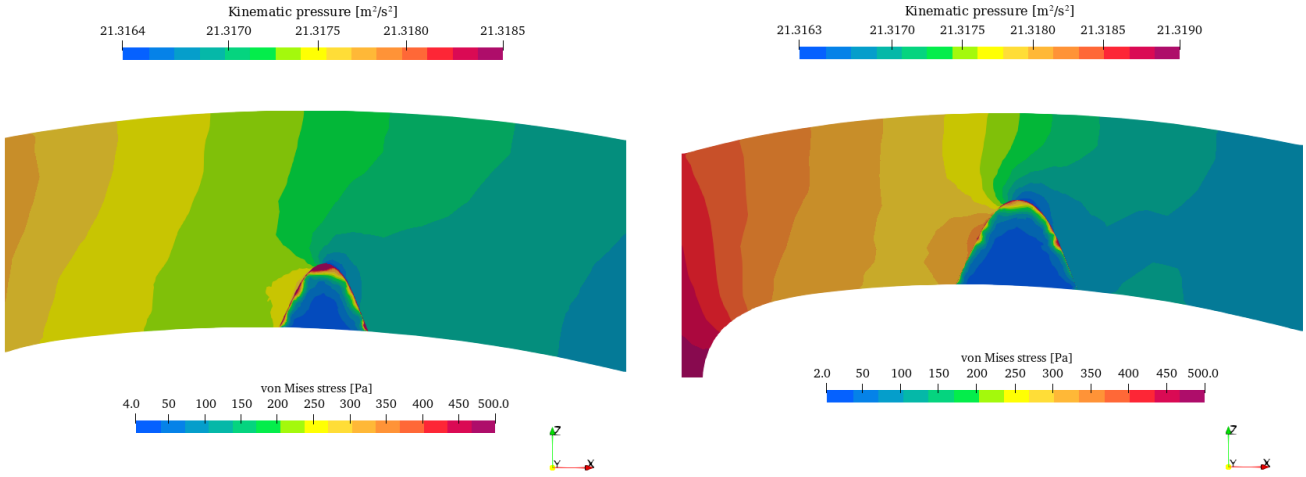

Slika 16. Usporedba tlak-naprezanje II

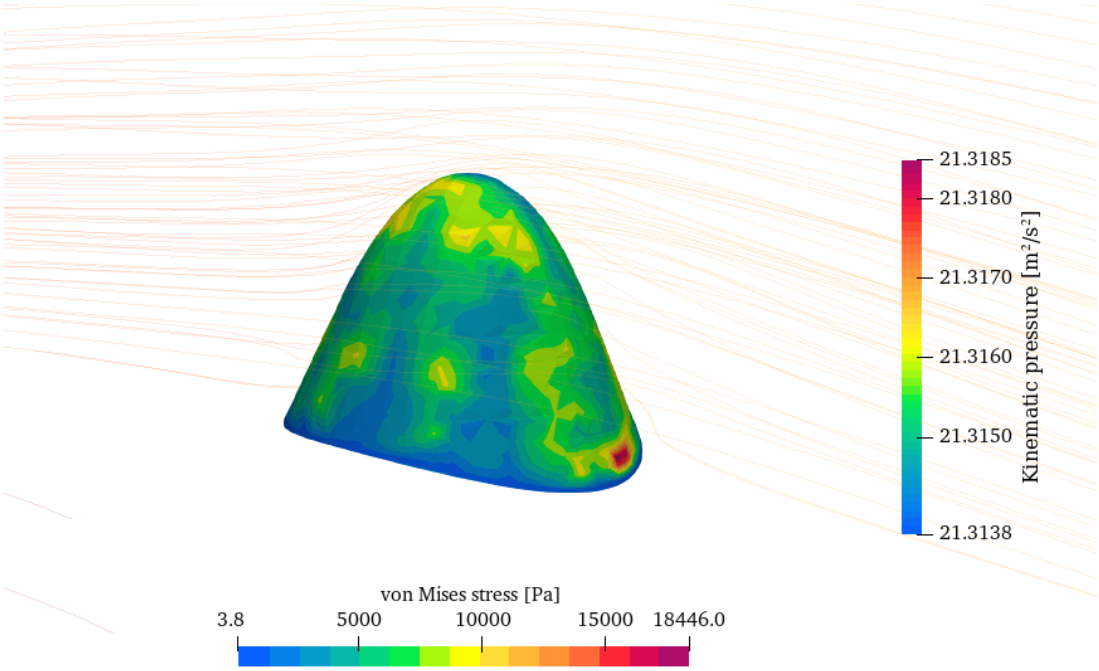

Slika 17. Usporedba polja tlak-naprezanje, model 1

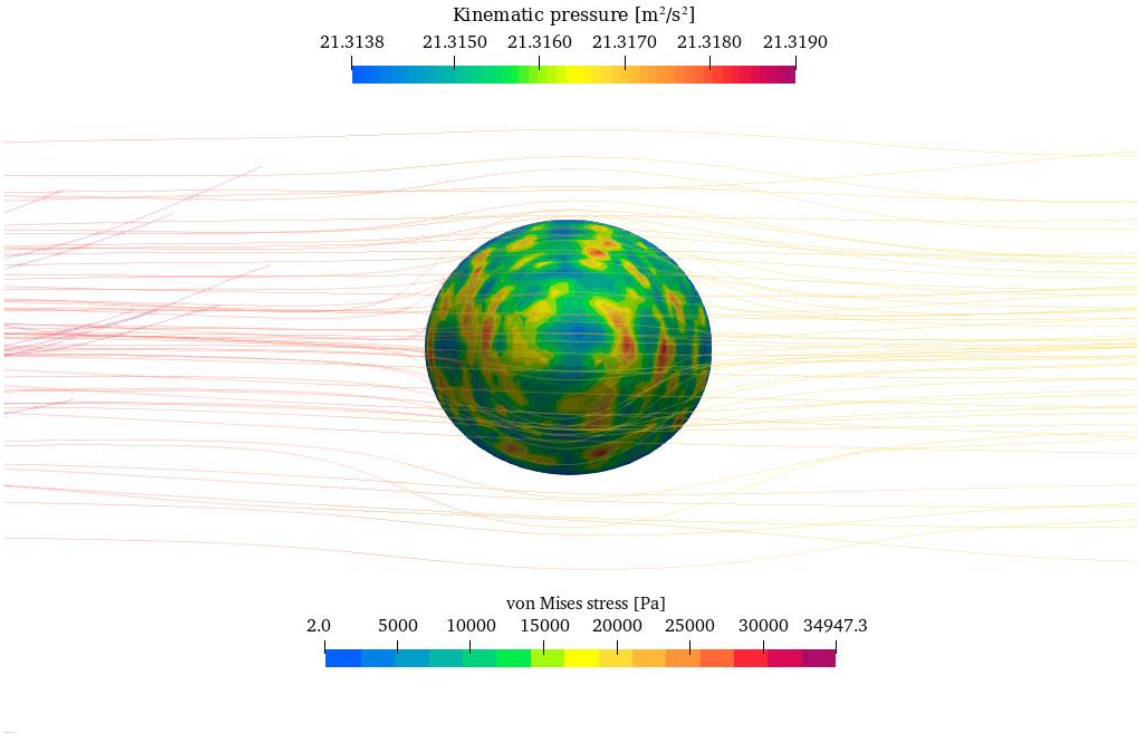

Slika 18. Usporedba polja tlak-naprezanje, model 2

Sljedeće slike prikazuju pomake i ekvivalentna naprezanja u trenutku maksimalne brzine tj. $t = 0.56$ s.

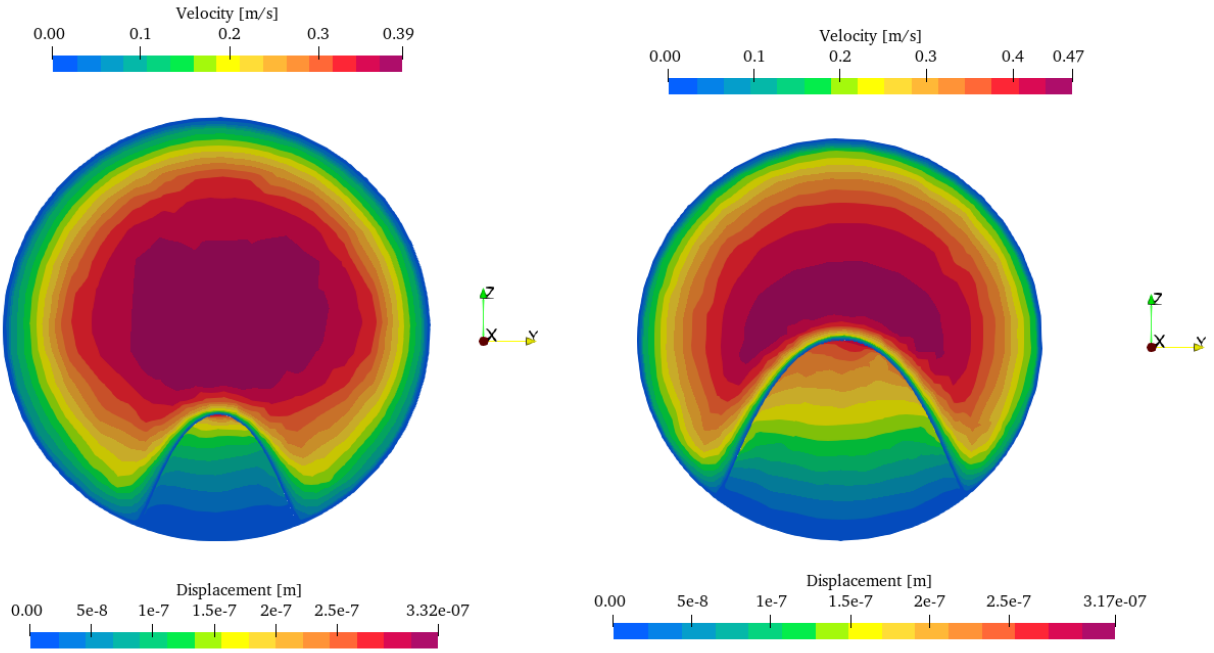

Slika 19. Usporedba brzina-pomak I

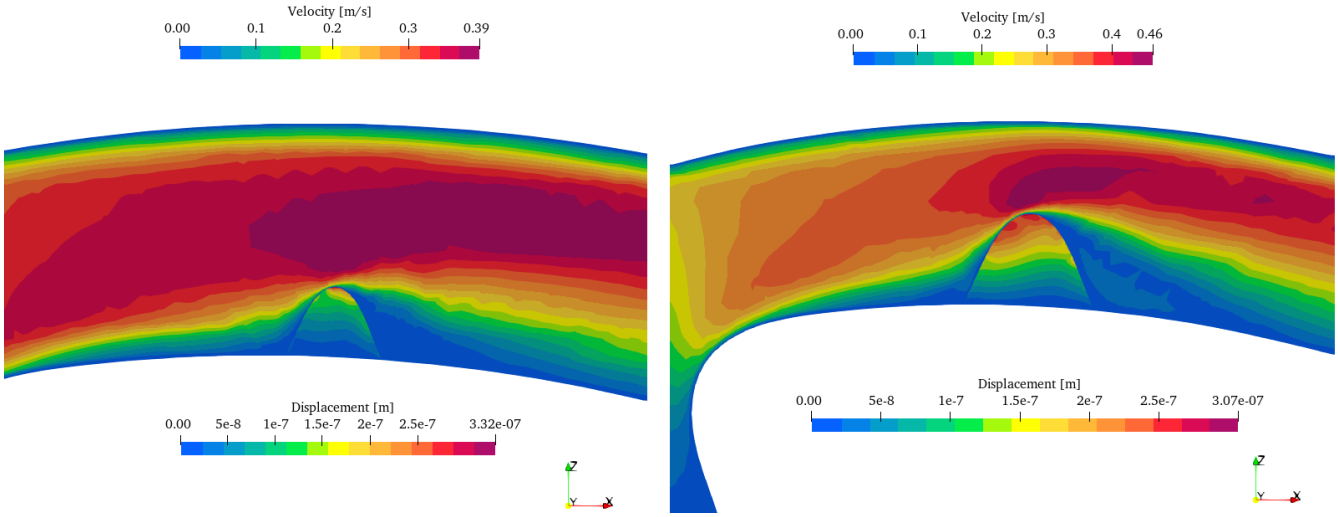

Slika 20. Usporedba brzina-pomak II

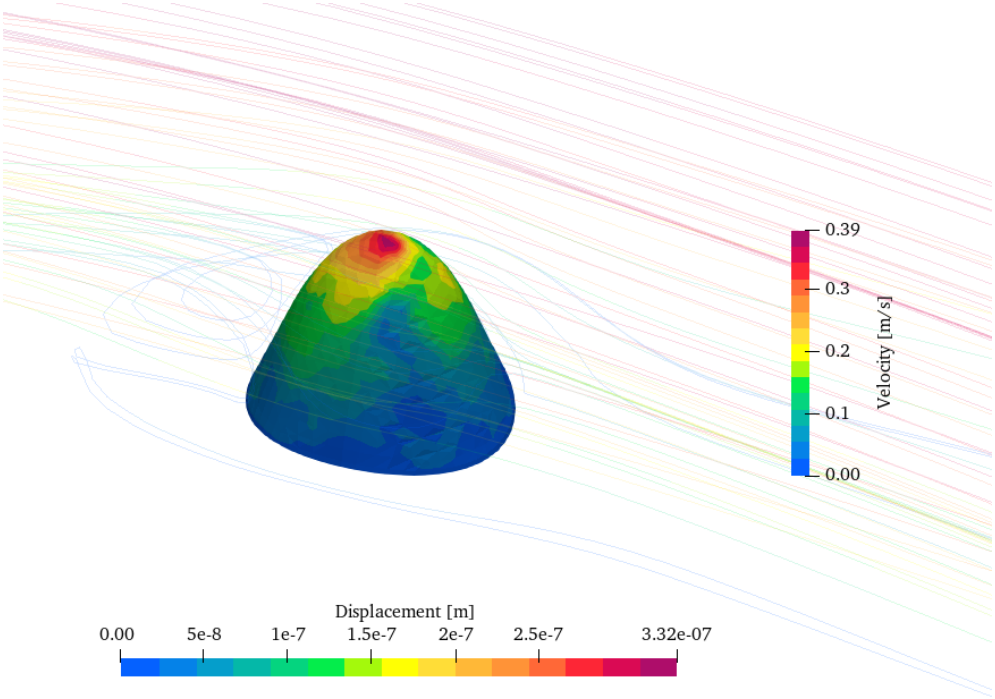

Slika 21. Usporedba polja brzina-pomak, model 1

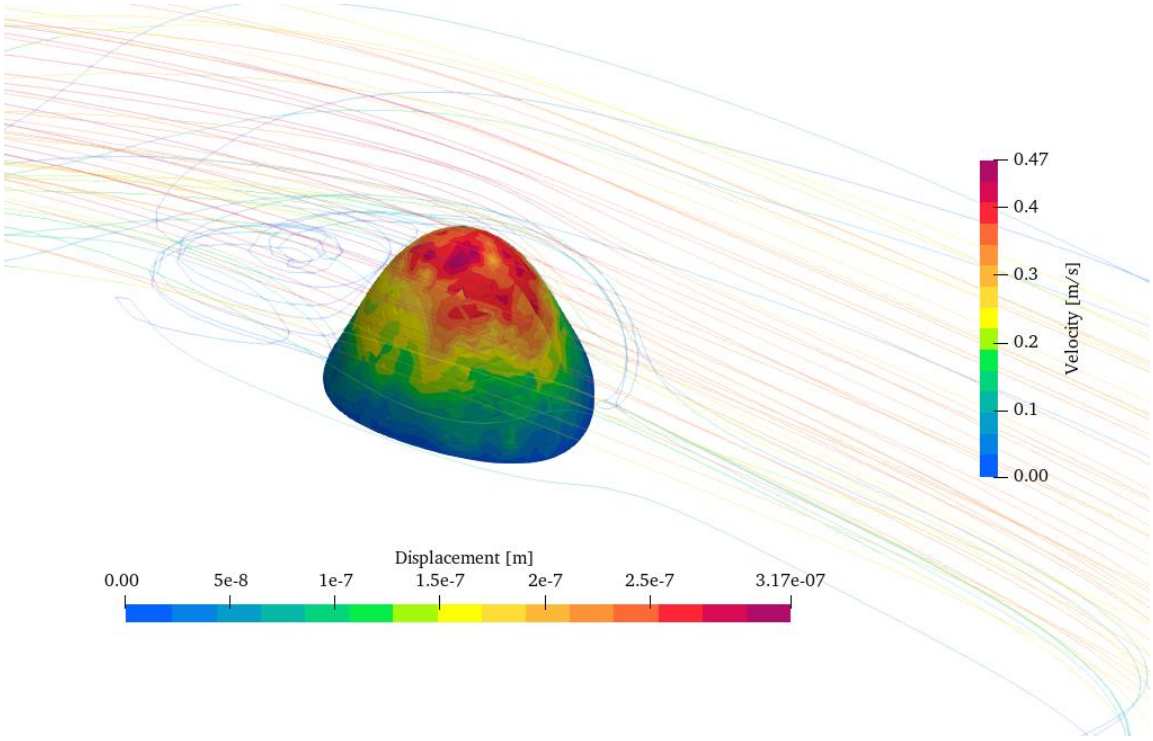

Slika 22. Usporedba polja brzina-pomak, model 2

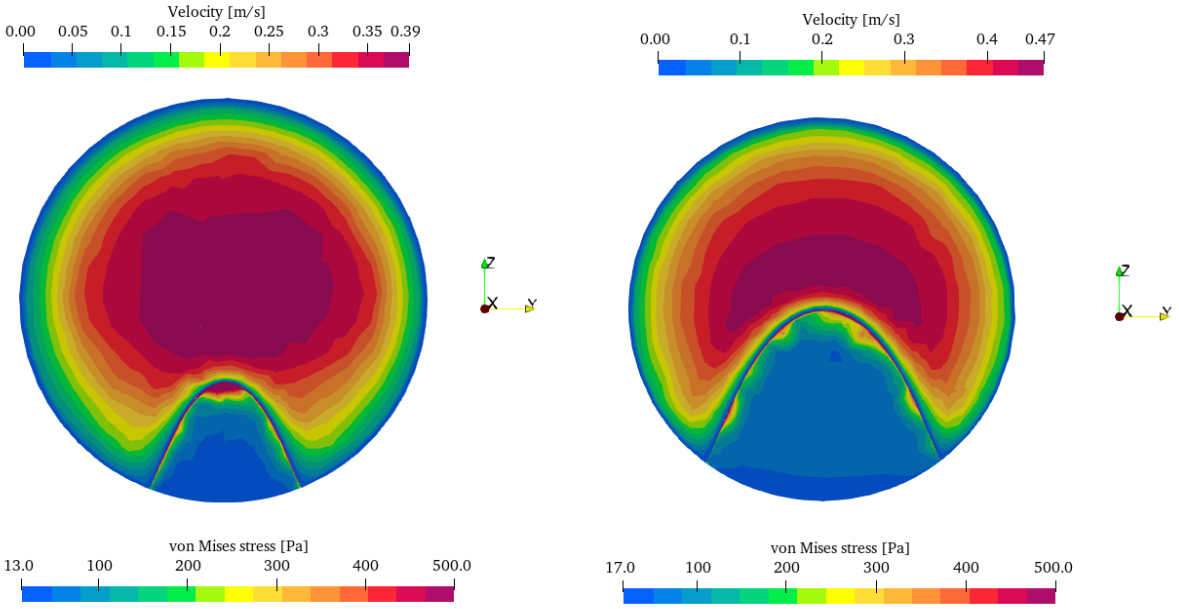

Slika 23. Usporedba brzina-naprezanje I

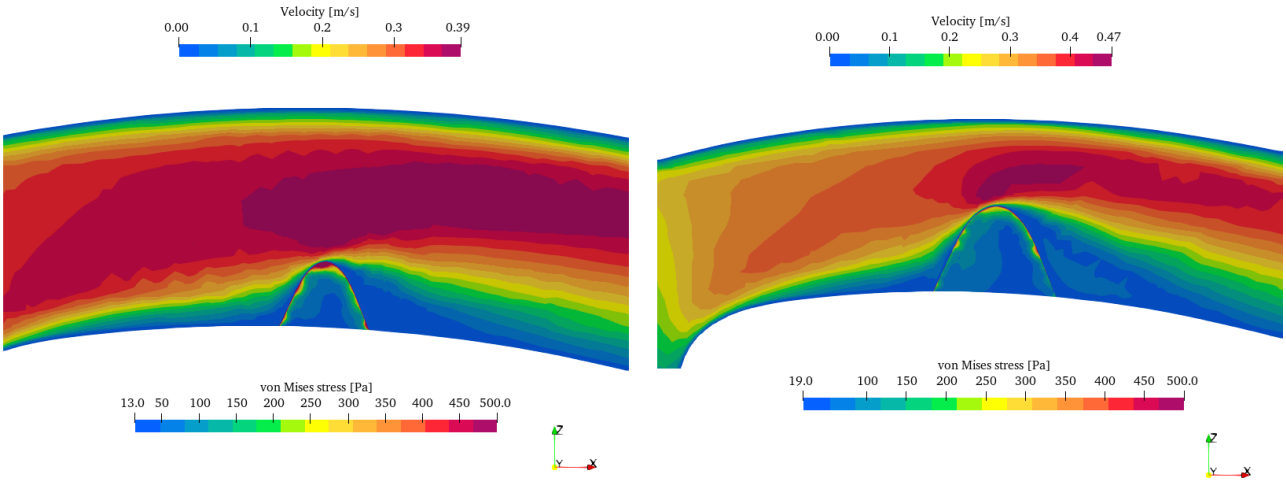

Slika 24. Usporedba brzina-naprezanje II

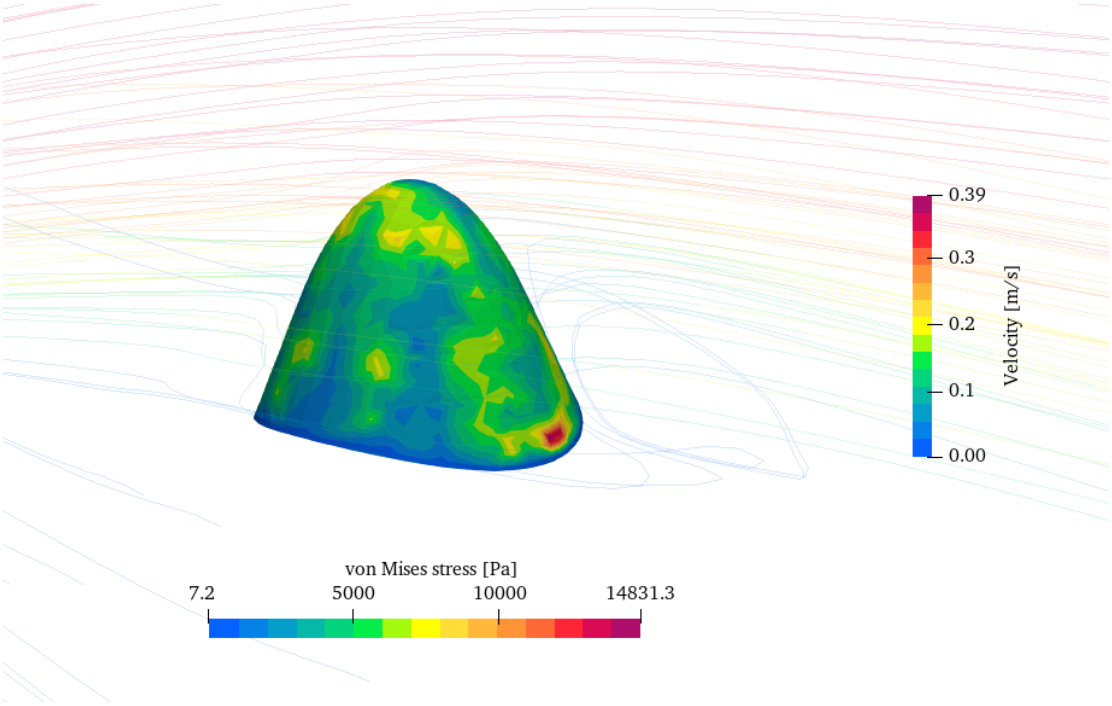

Slika 25. Usporedba polja brzina-naprezanje, model 1

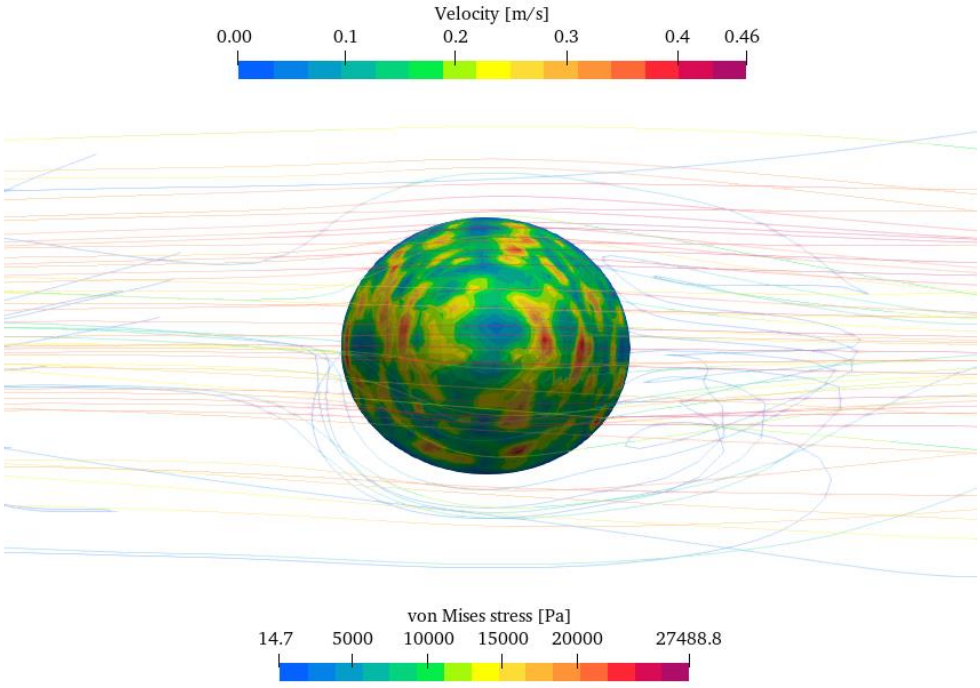

Slika 26. Usporedba polja brzina-naprezanje, model 2

1. INTRODUCTION

According to the World Health Organization, ischemic heart disease and strokes are the leading causes of death worldwide. The majority of cardiovascular diseases are caused by atherosclerosis, which is the formation and progression of plaque in the inner lining of the arterial wall, also known as atheroma. The initial stage of atherosclerosis is asymptomatic; however, the progressive evolution and accumulation of plaque over decades causes a significant reduction in lumen size known as stenosis. The progression of atherosclerotic plaque has been correlated with the presence of low wall shear stress (WSS) on the artery wall. The zones of low shear stress are associated with permanent endothelium inflammation, thus providing favorable conditions for the plaque formation. This cholesterol-rich tissue causes narrowing of the lumen, rupture or erosion of the arterial wall, hardening of the arteries, and loss of their elasticity, which leads to an eventual or complete reduction in the blood flow through the vessels [1].

Hemodynamics, the study of blood flow, is essential to understanding the mechanisms behind the development of cardiovascular diseases. In vivo studies that involve blood flow are usually difficult to perform due to ethical issues, high costs, and technical complications [2]. Therefore, numerical simulations along with medical imaging can provide valuable information on the hemodynamic effects and anatomic alterations due to the presence of stenosis, which can induce significant pressure drops, increased wall shear stress, separation, and plaque rupture. The prevention of coronary artery disease (CAD) is important as its occurrence is now seen as one of the largest economic burdens on global society [3]. This is the reason why the identification of vulnerable plaque, at high risk of rupturing, remains the most important task in the field. This thesis aims to develop a simplified dynamic model for coronary arteries, which predicts the vulnerable atherosclerotic plaque and thus identifying patients at high risk of a heart attack. This model would allow the non-invasive analysis of the patient-specific situation and thus carry out the necessary interventions for plaque stabilization and heart attack prevention [4].

The goal of this thesis is to reconstruct a simplified geometrical model of the coronary artery lumen with the accumulated plaque based on the computerized tomography (CT) scans and perform a numerical fluid-structure interaction (FSI) simulation assuming a rigid artery wall and incompressible hyperelastic plaque body.

2. MEDICAL INTRODUCTION

2.1. Anatomy and physiology of the cardiovascular system

The cardiovascular system, also called the circulatory system, maintains the distribution of blood throughout the body and is composed of the heart and the blood vessels: arteries, capillaries, and veins. The circulatory system is composed of two parts: pulmonary circulation and systemic circulation. The pulmonary circulation, between the heart and lungs, transports deoxygenated blood to the lungs to get oxygen, and then back to the heart. The systemic circulation carries oxygenated blood away from the heart to the tissues and cells, and then back to the heart. In this way, all the body's cells receive blood and oxygen.

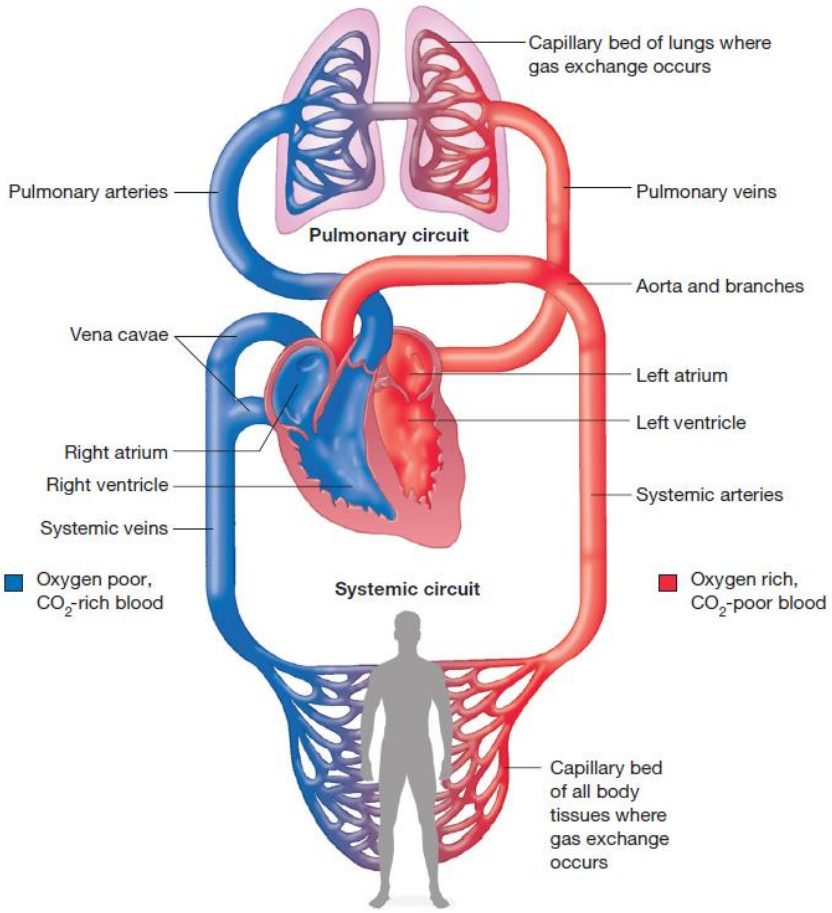

Figure 2-1. A schematic of the circulatory system [5]

In addition to distributing oxygen and other nutrients, such as glucose and amino acids, the cardiovascular system also collects waste products from the body's cells. Carbon dioxide and other waste products produced by the metabolic reactions are transported by the cardiovascular system to the lungs, liver, and kidneys, where they are eliminated from the body [1].

2.2. Heart

The human heart is a muscular organ containing four chambers that are situated just to the left of the midline of the thoracic cavity. It is approximately the size of a man's closed fist. The upper two chambers (atria) are divided by a wall-like structure called the interatrial septum. The lower two chambers (ventricles) are divided by a similar structure called the interventricular septum. Between each atrium and ventricle, valves allow blood to flow in one direction, preventing backflow [2].

The wall of the heart is quite thick and is composed of three layers (see Fig. 2-2):

1. The *endocardium* is the inner layer of the heart lining the heart chambers. It is a very smooth, thin layer that serves to reduce friction as the blood passes through the heart chambers.

2. The *myocardium* is the thick, muscular middle layer of the heart. Contraction of this muscle layer develops the pressure required to pump blood through the blood vessels.

3. The *epicardium* is the outer layer of the heart. The heart is enclosed within a double-layered pleural sac, called the pericardium. The epicardium is the visceral pericardium or the inner layer of the sac. The outer layer of the sac is the parietal pericardium. The fluid between the two layers of the sac reduces friction as the heart beats.

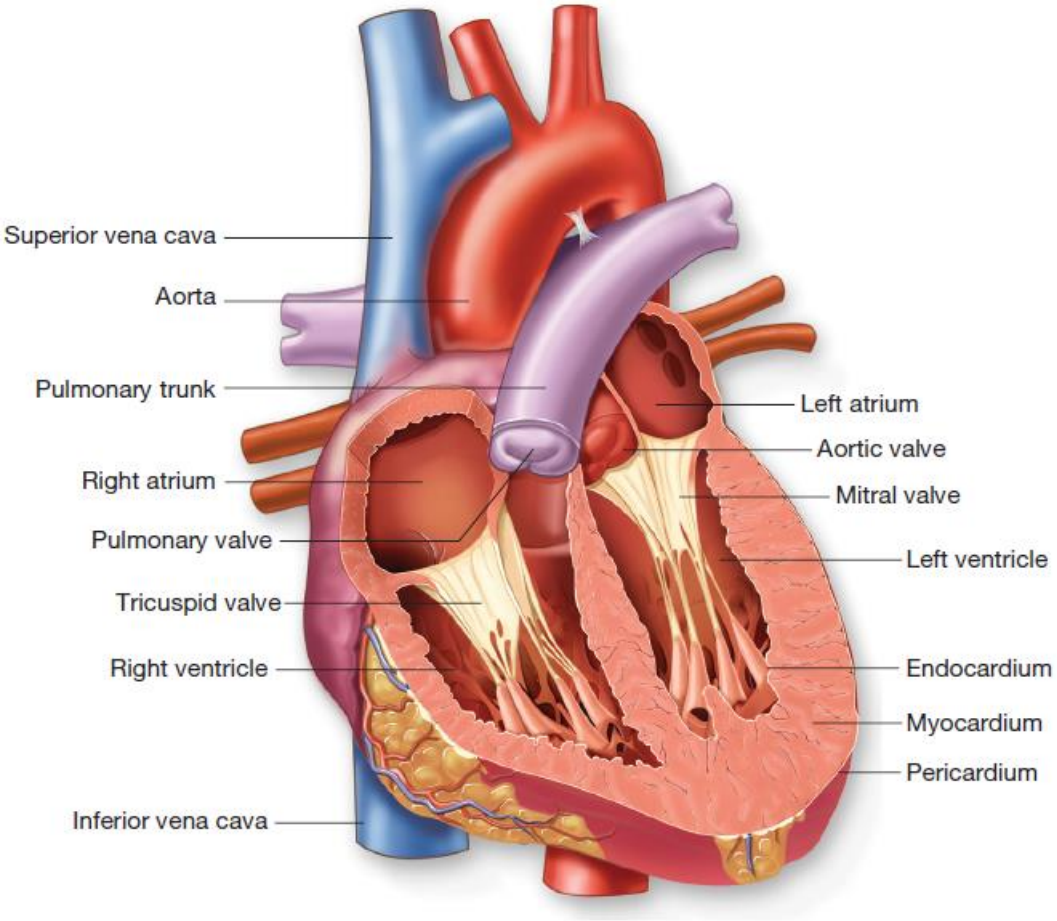

Figure 2-2. Internal view of the heart [5]

In a healthy person, the blood flow through the heart is very regular (see Fig. 2-3). It travels from the heart to the lungs, where it receives oxygen, before returning to the heart and then to the body tissues and parts. The normal process of blood flow is:

- Deoxygenated blood from all the tissues in the body enters a relaxed right atrium via two large veins called the superior vena cava and inferior vena cava.
- The right atrium contracts and the blood flows through the tricuspid valve into the relaxed right ventricle.
- The right ventricle then contracts and the blood is pumped through the pulmonary valve into the pulmonary artery, carrying it to the lungs for oxygenation.
- The left atrium receives blood returning to the heart after being oxygenated by the lungs. This blood enters the relaxed left atrium from the four pulmonary veins.

- The left atrium contracts and blood flows through the mitral valve into the relaxed left ventricle.
- When the left ventricle contracts, the blood is pumped through the aortic valve and into the aorta, the largest artery in the body. The aorta carries blood to all parts of the body.

It can be seen that the heart chambers alternate between relaxing, in order to fill, and contracting to push blood forward. The period of time a chamber is relaxed is diastole. The contraction phase is systole.

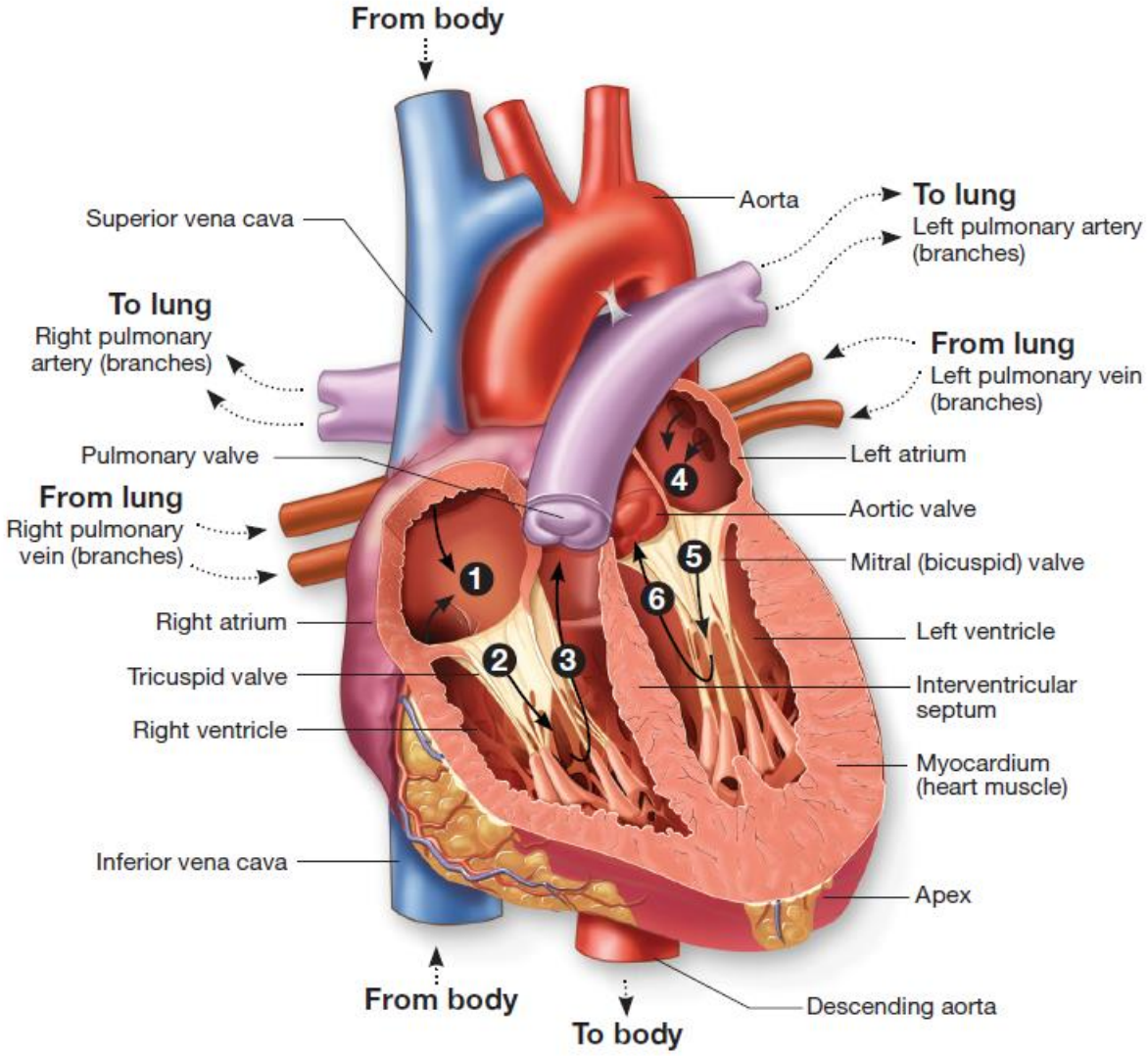

Figure 2-3. Blood flow through the chambers of the left and right side of the heart [5]

2.3. The blood vessels and circulation

The function of the circulation is to serve the needs of the body tissues:

- to transport nutrients to the body tissues,
- to transport waste products away,
- to transport hormones from one part of the body to another,
- to maintain an appropriate environment in all the tissue fluids of the body for survival and optimal function of the cells.

The blood vessels of the human body carry blood to every type of tissue and organ. There are five general classes of blood vessels in the cardiovascular system:

- arteries
- arterioles
- capillaries
- venules
- veins

The function of the *arteries* is to transport blood under high pressure to the tissues. For this reason, the arteries have strong vascular walls, and blood flows at a high velocity in the arteries.

The *arterioles* are the last small branches of the arterial system; they act as control conduits through which blood is released into the capillaries. Arterioles have strong muscular walls that can close the arterioles completely or can, by relaxing, dilate the vessels severalfold, thus having the capability of vastly altering blood flow in each tissue in response to its needs.

The function of the *capillaries* is to exchange fluid, nutrients, electrolytes, hormones, and other substances between the blood and the interstitial fluid. To serve this role, the capillary walls are thin and have numerous minute capillary pores permeable to water and other small molecular substances.

The *venules* collect blood from the capillaries and gradually coalesce into progressively larger veins.

The *veins* function as conduits for the transport of the blood from the venules back to the heart. The venous walls are thin because the pressure in the venous system is very low. Even so, they are muscular enough to contract or expand and thereby serve as a controllable reservoir for the extra blood, either a small or a large amount, depending on the needs of the circulation [3].

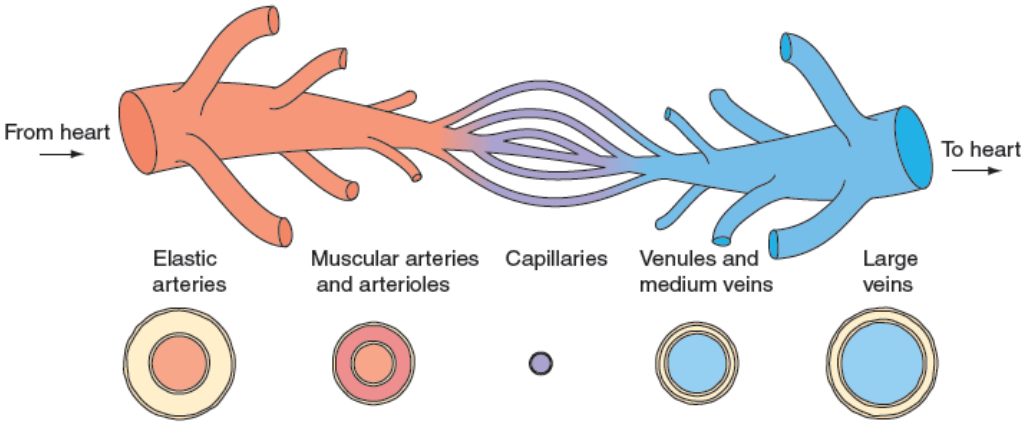

Figure 2-4. The structure and diameter of blood vessels [6]

About 84 % of the entire blood volume of the body is in the systemic circulation and 16 % is in the heart and lungs. Of the 84 % in the systemic circulation, approximately 64 % is in the veins, 13 % is in the arteries, and 7 % is in the systemic arterioles and capillaries. The heart contains 7 % of the blood, and the pulmonary vessels, 9 %. Most surprising is the low blood volume in the capillaries. However, the most important function of circulation occurs here - the alternating diffusion of substances between the blood and the tissues.

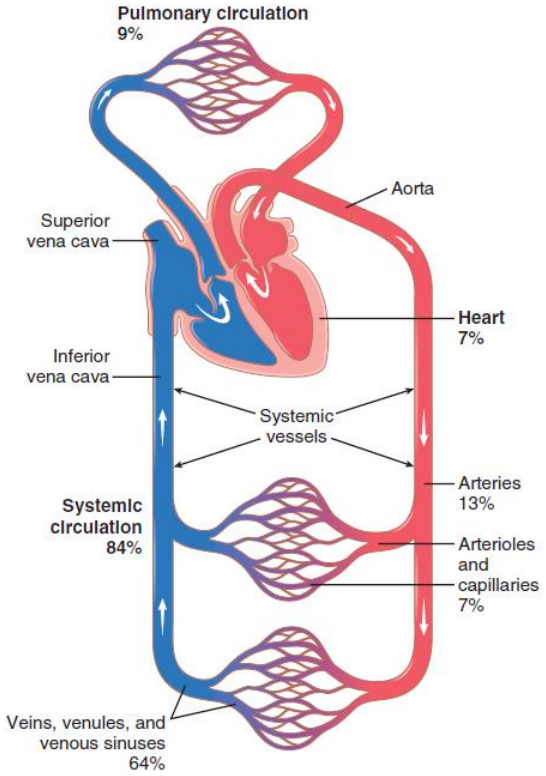

Figure 2-5. Distribution of blood in the different parts of the circulatory system [7]

2.4. Blood pressure

Blood pressure is defined as the force that blood exerts against the inner walls of blood vessels. Arterial blood pressure rises and falls according to cardiac cycle phases. The maximum pressure during ventricular contraction is called systolic pressure. The lowest pressure that remains in the arteries before the next ventricular contraction is called diastolic pressure. Blood pressure is almost always measured in millimeters of mercury (mm Hg) with a device called a sphygmomanometer. Its results are reported as a fraction of the systolic pressure over the diastolic pressure, which for a healthy person is 120/80 mm Hg.

The artery walls are distended as blood surges into them from the ventricles, but they recoil almost immediately. This expansion and recoiling can be felt as a pulse in an artery near the surface of the skin. The arterial blood pressure depends on heart rate, stroke volume, blood volume, peripheral resistance, and bloody viscosity.

Heart action determines the amount of blood entering the arterial system with each ventricular contraction. Stroke volume is defined as the volume of blood discharged from the ventricle with each contraction. An average adult male's stroke volume is about 70 mL. The cardiac output is defined as the volume discharged from the ventricle per minute. It is calculated by multiplying the stroke volume by the heart rate, in beats per minute. The average cardiac output of an adult person at rest is about 5000 mL/min. Blood pressure varies with cardiac output and increases or decreases based upon similar changes in stroke volume or heart rate.

Blood volume is defined as the sum of formed elements and plasma volumes in the vascular system. Blood volume varies with age, body size, and gender. Most adults have approximately 5 L of blood, which makes up 8 % of the body weight in kilograms. Blood pressure and volume are usually directly proportional. Any changes in volume can initially alter the pressure.

The resistance of arteries to blood flow is defined as peripheral resistance. The degree of peripheral resistance is determined by the blood vessel diameter and the force of contraction exerted by vascular smooth muscle. Therefore, peripheral resistance is a factor that accounts for blood pressure.

The viscosity is defined as the resistance of a fluid to flow. In a biological fluid, viscosity is caused by the attraction of molecules or cells to one another. The higher the viscosity, the greater the resistance to flowing. As the blood viscosity is increased, the greater the force is needed to move the blood. Blood pressure rises as blood viscosity increases and vice versa.

2.5. Coronary circulation

About one-third of all deaths in industrialized countries of the Western world result from coronary artery disease, and almost all elderly people have at least some impairments in coronary artery circulation. For this reason, understanding the normal and pathological physiology of coronary circulation is one of the most important subjects in medicine.

Figure 2-6 shows the heart and its coronary blood supply. Note that the main coronary arteries lie on the surface of the heart and smaller arteries then penetrate from the surface into the cardiac muscle mass. It is almost entirely through these arteries that the heart receives its nutritive blood supply. Only the inner 1/10 millimeter of the endocardial surface can obtain significant nutrition directly from the blood inside the cardiac chambers, so this source of muscle nutrition is minuscule.

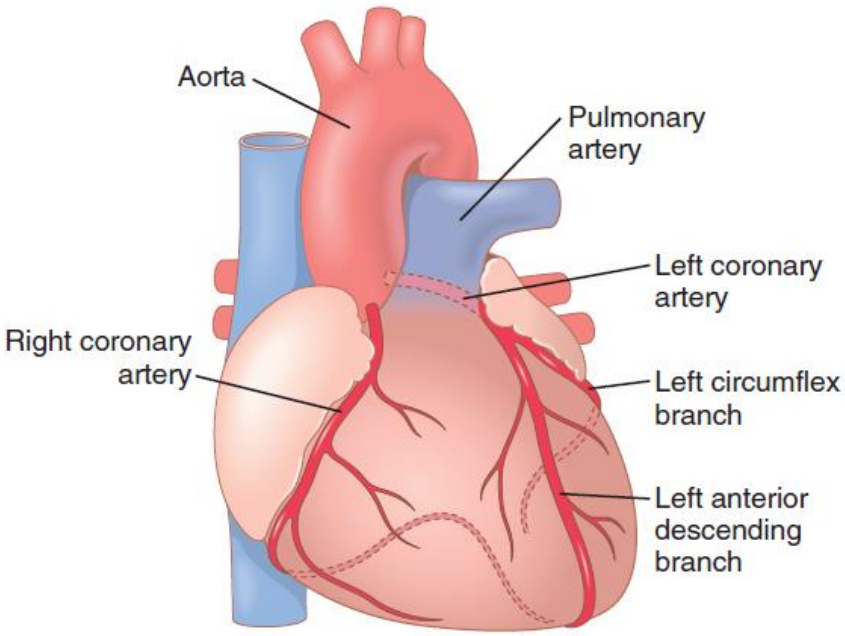

Figure 2-6. The coronary arteries [7]

The left coronary artery supplies mainly the anterior and left lateral portions of the left ventricle, whereas the right coronary artery supplies most of the right ventricle, as well as the posterior part of the left ventricle in 80 to 90 % of people.

Most of the coronary venous blood flow from the left ventricular muscle returns to the right atrium of the heart by way of the coronary sinus, which is about 75 % of the total coronary blood flow. On the other hand, most of the coronary venous blood from the right ventricular muscle returns through small anterior cardiac veins that flow directly into the right atrium, not by way of the coronary sinus. A very small amount of coronary venous blood also flows back into the heart through very minute thebesian veins, which empty directly into all chambers of the heart.

The normal coronary blood flow in the resting human being averages 70 ml/min/100 g of heart weight, or about 225 ml/min, which is about 4 to 5 % of the total cardiac output. During strenuous exercise, the heart of a young adult increases its cardiac output four to sevenfold, pumping blood against higher-than-normal arterial pressure. Consequently, the work output of the heart under severe conditions may increase sixfold to ninefold. At the same time, the coronary blood flow increases threefold to fourfold to supply the extra nutrients needed by the heart. This increase is not as significant as the increase in workload, implying that the ratio of heart energy expenditure to coronary blood flow increases. As a result, the "efficiency" of cardiac energy utilization increases to compensate for the relative deficiency of coronary blood supply.

2.5.1. Phasic changes in coronary blood flow during systole and diastole

Figure 2-7 shows the changes in blood flow through the nutrient capillaries of the left ventricular coronary system in ml/min in the human heart during systole and diastole, as extrapolated from studies in experimental animals. This diagram shows that the coronary capillary blood flow in the left ventricle muscle falls to a low value during systole, which is opposite to flow in other vascular beds in the body. The reason for this phenomenon is the strong compression of the intramuscular blood vessels by the left ventricular muscle during systolic contraction.

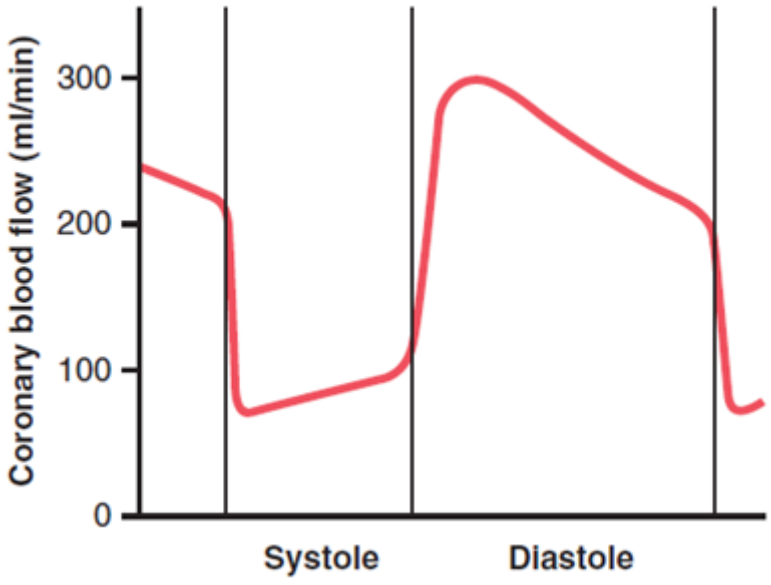

Figure 2-7. The phasic flow of blood through the coronary capillaries of the human left ventricle during cardiac systole and diastole [7]

During diastole, the cardiac muscle relaxes and no longer obstructs blood flow through the left ventricular muscle capillaries, so blood flows rapidly during all of the diastole.

Blood flow through the coronary capillaries of the right ventricle also undergoes phasic changes during the cardiac cycle. However, because the force of contraction of the right ventricular muscle is much lower than that of the left ventricular muscle, the inverse phasic changes in the right ventricular muscle are only partial, as opposed to those in the left ventricular muscle.

2.5.2. Control of coronary blood flow

The primary regulator of coronary blood flow is local muscle metabolism. Local arteriolar vasodilation in response to the nutritional needs of cardiac muscle controls blood flow through the coronary system. That is, as the vigor of cardiac contraction increases, so does the rate of coronary blood flow. Reduced heart activity, on the other hand, is accompanied by decreased coronary flow. This local regulation of coronary blood flow is similar to what occurs in many other body tissues, particularly the skeletal muscles.

The oxygen demand is a major factor in the regulation of local coronary blood flow. Blood flow in the coronary arteries is usually regulated almost exactly in proportion to the need for oxygen by the cardiac musculature. Normally, as the blood flows through the heart muscle, about 70% of the oxygen in the coronary arterial blood is removed. Because there isn't much oxygen left, only a small amount of extra oxygen can be delivered to the heart musculature unless coronary blood flow increases. Fortunately, the coronary blood flow increases almost in direct proportion to any additional metabolic consumption of oxygen by the heart. The exact mechanism by which increased oxygen consumption causes coronary dilation is unknown. Many researchers believe that when the oxygen concentration in the heart drops, vasodilator substances are released from the muscle cells and dilate the arterioles [3].

2.6. Ischemic heart disease

Ischemic heart disease, caused by insufficient coronary blood flow, is the leading cause of death in Western culture. This causes the death of approximately 35 % of people aged 65 and older in the United States. Some deaths occur suddenly as a result of an acute coronary occlusion or heart fibrillation, whereas others occur gradually over weeks to years as a result of progressive weakening of the heart pumping process.

Atherosclerosis is a frequent cause of diminished coronary blood flow. The atherosclerotic process is discussed in detail in Chapter 2.6.3. In short, people with a genetic predisposition to

atherosclerosis, who are overweight or obese and lead a sedentary lifestyle, or who have high blood pressure and endothelial cell damage in the coronary blood vessels, have large amounts of cholesterol deposited beneath the endothelium at many points in arteries throughout the body. These deposit areas are gradually invaded by fibrous tissue and frequently become calcified. As a result, atherosclerotic plaques form and protrude into vessel lumens, blocking or partially blocking blood flow. The first few centimeters of the major coronary arteries are a common site for the formation of atherosclerotic plaques.

2.6.1. Acute coronary syndrome

Acute coronary artery occlusion occurs most frequently in people with pre-existing atherosclerotic coronary heart disease, and only rarely in people with normal coronary circulation. Acute occlusion can result from any one of several effects, two of which are the following:

- The atherosclerotic plaque can cause a local blood clot called a thrombus that occludes the artery.
- Many clinicians believe that local muscular spasms of a coronary artery also can occur which may lead to secondary thrombosis of the vessel.

2.6.2. Collateral circulation in the heart

The degree of heart muscle damage caused by either slowly developing atherosclerotic constriction of the coronary arteries or by sudden coronary occlusion is determined in large part by the degree of collateral circulation that has already developed or that can open within minutes after the occlusion.

There are almost no large communications between the larger coronary arteries in a healthy heart. Many anastomoses do exist, however, among the smaller arteries ranging in diameter from 20 to 250 micrometers, as illustrated in Fig. 2-9.

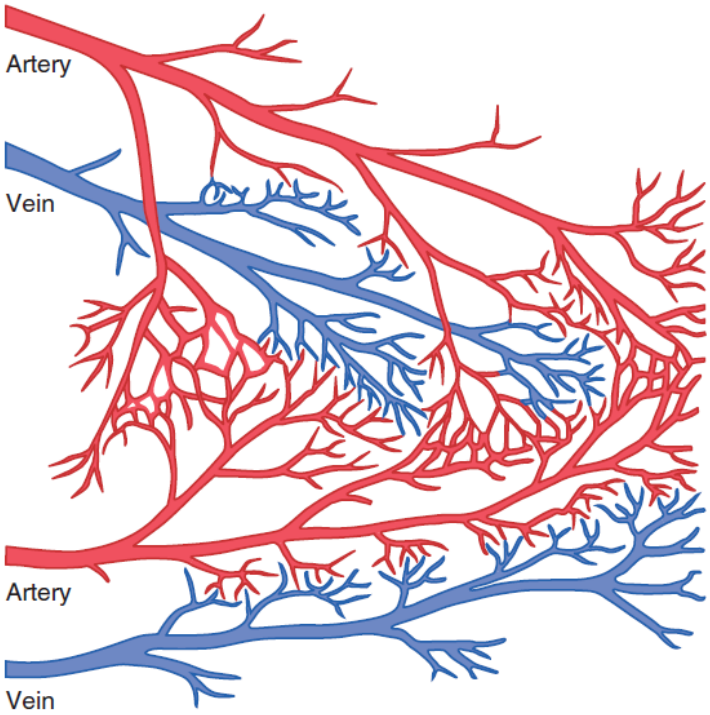

Figure 2-8. Minute anastomoses in the normal coronary arterial system [7]

When a sudden occlusion occurs in one of the larger coronary arteries, the small anastomoses dilate within seconds. However, blood flow through these minute collaterals is typically less than half of what is required to keep most of the cardiac muscle that they now supply alive. For the next 8 to 24 hours, the diameters of the collateral vessels do not increase significantly. However, collateral flow begins to increase, doubling by the second or third day and frequently returning to normal or nearly normal coronary flow within a month. Many patients recover almost completely from various degrees of coronary occlusion due to the development of collateral channels when the area of muscle involved is not too large.

When atherosclerosis constricts the coronary arteries gradually over time rather than suddenly, collateral vessels can form at the same time as the atherosclerosis becomes more and more severe. As a result, the individual may never experience an acute episode of cardiac dysfunction. Eventually, however, the sclerotic process progresses beyond the capacity of even the collateral blood supply to provide the required blood flow. Sometimes the collateral blood vessels themselves develop atherosclerosis. When this occurs, the heart muscle becomes severely limited in its work output, and the heart cannot pump even normally required amounts of blood flow. This is one of the leading causes of cardiac failure in the elderly.

2.6.3. Atherosclerosis

Atherosclerosis is a disease of the large and intermediate-sized arteries in which fatty lesions called atheromatous plaques develop on the inside surfaces of the arterial walls. Arteriosclerosis, in contrast, is a general term that refers to thickened and stiffened blood vessels of all sizes.

One abnormality that can be measured very early in blood vessels that later become atherosclerotic is damage to the vascular endothelium. This damage, in turn, increases the expression of adhesion molecules on endothelial cells and decreases their ability to release nitric oxide and other substances that help prevent the adhesion of macromolecules, platelets, and monocytes to the endothelium. After the damage to the vascular endothelium occurs, circulating monocytes and lipids (mostly LDLs) begin to accumulate at the site of injury (Fig. 2-9A). The monocytes cross the endothelium, enter the intima of the vessel wall, and differentiate to become macrophages, which then ingest and oxidize the accumulated lipoproteins, giving the macrophages a foamlike appearance. These macrophage foam cells then aggregate on the blood vessel and form a visible fatty streak.

With time, the fatty streaks grow larger and coalesce, and the surrounding fibrous and smooth muscle tissues proliferate to form larger and larger plaques (see Fig. 2-9B). Also, the macrophages release substances that cause inflammation and further proliferation of smooth muscle and fibrous tissue on the inside surfaces of the arterial wall. The lipid deposits plus the cellular proliferation can become so large that the plaque bulges into the lumen of the artery and greatly reduces blood flow, sometimes completely occluding the vessel. Even without occlusion, the fibroblasts of the plaque eventually deposit extensive amounts of dense connective tissue, and sclerosis becomes so great that the arteries become stiff. Later, calcium salts often precipitate with the cholesterol and other lipids of the plaques, leading to bony-hard calcifications that can make the arteries rigid tubes. Both of these later stages of the disease are called “hardening of the arteries.”

Atherosclerotic arteries lose most of their distensibility, and because of the degenerative areas in their walls, they are easily ruptured. Also, where the plaques protrude into the flowing blood, their rough surfaces can cause blood clots to develop, with resultant thrombus or embolus formation leading to a sudden blockage of all blood flow in the artery.

Almost half of all deaths in the United States and Europe are due to vascular disease. About two-thirds of these deaths are caused by thrombosis of one or more coronary arteries. The remaining one-third is caused by thrombosis or hemorrhage of vessels in other organs of the body, especially the brain (causing strokes), but also the kidneys, liver, gastrointestinal tract, limbs, and so forth.

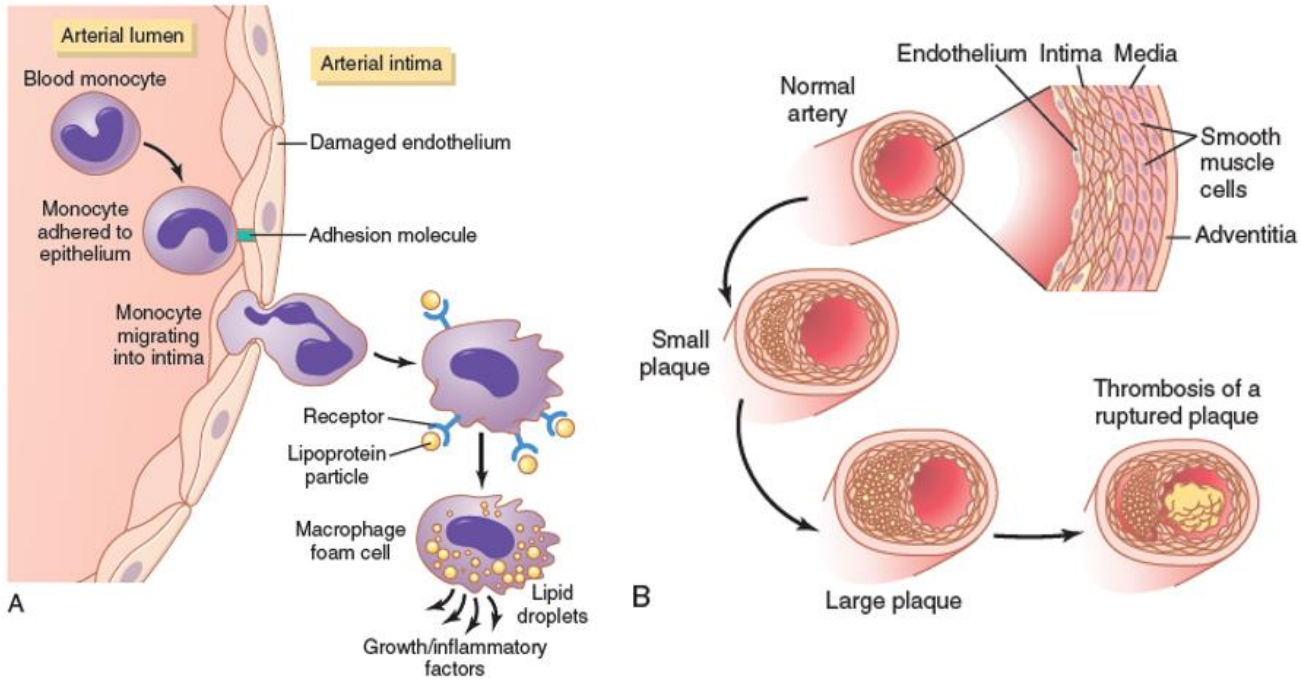

Figure 2-9. Development of atherosclerotic plaque [7]

2.6.4. Prevention of atherosclerosis

In some people with perfectly normal levels of cholesterol and lipoproteins, atherosclerosis still develops. Some of the factors that are known to predispose to atherosclerosis are:

- physical inactivity and obesity,
- diabetes mellitus,
- hypertension,
- hyperlipidemia,
- cigarette smoking.

The most important measures to protect against the development of atherosclerosis and its progression to serious vascular disease are:

- maintaining a healthy weight, being physically active, and eating a diet that contains mainly unsaturated fat with a low cholesterol content;
- preventing hypertension by maintaining a healthy diet and being physically active, or effectively controlling blood pressure with antihypertensive drugs if hypertension does develop;
- effectively controlling blood glucose with insulin treatment or other drugs if diabetes develops;
- avoiding cigarette smoking.

3. MATHEMATICAL MODEL

The Finite Volume Method (FVM) is a numerical technique that transforms the partial differential equations representing conservation laws over differential volumes into discrete algebraic equations over finite volumes (or elements or cells). In a similar fashion to the finite difference or finite element method, the first step in the solution process is the discretization of the geometric domain, which, in the FVM, is discretized into non-overlapping elements or finite volumes. The partial differential equations are then discretized into algebraic equations by integrating them over each discrete element. The system of algebraic equations is then solved to compute the values of the dependent variable for each of the elements.

In the finite volume method, some of the terms in the conservation equation are turned into face fluxes and evaluated at the finite volume faces. Because the flux entering a given volume is identical to that leaving the adjacent volume, the FVM is strictly conservative. This inherent conservation property of the FVM makes it the preferred method in Computational Fluid Dynamics (CFD). Another important attribute of the FVM is that it can be formulated in the physical space on unstructured polygonal meshes. Finally, in the FVM it is quite easy to implement a variety of boundary conditions in a non-invasive manner since the unknown variables are evaluated at the centroids of the volume elements, not at their boundary faces.

These characteristics have made the Finite Volume Method quite suitable for the numerical simulation of a variety of applications involving fluid flow and heat and mass transfer, and developments in the method have been closely entwined with advances in CFD. From a limited potential at inception confined to solving simple physics and geometry over structured grids, the FVM is now capable of dealing with all kinds of complex physics and applications [4].

3.1. The Semi-Discretized Equation

In the first step of the finite volume discretization process, the governing equations are integrated over the cells (or finite volumes) into which the domain has been subdivided, then the Gauss theorem is applied to transform the volume integrals of the convection and diffusion terms into surface integrals. Following this step, the surface and volume integrals are transformed into discrete ones and integrated numerically through the use of integration points (ip). The conservation equation for a general scalar variable can be expressed as:

$$\underbrace{\frac{\partial(\rho\phi)}{\partial t}}_{\text{transient term}} + \underbrace{\nabla\cdot(\rho\mathbf{v}\phi)}_{\text{convective term}} = \underbrace{\nabla\cdot\left(\Gamma^{\phi}\nabla\phi\right)}_{\text{diffusion term}} + \underbrace{Q^{\phi}}_{\text{source term}} . \tag{3.1}$$

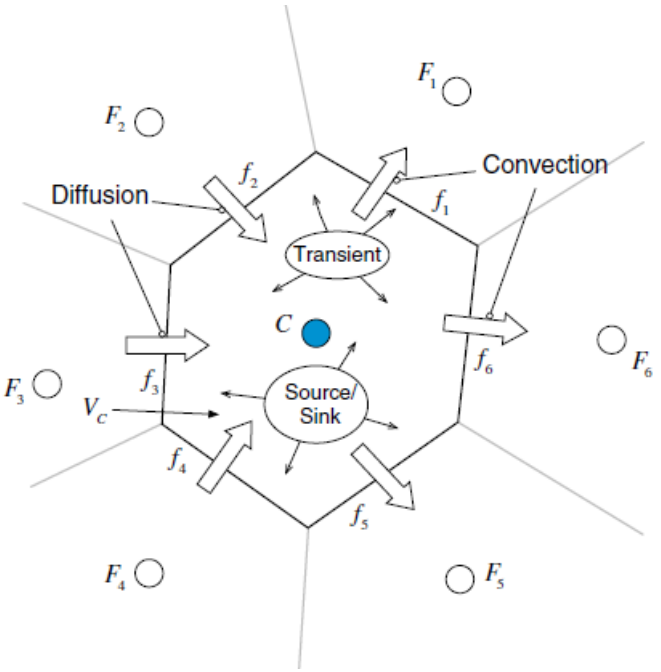

Figure 3-1. Conservation in a discrete element [8]

The temporal derivative in Eqn. (3.1) represents the inertia of the system. Inertia can be described as the potential of the system (CV) to accumulate the general property ϕ. The convection term can be presented as a coordinate transformation, on the amount of the property ϕ which is transported into and out of the system with the convective velocity **v**. The diffusion term represents the gradient transport of the property ϕ, in which Γ^{ϕ} is the diffusion coefficient. Source or sink terms define the local production or destruction of the general property ϕ [5].

3.2. Fluid governing equations

Eqn. (3.1) represents one of the fundamental equations in continuum mechanics. It describes how a scalar quantity is transported through space. When the general property ϕ is replaced with some other properties, other transport equations may be written. The fluid flow in this thesis is considered to be isothermal and laminar, while the fluid, that is blood, is assumed to be incompressible and Newtonian. The fluid flow is governed by the mass and the linear momentum conservation laws.

3.2.1. Continuity equation

The principle of conservation of mass indicates that in the absence of mass sources and sinks, a region will conserve its mass on a local level. Considering the material volume of fluid shown in Fig. 3-2 of mass m, density ρ, and velocity $\mathbf{v}$, conservation of mass in the material coordinate system can be written as:

$$\left(\frac{dm}{dt}\right)_{MV} = 0\,. \tag{3.2}$$

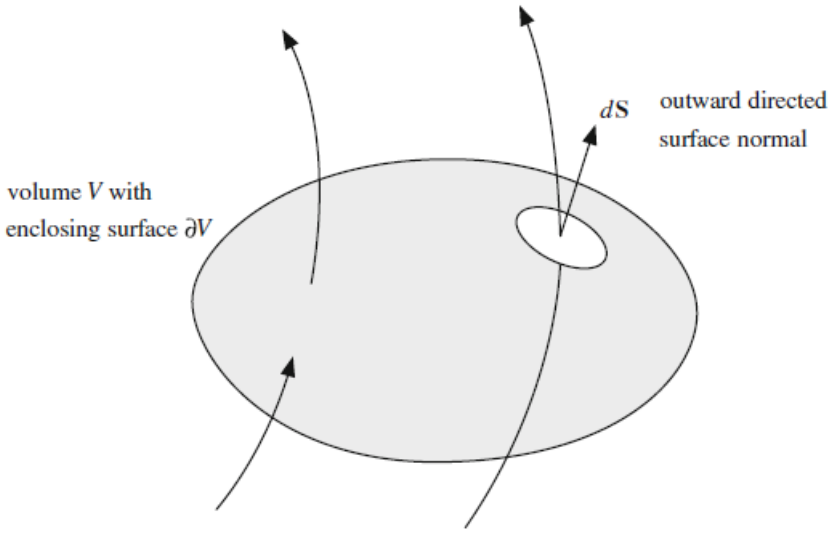

Figure 3-2. Conservation of mass for a material volume of a fluid of mass *m* [8]

The equivalent expression of mass conservation in an Eulerian coordinate system is:

$$\frac{\partial \rho}{\partial t} + \nabla \cdot (\rho \mathbf{v}) = 0\,. \tag{3.3}$$

In the case of incompressible flow, Eqn. (3.2) can be further simplified, as follows:

$$\nabla \cdot \mathbf{v} = 0\,. \tag{3.4}$$

3.2.2. Momentum equation

The principle of conservation of linear momentum states that a body retains its total momentum in the absence of any external force acting on it. Since momentum is a vector quantity, its components in any direction will also be conserved.

For the material volume of a substance, Newton's Second Law of motion asserts that the momentum of this specific volume can change only in the presence of a net force acting on it, which could include both surface forces and body forces. Therefore, by considering the material

volume of fluid shown in Fig. 3-3 of mass m, density ρ, and velocity $\mathbf{v}$, Newton's law in Lagrangian coordinates can be written as:

$$\left[\frac{d(m\mathbf{v})}{dt}\right]_{MV} = \left(\int_V \mathbf{f}\, dV\right)_{MV}, \tag{3.5}$$

where $\mathbf{f}$ is the external force per unit volume acting on the material volume.

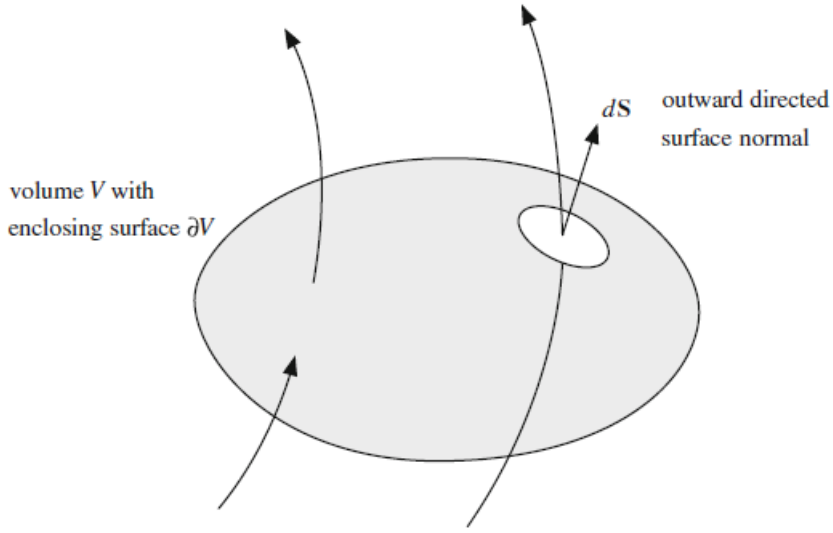

Figure 3-3. Conservation of linear momentum for a material volume of a fluid of mass *m* [8]

The equivalent expression of momentum conservation in an Eulerian coordinate system is:

$$\frac{\partial(\rho\mathbf{v})}{\partial t} + \nabla\cdot(\rho\mathbf{v}\mathbf{v}) = \underbrace{\mathbf{f}_b}_{\text{body forces}} + \underbrace{\nabla\cdot\boldsymbol{\sigma}}_{\text{surface forces}}. \tag{3.6}$$

In the case of incompressible flow, Eqn. (3.6) can be transformed into:

$$\underbrace{\frac{\partial\mathbf{v}}{\partial t}}_{\text{local rate of change}} + \underbrace{\nabla\cdot(\mathbf{v}\mathbf{v})}_{\text{convection}} = \underbrace{\nu\nabla^2\mathbf{v}}_{\text{diffusion}} - \underbrace{\frac{1}{\rho}\nabla p}_{\text{pressure gradient}} + \underbrace{\mathbf{f}_b}_{\text{body forces}}, \tag{3.7}$$

where $\mathbf{v}$ is the fluid velocity, ν is the fluid kinematic viscosity, p is the fluid pressure, and ρ is the fluid density. In Eqn. (3.7) Cauchy stress tensor is written as a sum of the pressure gradient ∇p and the viscous stress tensor which exist in the diffusion term. Velocity $\mathbf{v}$ in Eqn. (3.7) can be a transporting and a transported variable, thus making the convection term non-linear. The continuity equation (3.4) and the momentum equation (3.7) represent the Navier-Stokes equations for incompressible flow.

3.3. Solid governing equations

The deformation of the solid, assumed to be hyperelastic and incompressible, can be described by the linear momentum conservation law:

$$\rho \frac{\partial^2 \mathbf{u}}{\partial t^2} = \nabla \cdot \boldsymbol{\sigma} + \rho \mathbf{f}_b, \tag{3.8}$$

where $\boldsymbol{\sigma}$ is the Cauchy stress tensor, $\mathbf{f}_b$ represents the body force, ρ is the density of the element and $\mathbf{u}$ denotes the displacement vector.

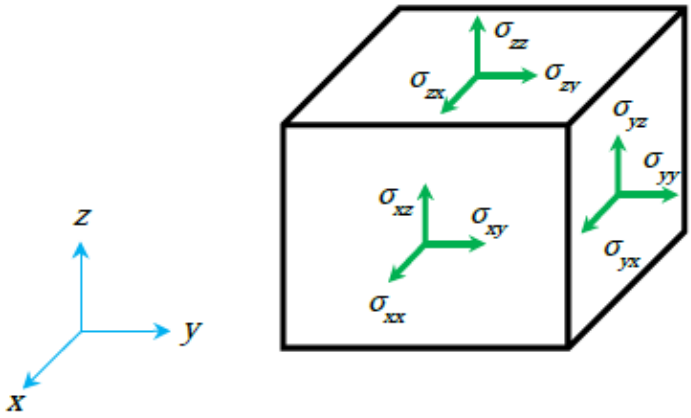

Figure 3-4. Stress components on infinitesimal solid element [4]

The Cauchy stress tensor $\boldsymbol{\sigma}$ can be expressed by the following equation:

$$\boldsymbol{\sigma} = -p\mathbf{I} + 2\frac{\partial W}{\partial I_1}\mathbf{b} - 2\frac{\partial W}{\partial I_2}\mathbf{b}^{-1}, \tag{3.9}$$

where $\mathbf{b} = \mathbf{F} \cdot \mathbf{F}^{\mathrm{T}}$ is the left Cauchy-Green tensor, $\mathbf{F} = \mathbf{I} + (\nabla \mathbf{u})^{\mathrm{T}}$ is the deformation gradient tensor, $\mathbf{I}$ is the second-order identity tensor and p is a scalar, which has to be determined. I_1 and I_2 represent deviatoric strain invariants, which are equal to $I_1 = \mathrm{tr}(\mathbf{F})$, $I_2 = \frac{1}{2}[(\mathrm{tr}\mathbf{F})^2 - \mathrm{tr}(\mathbf{F})^2]$ and due to incompressibility constraint, $I_3 = \det(\mathbf{F}) = 1$. Therefore, the two principal invariants I_1 and I_2 are the only independent deformation variables [6].

To account for finite strains, the neo-Hookean hyperelastic material model is used. The neo-Hookean strain energy density function is perhaps the simplest model for an incompressible isotropic rubber-like material. It is characterized by:

$$W = c_1(I_1 - 3), \tag{3.10}$$

where $c_1 = \mu_1/2$ and the shear modulus $\mu = \mu_1$, which is then transformed into:

$$W = \frac{\mu}{2}(I_1 - 3). \tag{3.11}$$

This strain-energy function involves a single parameter only and provides a mathematically simple and reliable constitutive model for the nonlinear deformation behavior of isotropic rubber-like materials. It relies on phenomenological considerations and includes typical effects known from nonlinear elasticity within the small strain domain.

Taking Eqns. (3.9) and (3.11) into account, the Cauchy stress tensor $\boldsymbol{\sigma}$ may be expressed as:

$$\boldsymbol{\sigma} = -p\mathbf{I} + \mu\mathbf{b} \tag{3.12}$$

3.4. FSI coupling methods

Three different coupling procedures can be used to solve fluid-structure interaction (FSI) problems:

a) separate analysis method, or hybrid method,
b) single analysis method,
c) single fluid-structure domain.

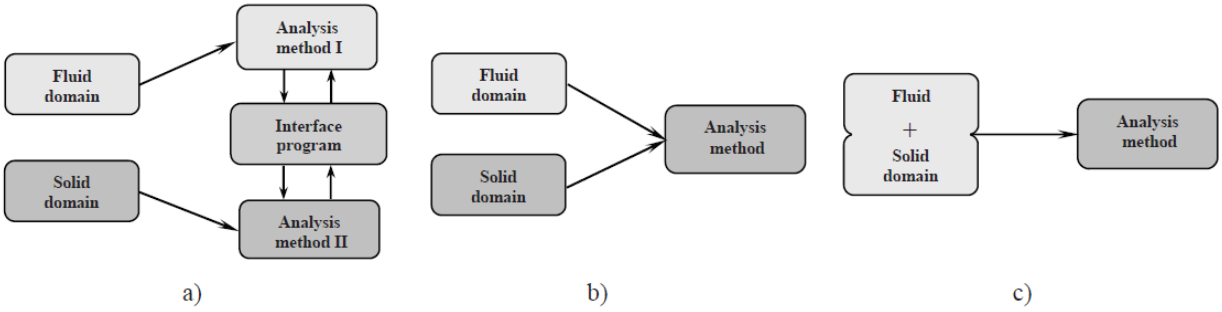

Figure 3-5. Fluid-structure coupling procedures [10]

The first two are partitioned methods, which solve the solid and fluid domains separately using their respective mesh discretization and numerical method. The coupling is accomplished by passing information across the fluid-solid interface. The difference between the two approaches is in the method used to discretize the separate domains. In the former, two different methods are used (e.g. Finite Element (FE) for the solid domain and Finite Volume (FV) for the fluid domain), whereas in the latter the same method is used for both domains (e.g. FE or FV). The third method, known as the monolithic approach, solves the coupled problem as one entity using a single numerical procedure. Both partitioned and monolithic approaches have advantages and disadvantages, and the choice may depend on the FSI problem [7].

Currently, only the partitioned approach is implemented in OpenFOAM FSI solver *solids4foam*. The solver is based on the cell-centered finite volume discretization method for both domains and the strongly coupled partitioned solution procedure (Fig 3-5.b).

3.4.1. Conditions at the fluid-solid interface

The fluid and solid models are coupled by kinematic and dynamic conditions which must be satisfied at the fluid-solid interface. The kinematic condition states that the velocity and displacement must be continuous across the interface:

$$\mathbf{v}_{F,i} = \mathbf{v}_{S,i}, \tag{3.13}$$

$$\mathbf{u}_{F,i} = \mathbf{u}_{S,i} \tag{3.14}$$

where subscripts F and S represent the quantities corresponding to the fluid and solid regions of the model, respectively, and subscript i represents the quantities at the fluid-solid interface.

The dynamic condition follows from the linear momentum conservation law and states that forces are in equilibrium at the interface:

$$\mathbf{n}_i \cdot \boldsymbol{\sigma}_{F,i} = \mathbf{n}_i \cdot \boldsymbol{\sigma}_{S,i} \tag{3.15}$$

where $\mathbf{n}_i$ is the unit normal vector at the interface.

In the partitioned computational approach, force (traction) is usually calculated at the fluid side of the interface and applied as a boundary condition on the solid side of the interface. The traction is calculated by using the fluid stress tensor consisting of the isotropic and viscous components. The viscous (deviatoric) component, defined by Newton's law of viscosity, is:

$$\boldsymbol{\tau} = \mu \left[\nabla \mathbf{v} + (\nabla \mathbf{v})^{\mathrm{T}}\right] \tag{3.16}$$

where $\mu = \rho\nu$ is fluid dynamic viscosity. The stress tensor for an incompressible Newtonian fluid reads as follows:

$$\boldsymbol{\sigma}_{F,i} = -p\mathbf{I} + \boldsymbol{\tau} = -p\mathbf{I} + \mu \left[\nabla \mathbf{v} + (\nabla \mathbf{v})^{\mathrm{T}}\right] \tag{3.17}$$

and the traction at the interface reads:

$$\mathbf{t}_{F,i} = \mathbf{n}_i \cdot \boldsymbol{\sigma}_{F,i} = -p\mathbf{n}_i + \mu \mathbf{n}_i \cdot \nabla \mathbf{v}_t - 2\mu(\nabla_s \cdot \mathbf{v})\mathbf{n}_i + \mu \nabla_s \mathbf{v}_n, \tag{3.18}$$

where $\mathbf{v}_t = (\mathbf{I} - \mathbf{nn}) \cdot \mathbf{v}$ is the tangential velocity component, $\nabla_s = \nabla - \mathbf{nn} \cdot \nabla$ is the surface tangential gradient operator and $\mathbf{v}_n = \mathbf{n} \cdot \mathbf{v}$ is the normal velocity component. The third and the fourth term on the right-hand side of equation (3.17) can usually be omitted. Otherwise, these terms can be calculated directly at the solid side of the interface taking that the kinematic condition is valid.

3.4.2. Solution procedure for fluid-structure interaction

As mentioned earlier, the partitioned approach is adopted for the fluid-structure interaction solution procedure, where the flow model and the structural model are solved separately using different solvers in the FV framework. The coupled fluid-structure interaction problem is decomposed using the Dirichlet-Neumann procedure, where the flow model is solved for a given velocity (or displacement) of the fluid-structure interface, while the structural model is solved for a given force exerted on the interface.

The equilibrium of the force and velocity (or displacement) on the fluid-structure interface is enforced in each time step using a strongly coupled procedure by performing iterations between the fluid and solid solvers. To that end, the Gauss-Seidel iteration scheme with fixed relaxation or convergence acceleration using Aitken (dynamic) relaxation and the interface quasi-Newton procedure, with the approximation for the inverse of the Jacobian from a least-squares model (IQN-ILS) are available. The Aitken relaxation procedure and the IQN-ILS procedure are preceded by two fixed-relaxation iterations.

The fluid-structure interaction solution procedure is summarized in the following algorithm:

1: Switch to the next time step.
2: Predict interface displacement and calculate initial interface residual.
3: Start the FSI strongly coupled iterative procedure.
4: Switch to the next iteration.
5: Calculate the vertex-displacements of the fluid side of the interface.
6: Solve mesh motion equation.
7: Move the fluid mesh.
8: Solve the fluid model.
9: Transfer the face-center forces from the fluid to the solid side of the interface.
10: Solve the structural model.
11: Transfer the vertex-displacements from the solid to the fluid side of the interface.
12: Calculate interface residual at the fluid side of the interface.
13: if converged then
14: Go to the next time step (line 1)
15: else
16: Go to the next iteration (line 4)
17: end if

3.4.3. Interpolation at the fluid-structure interface

Traction (pressure and viscous forces) calculated at the boundary faces of the fluid side of the interface must be transferred to the boundary faces of the solid side of the interface; it is applied as the boundary condition for the solid model. In general, meshes at the solid and fluid side of the interface are not conformal and an interpolation procedure between the models is required. To this end, two different interpolation techniques are used:

1. *face-interpolation procedure* for the interpolation from the boundary cell faces of the fluid side of the interface to the boundary cell faces of the solid side of the interface,
2. *vertex-interpolation procedure* for the interpolation of the vertex-displacement field from the solid side of the interface to the vertices of the fluid side of the interface.

To map fields (e.g. traction, velocity, displacement) between the fluid and solid interfaces the General Grid Interface (GGI) class is used. [8]

4. THE CORONARY ARTERY MODEL DEVELOPMENT

This chapter will describe the entire parameters necessary for the numerical simulation, including the mesh, time step discretization, boundary, and numerical setup. The first part will focus on the CFD simulation, which was done to acquire boundary conditions at the outlet of coronary arteries. Even though the pressure waveform is relatively the same, the coronary flow waveform differs significantly from the aortic flow. This phenomenon makes the coronary flow model more complex and more difficult to simulate, which will be discussed later in the chapter. The second part will focus on the FSI setup and how the CFD results were implemented.

4.1. Geometry

The responsibility of coronary arteries is to supply oxygen-rich blood to the heart. There are two main coronary arteries arising from the aortic root, namely the left main (LM) and the right coronary artery (RCA), where the LM typically divides into two branches, the left anterior descending (LAD) and the left circumflex (LCx), although occasionally it trifurcates into the LAD, LCx and ramus intermedius (RI) arteries as seen in Fig. 4-1. The LAD is responsible for delivering blood to the anterior wall and apex of the left ventricle, the heart's main pumping chamber. Coronary circulation was thoroughly explained in Chapter 2.

The computerized tomography (CT) scans from which the geometry was extracted were provided by the AZ Delta hospital in Belgium. The CT scan data is in DICOM format, and it consists of a large number of 2D images, each representing a slice of the geometry. 3D models were obtained by volume rendering of CT scans and subsequent editing. A detailed description of the geometry extraction is given in [9]. The extracted geometry is shown in Fig. 4-1 and Fig. 4-2:

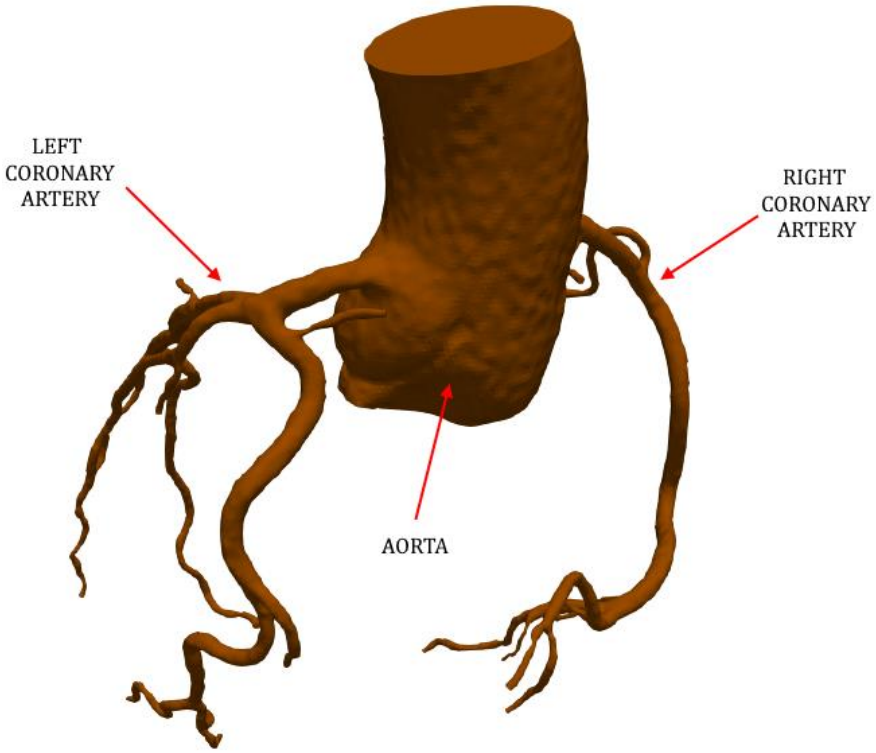

Figure 4-1. The patient-specific coronary arteries

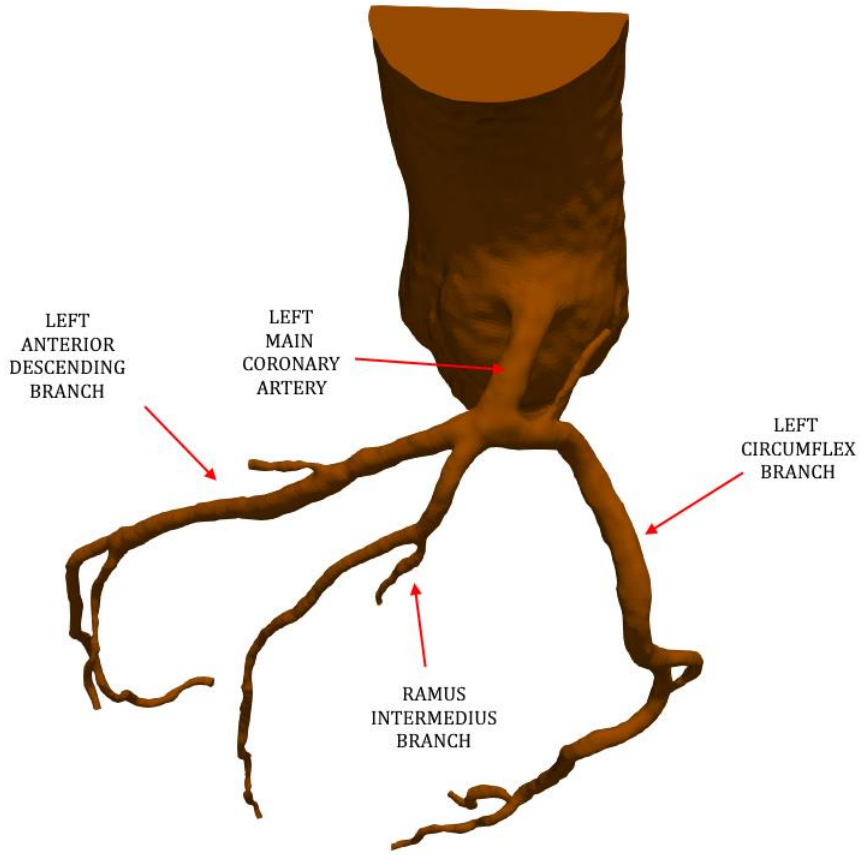

Figure 4-2. The left coronary artery trifurcation

4.1.1. The simplified geometry model

The simplified geometry was modeled in SolidWorks 2020 SP3. The diameters and lengths of coronary arteries were measured in ParaView and averaged values were obtained for modeling. The model consists of aortic inlet, LM, LCx, LAD, and RI coronary arteries. Geometry was made including the aortic inlet due to the known pressure waveform in the aortic root during the heart cycle. The CFD simulation was conducted on a simplified geometry of a healthy artery to obtain the downstream conditions, whereas the FSI simulations were performed on a diseased geometry affected by the atherosclerosis.

4.2. CFD numerical model

4.2.1. Introduction

As previously stated, the coronary and the aortic flow are significantly different. This is explained by the fact that the coronary arteries are located in the muscular wall of the heart, so when the heart is in the contracting, the coronary arteries constrict and their resistance to blood flow is high, whereas in the diastole phase, when the heart muscle is relaxed, the flow increases. There is a paradox, at high pressure in the aortic root (during cardiac contraction) the coronary flow is small, and during cardiac relaxation, coronary flow increases. This means that the resistance of the coronary arteries changes during the heartbeat (and their diameter may also change significantly), which is not the case in systemic arteries, where we can expect constant peripheral resistance. As a result, the flow model in coronary arteries is more complex than that in systemic arteries.

This thesis focuses on the left coronary artery due to the known experimental data for the LCA. Another reason is that the myocardial infarction most often affects the left ventricle, whose energy and oxygen needs are higher. Less commonly, however, it can also affect the right ventricle or atria, usually the right [10]. The following figure describes the differences in cardiac circulation between the left and right coronary artery, which is explained in [11]:

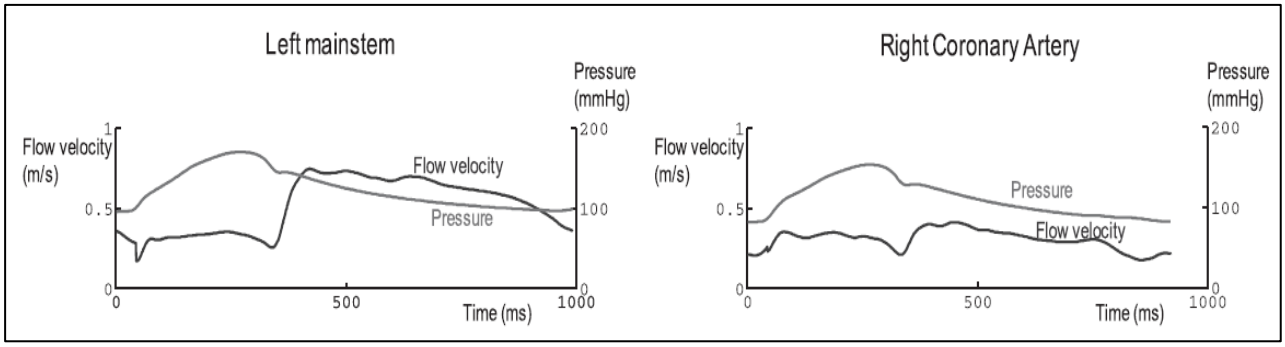

Figure 4-3. Representative simultaneous pressure and flow waveforms in the left main stem and proximal right coronary artery [15]

The following figure shows the measured pressure and volume flow waveform through the aortic valve for three subjects of different ages:

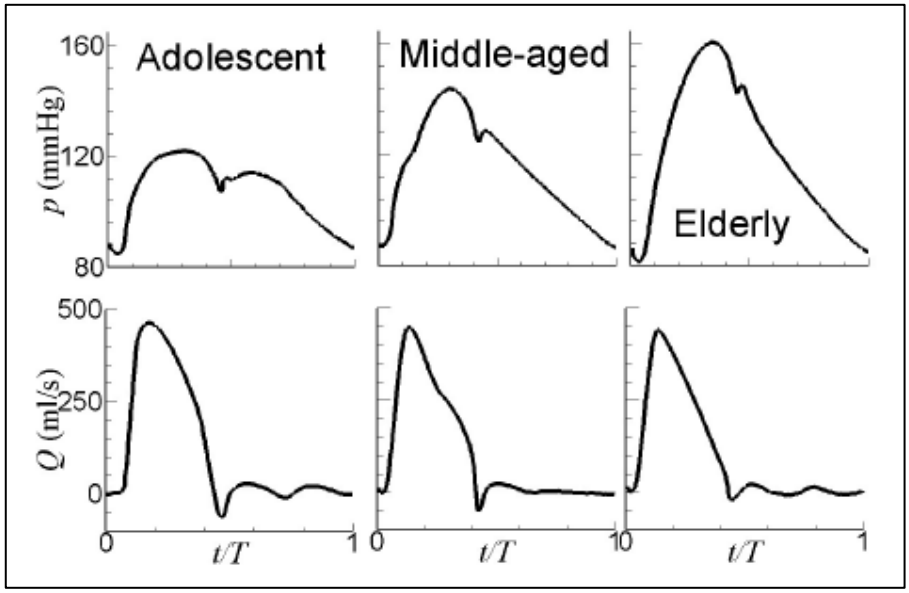

Figure 4-4. The measured pressure and flow waveform in the aortic valve for adolescents, middle-aged, and elderly during a heartbeat [16]

It can be seen from the figure that maximal flow and diastolic pressure remain more or less unchanged with age, while systolic pressure increases with age. This increase is due to changes in the arterial walls, in which due to the deterioration of elastin, the walls become stiffer, and for the same change in volume, the increase in pressure in the aorta is greater [12].

Fig. 4-5 shows the measured flow waveform through the left coronary artery for three subjects of different ages:

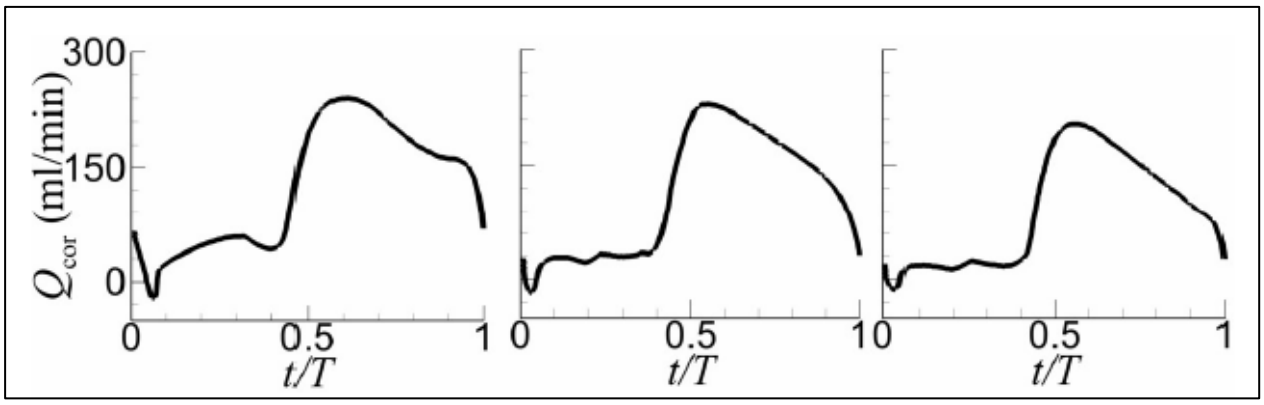

Figure 4-5. Blood flow waveform in the LCA for adolescents, middle-aged, and elderly during a heartbeat [16]

4.2.2. Geometry

The simplified CFD geometry model of a healthy artery was designed in SolidWorks. The model is shown in Fig 4-6:

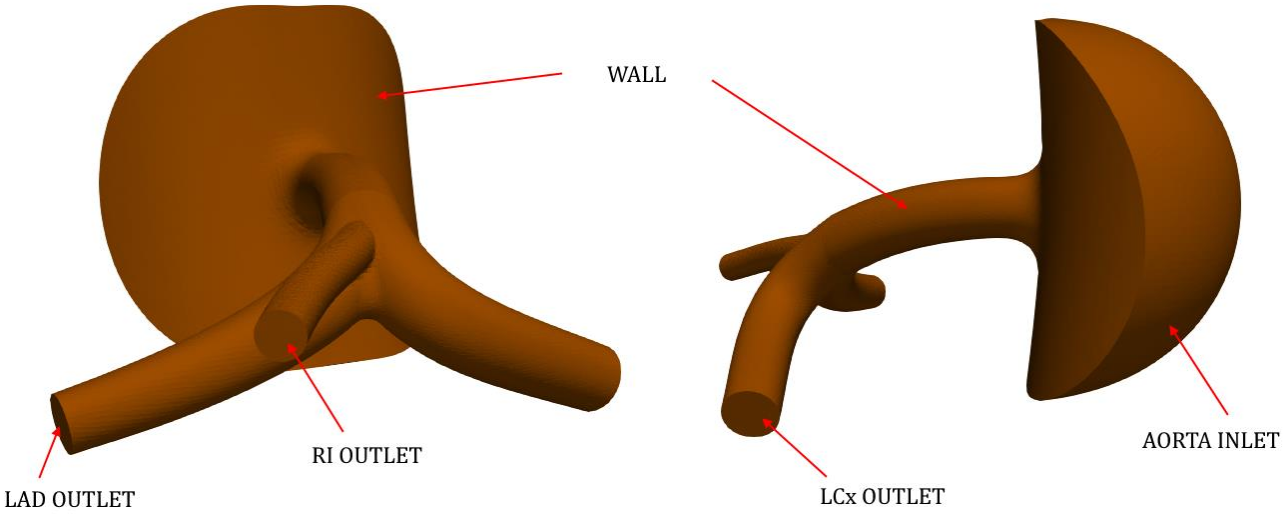

Figure 4-6. The left coronary artery geometry model

4.2.3. Mesh

The computational mesh used in this work was made by an open-source cross-platform library for automatic mesh generation that is built on top of OpenFOAM called cfMesh®. It is licensed under GPL (General Public License), and compatible with all recent versions of OpenFOAM.
cfMesh supports a variety of 3D and 2D workflows built by using components from the main library that are extensible and can be combined to create a variety of meshing workflows. The core library utilizes mesh modifier concept, which enables efficient parallelization using both shared-memory parallelization (SMP) and distributed memory parallelization (MPI). [13].

Meshing workflows implemented in cfMesh require input geometry in a form of surface triangulation such as STL (Stereo Lithography) files. STL files are then converted into FMS (File Management System) files because they can store patch information. The volume mesh was created by typing the *cartesianMesh* command in a shell window, which generates 3D meshes consisting of predominantly hexahedral cells with polyhedra in the transition regions between the cells of different sizes. The *checkMesh* command performs basic topology and geometric checks on the input mesh and evaluates mesh statistics and quality parameters.
The computational mesh consists of 133,998 mostly hexahedral cells. The mesh quality satisfied quality indicator (negative cells, skewness and orthogonality) thresholds. It is shown in the following figures:

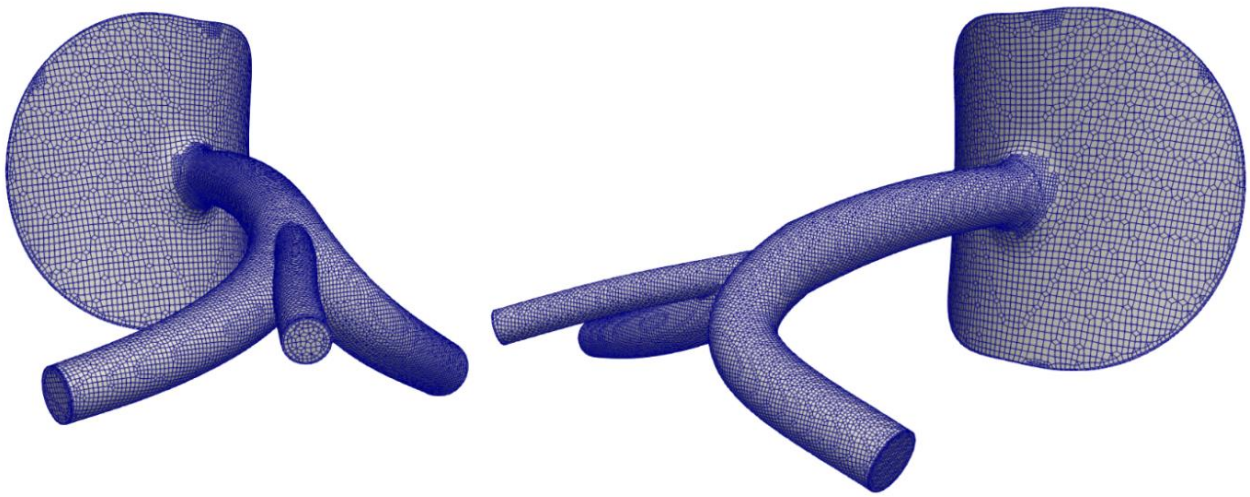

Figure 4-7. Surface mesh of a simplified healthy coronary artery

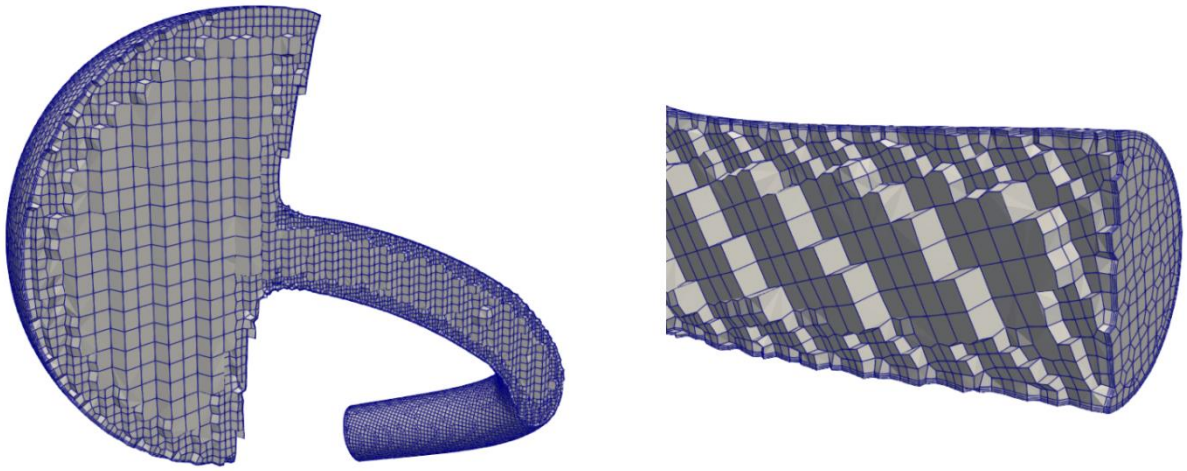

Figure 4-8. Volume mesh of a simplified healthy coronary artery

4.2.4. Boundary conditions

Each boundary condition has a physical meaning described mathematically via an equation, which in the context of a numerical method has to be translated into an algebraic relation. The geometry consists of six patches, whose boundary conditions are given in Table 4-1. As already mentioned, the fluid flow is considered to be isothermal and laminar, while the blood is assumed as incompressible and Newtonian. Therefore, it is only necessary to define boundary conditions of the velocity U and pressure p.

Table 4-1: Boundary conditions

Patch	**Boundary condition**	
	U	p
aorta_in	newFlowRateInletVelocity	zeroGradient
lad_out	zeroGradient	flowRateOutletPressure
ri_out	zeroGradient	flowRateOutletPressure
lcx_out	zeroGradient	flowRateOutletPressure
wall	noSlip	zeroGradient

The boundary condition *newFlowRateInletVelocity* is a velocity inlet boundary condition either correcting the extrapolated velocity or creating a uniform velocity field normal to the patch adjusted to match the specified flow rate [14]. The experimental volume flow data is written in a text file and is set to the inlet boundary. Thus, the velocity boundary condition is defined by the volume flow rate. The *new* part indicates that the flow rate can be scaled with the desired factor. In the case of a different time step of the numerical simulation and the data from the text file, the intermediate values are linearly interpolated.

The boundary condition *flowRateOutletPressure* is a pressure outlet boundary condition, which corrects the extrapolated pressure to match the specified flow rate. The flow rates in this simulation are distributed according to the face surface ratios of the outlets.

zeroGradient boundary condition extrapolates the values from the domain to patches, whereas *noSlip* indicates that there is no relative velocity between the fluid and the wall, i.e., it fixes the velocity to zero at walls.

The coronary volume flow rate waveform at the inlet is plotted and shown in Fig. 4-9:

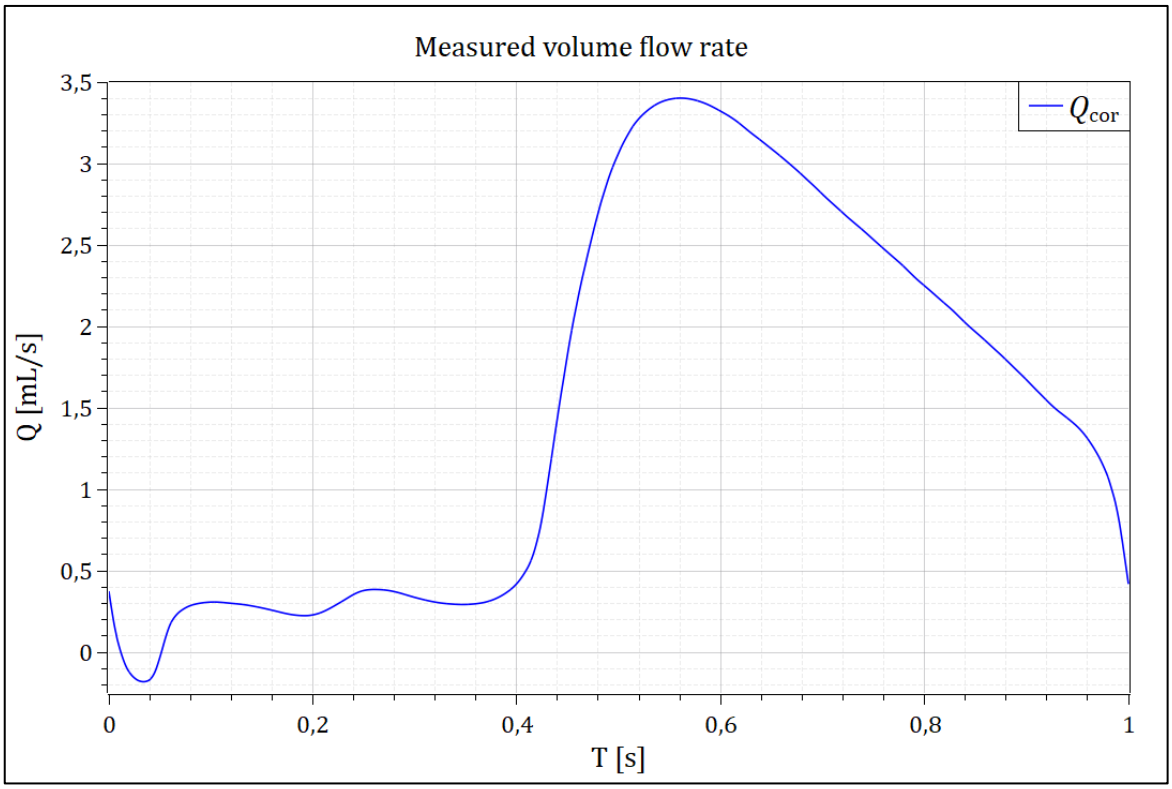

Figure 4-9. Coronary flow rate waveform during a heartbeat

The reference pressure cell is chosen at the center of the aorta inlet, as the experimental data is known for pressure distribution in the aortic valve during a heartbeat.

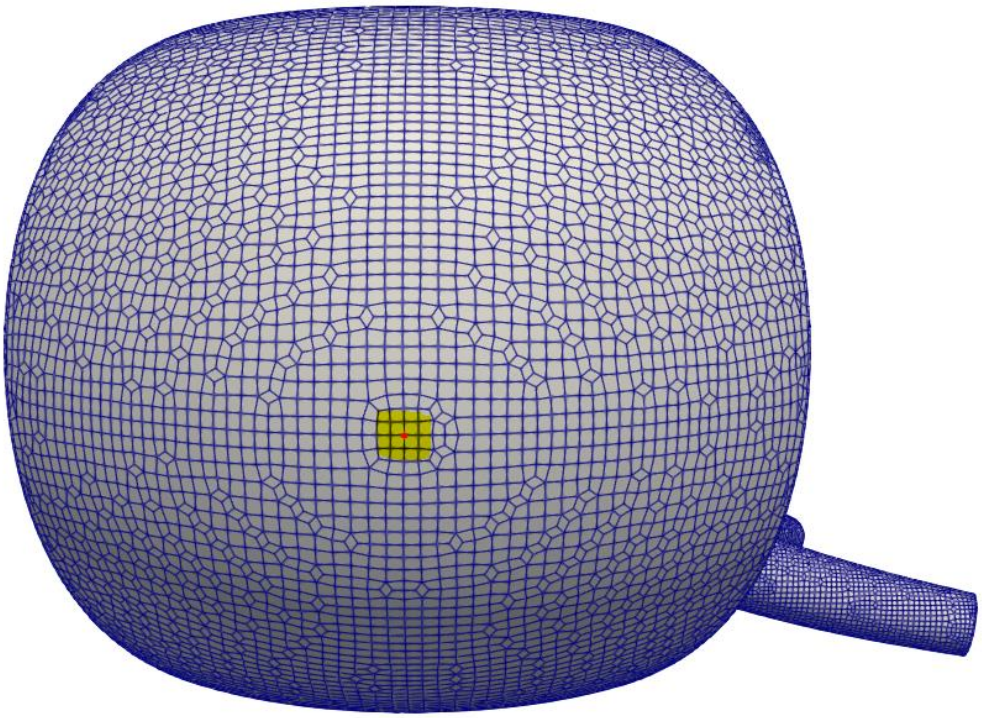

Figure 4-10. Reference pressure cell

The pressure profile in aortic valve is given in Fig. 4-11:

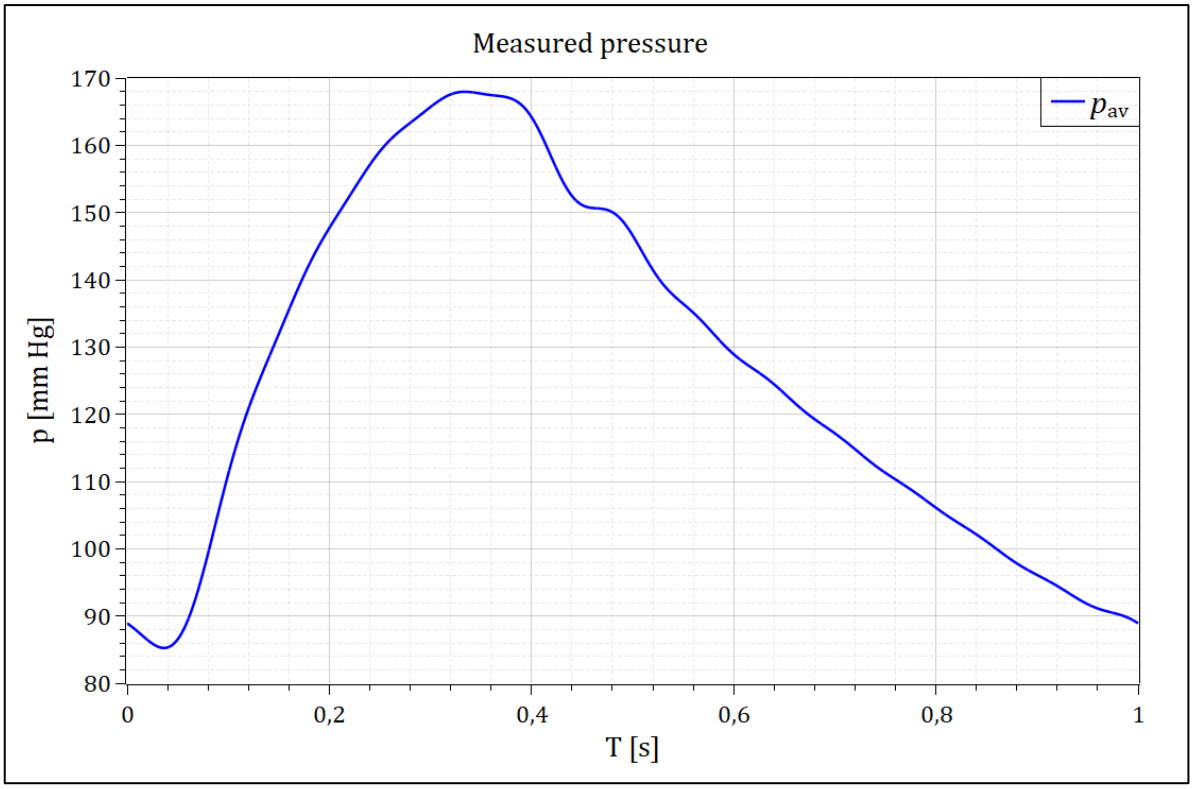

Figure 4-11. Pressure profile in the aortic valve during a heartbeat

The combination of these two boundary conditions represent the most realistic hemodynamic conditions in coronary artery circulation.

The following figure represents an overview of the arterial tree circulation based on experimental data, with each physical property having its own unit of measurement to improve the visibility of each curve. Q_{av} represents aortic valve flow rate, p_{av} is aortic valve pressure and Q_{cor} is coronary flow rate.

The flow phase difference in clearly visible. In this thesis, the pressure profile from the aortic root was used as a pressure in the reference cell. The use of the aortic pressure profile at the inlet is justified because of the similar pressure profiles in these two vessels, as shown in Fig 4-3. These assumptions were necessary due to the unknown experimental pressure data in coronary arteries.

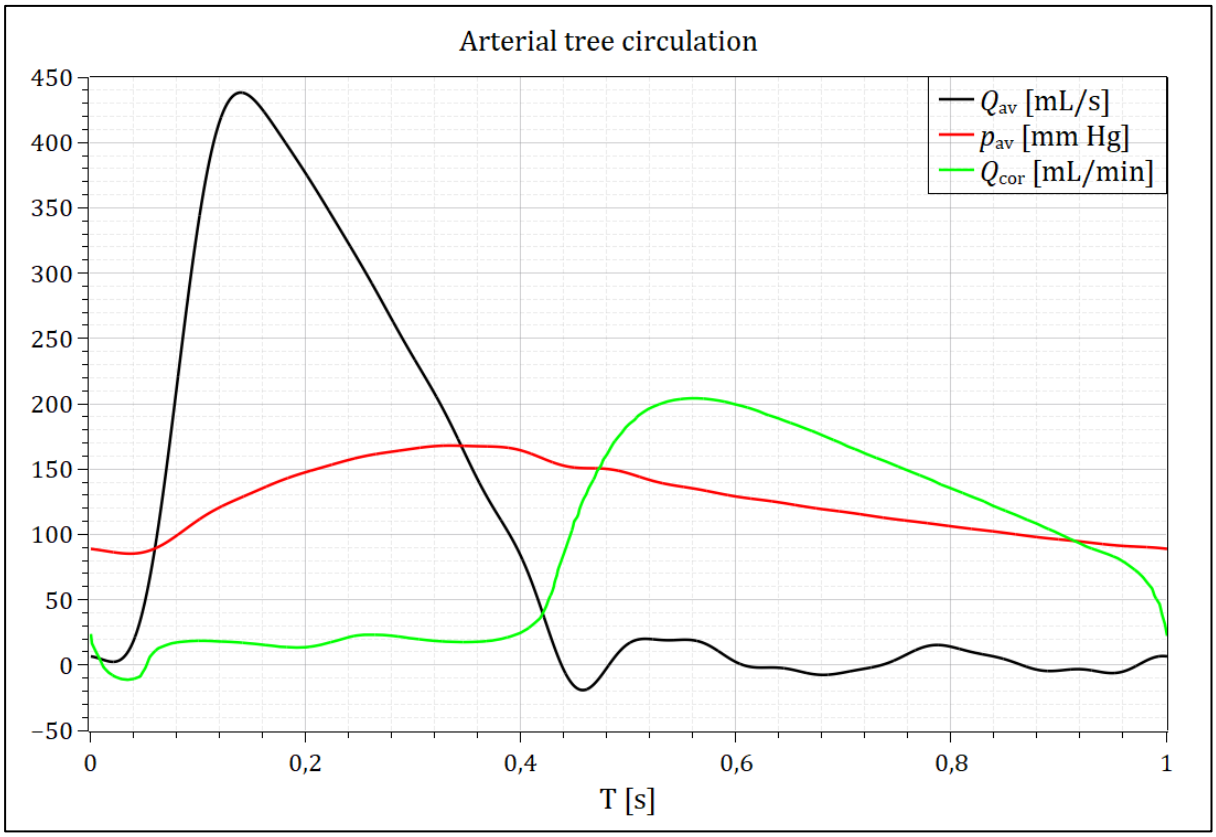

Figure 4-12. Arterial tree circulation

4.2.5. Solver control

Calculations were performed using the *pimpleFoam* numerical solver for incompressible transient flows. The PIMPLE algorithm is a combination of the PISO (Pressure Implicit with Splitting of Operator) and SIMPLE (Semi-Implicit Method for Pressure-Linked Equations) algorithms. The SIMPLE algorithm is used for stationary, while PISO is used for transient flows. The PIMPLE algorithm can be thought of as SIMPLE for each time step. For this reason, better stability over PISO is achieved, especially when it comes to large time steps in which the maximum Courant number can be continuously above 1 or when the nature of the solution is inherently unstable. The PIMPLE algorithm provides the pressure and velocity coupling, while the GAMG (Geometric Agglomerated Algebraic Multigrid Solver) solver performs pressure correction.

The CFD model is discretized in space using the second-order accurate cell-centered finite volume method and temporal discretization is performed using the second-order accurate implicit scheme. The under-relaxation factors λ_ϕ are used to promote convergence and stabilize the iterative solution process, whilst slowing down the changes in physical property ϕ between iterations. The

under-relaxation factors vary between 0 and 1. A value close to 1 implies little under relaxation, while a value close to 0 produces heavy under relaxation effects with very small changes in ϕ from iteration to iteration. The optimum under relaxation factor is problem dependent and is not governed by any general rule. The factors affecting λ_ϕ values include the type of problem solved, the size of the system of equation, the grid spacing and its expansion rate, and the adopted iterative method, among others. Usually, values of λ_ϕ are assigned based on experience or from preliminary calculations. The under-relaxation factors used in this simulation are $\lambda_U = 0.95$ and $\lambda_p = 0.9$, which proved to be stable. The solution converged when the pressure residual decreased under the 10^{-5} and the momentum residual under the 10^{-7}.

4.2.6. Results

The main feature of blood flow in the cardiovascular system is its pulsating and periodic nature, which means that the flow will be repeated from cycle to cycle for the same boundary conditions. To achieve periodic flow, it is necessary to perform the simulation sufficiently long until the influence of the initial conditions disappears. Even though the periodic nature was achieved in the first cycle, the results will be displayed for the last two cycles.

The goal of this simulation is to obtain a pressure waveform at the outlets during a heartbeat, which will be used as the boundary condition in the FSI simulation later on. This assumption is based on the development of collateral circulation, which occurs when atherosclerotic plaque gradually constricts the artery over time. Collateral flow represents the unchanged downstream conditions, whereas the upstream flow changes due to plaque growth.

Fig. 4-13 shows the volume flow rate waveform, which is based on the face surface ratios of the outlets i.e., it is based on the geometry of the vessels. This means that the velocity and pressure field at the outlets should have similar values. The small variations in values are due to the length differences of each branch and viscous flow, but as seen in Fig. 4-14 and Fig. 4-15, they are negligible. Approximately 52 % of the volume flow branches into the LAD outlet, 18 % into the RI outlet, and 30 % into the LCx outlet.

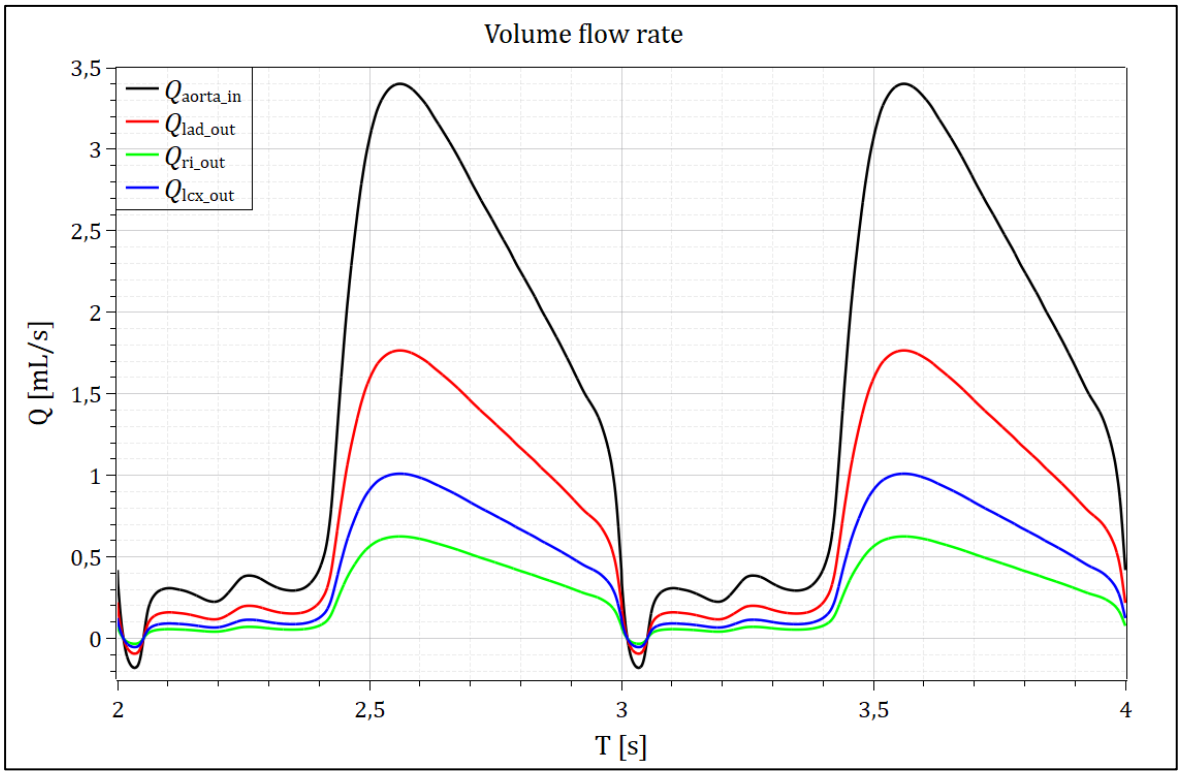

Figure 4-13. Volume flow rate waveform at the inlet and outlets

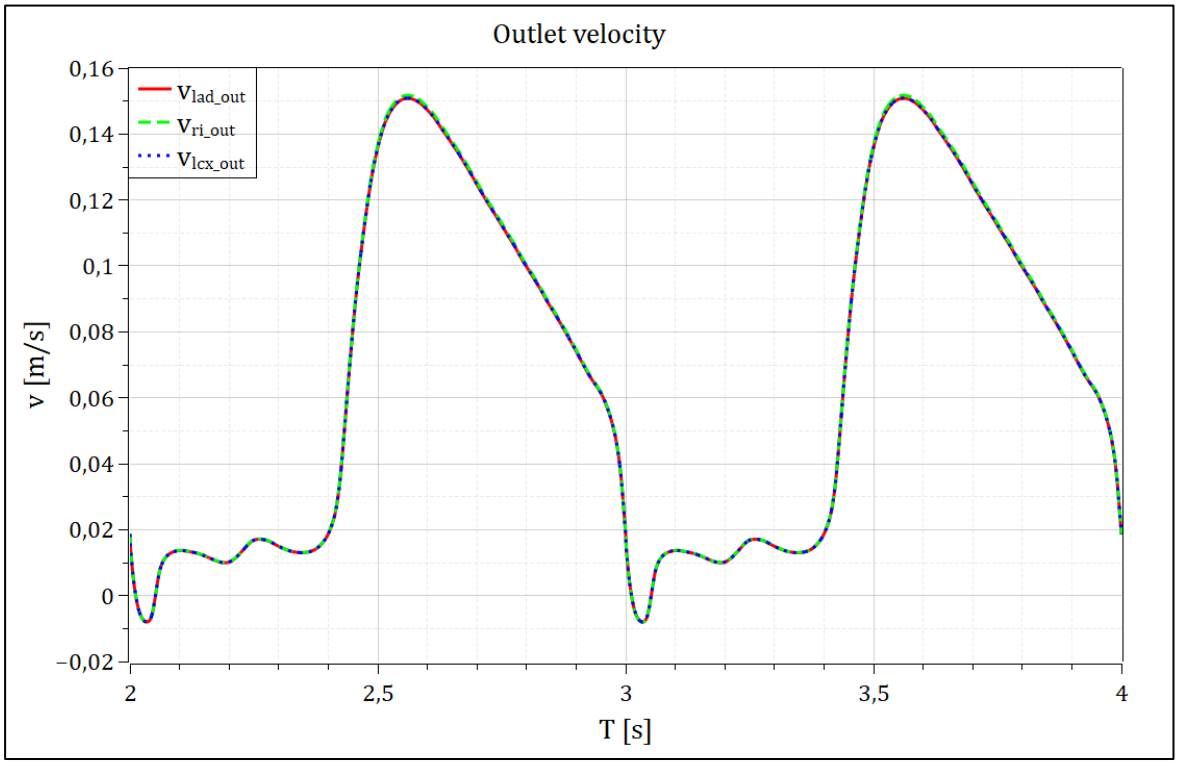

Figure 4-14. Outlet average velocity waveform

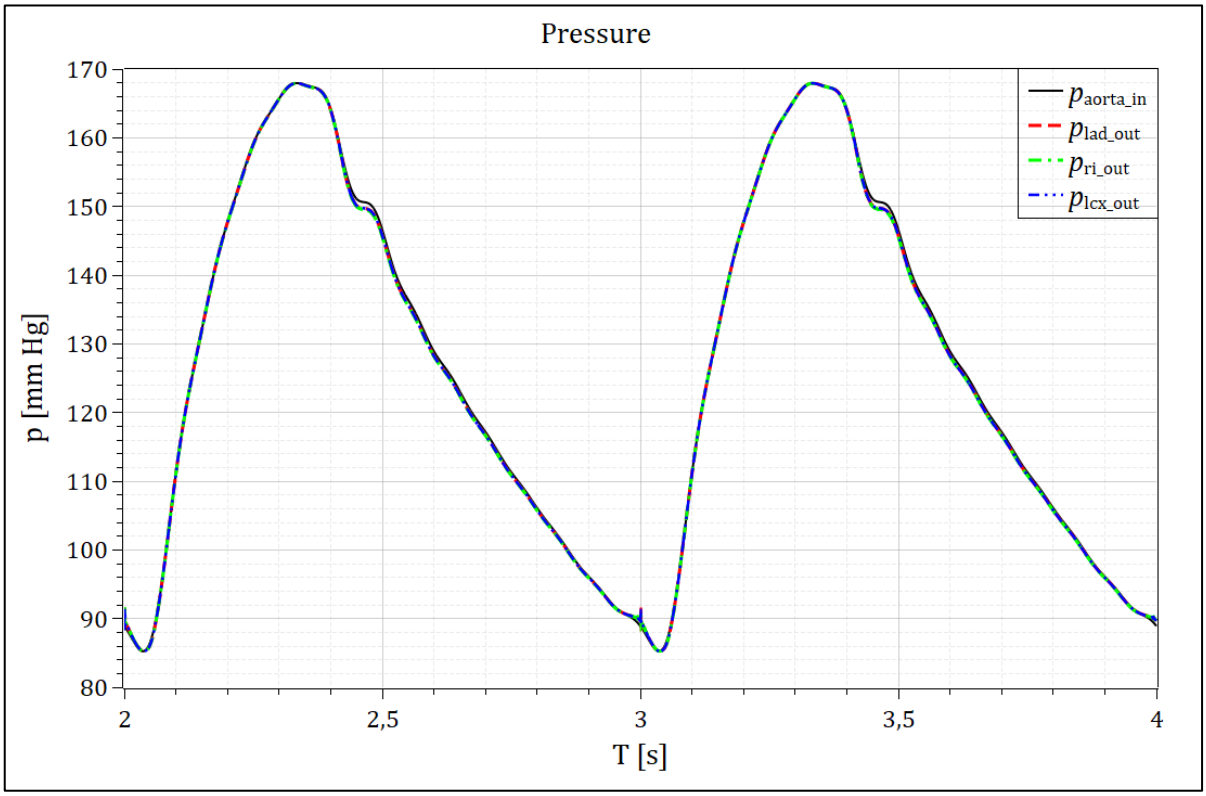

Figure 4-15. The pressure waveform at the inlet and outlets

4.3. FSI numerical model

This part of the chapter will mostly focus on the setup of the solid body and the fluid-solid interaction, as the fluid part was explained in the previous chapter. All existing differences between the fluid model used in CFD simulations and the fluid model used in FSI simulations will be emphasized.

4.3.1. Geometry

Two comparative geometry models were created to analyze the effect of different stenosis on the atherosclerotic artery. The first model was made with the 30 % stenosis, whereas the second with the 50 % stenosis. Plaque shoulder length is proportional to the plaque height. Geometry models are shown in the following figures:

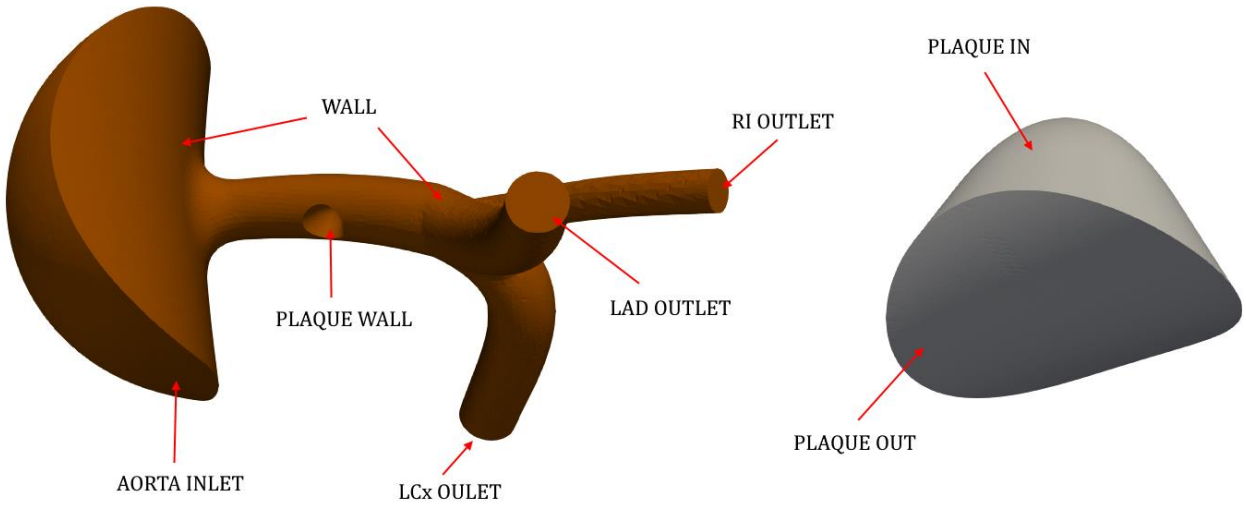

Figure 4-16. Geometry boundaries in FSI simulations showing fluid domain (brown) and solid domain (gray)

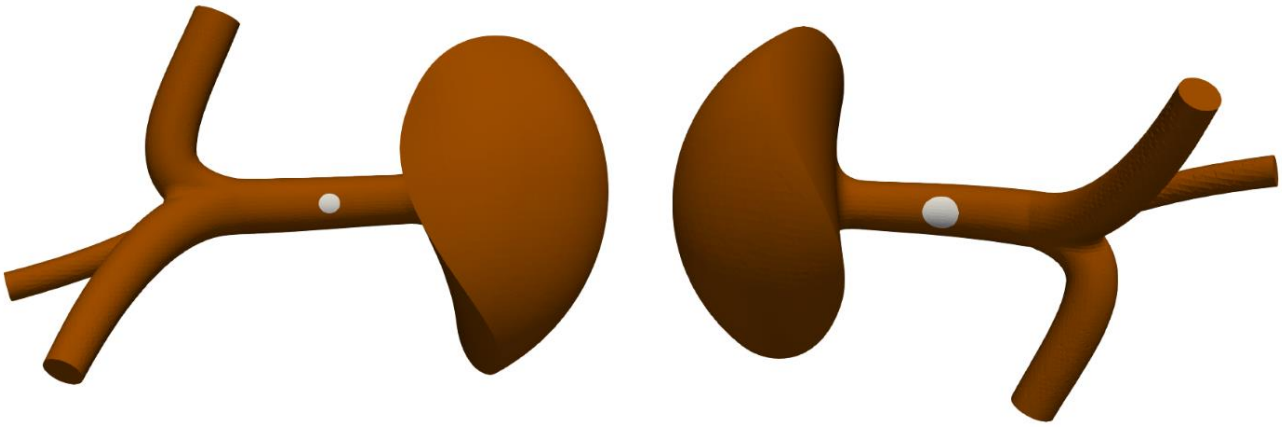

Figure 4-17. Geometry with 30 % stenosis (left) and 50 % stenosis (right)

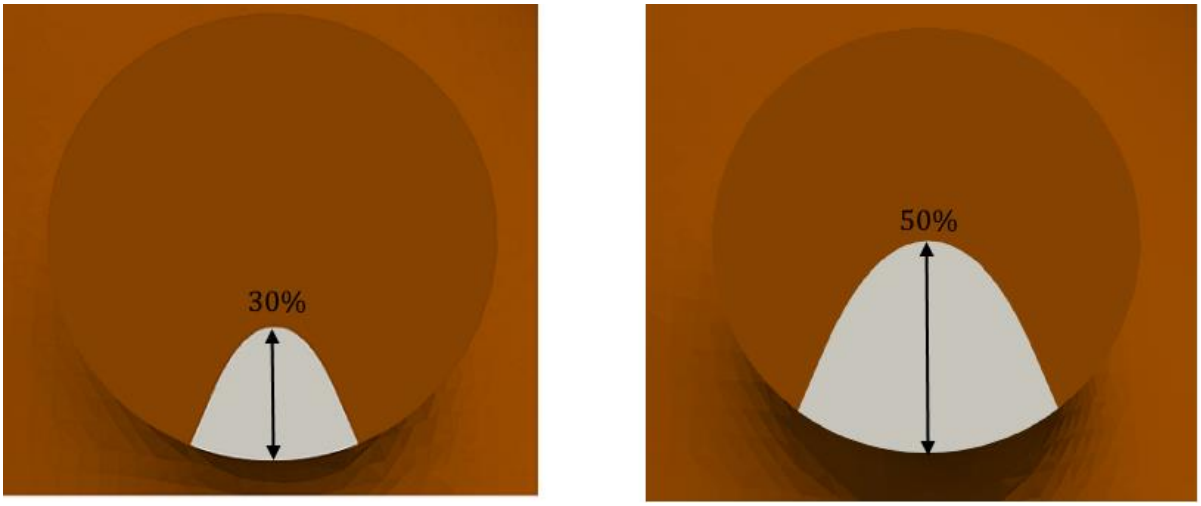

Figure 4-18. Schematic of different percentage stenoses

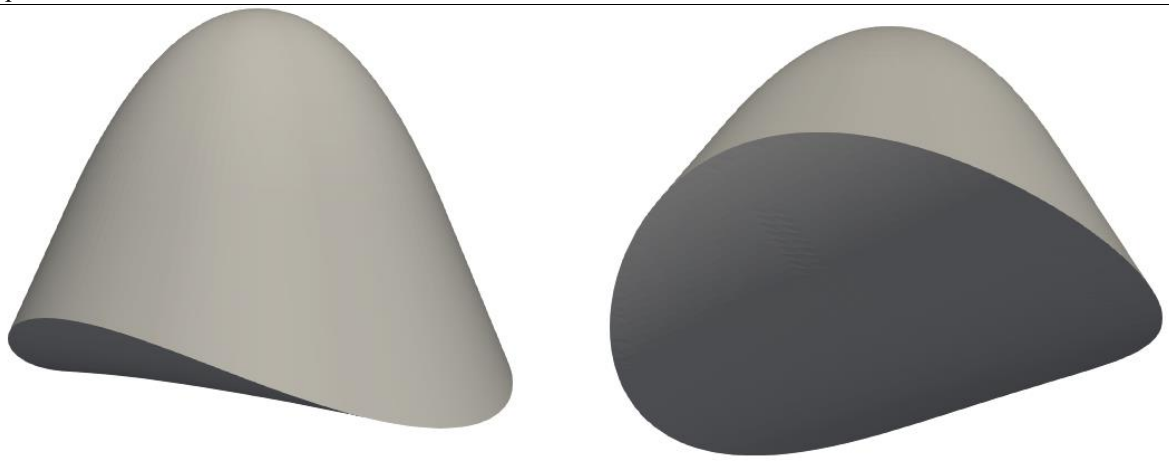

Figure 4-19. Atherosclerotic plaque geometry

4.3.2. Mesh

All four meshes were made with cfMesh and are mostly hexahedral. The mesh quality satisfied all the quality indicator thresholds. Index 1 will be used for the 30 % stenosis model, while index 2 for the 50 % stenosis model. Mesh information is given in the following table:

Table 4-2: Mesh properties

Region	Cell count
Fluid 1	141,366
Solid 1	4,858
Fluid 2	145,229
Solid 2	8,845

Mesh comparison is shown in the following figures:

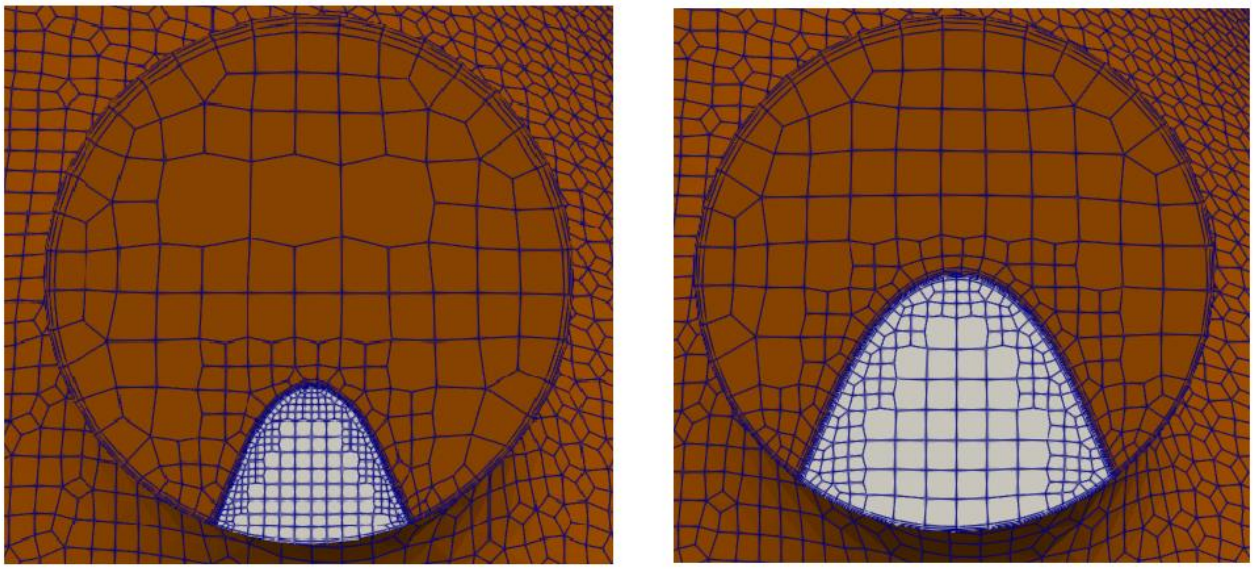

Figure 4-20. Cross section I of LM vessel at the maximum height of the plaque. On the left, geometry with 30 % stenosis is shown. On the right, geometry with 50 % stenosis is shown.

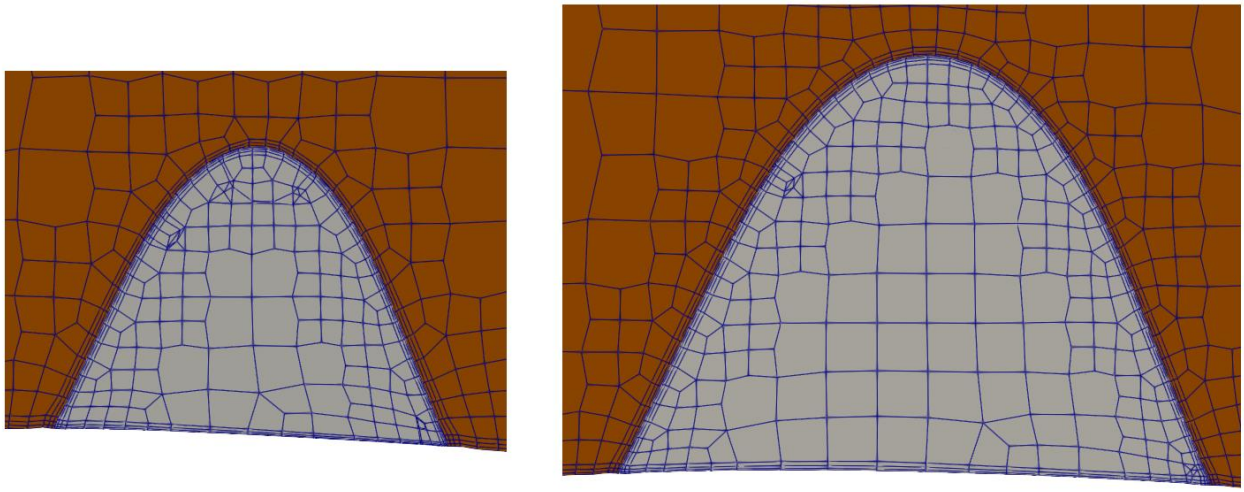

Figure 4-21. Cross section II of LM vessel at the maximum height of the plaque

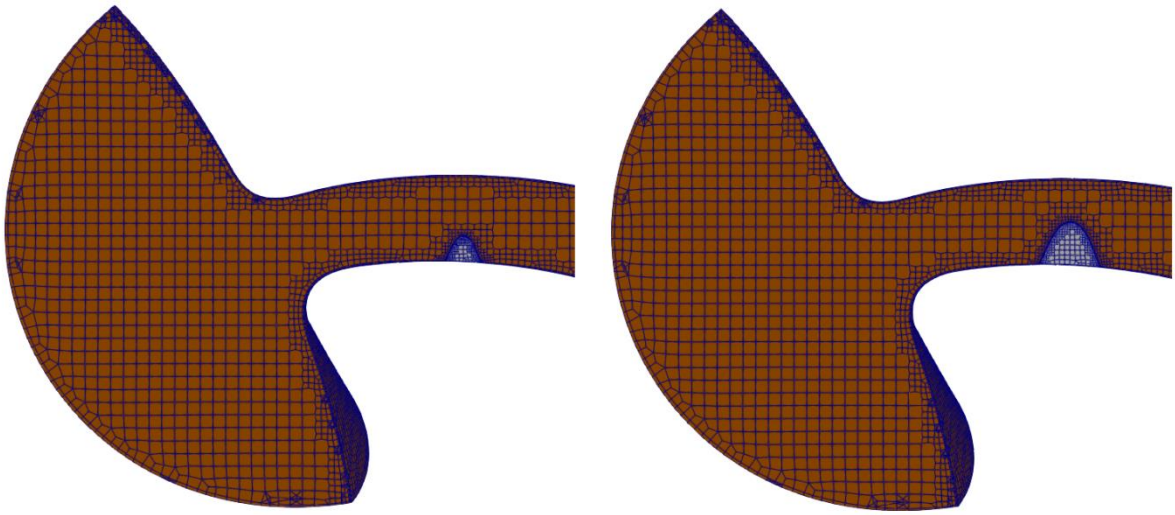

Figure 4-22. Cross section of LCA vessel

4.3.3. Boundary conditions

As it has been said in chapter 4.2, pressure boundary conditions at the outlets of the fluid domain are fixed using the results from the CFD simulation. As the pressure values are defined at the outlets, the reference pressure cell is no longer required at the inlet. Fluid boundary conditions are given in the following table:

Table 4-3: Fluid domain boundary conditions

Patch	**Boundary condition**	
	U	p
aorta_in	newFlowRateInletVelocity	zeroGradient
lad_out	zeroGradient	timeVaryingUniformFixedValue
ri_out	zeroGradient	timeVaryingUniformFixedValue
lcx_out	zeroGradient	timeVaryingUniformFixedValue
wall	noSlip	zeroGradient
plaque_wall	newMovingWallVelocity	zeroGradient

timeVaryingUniformFixedValue boundary condition represents a general fixed value condition with a time-varying value. *newMovingWallVelocity* boundary condition provides a velocity condition for cases with moving walls. It sets the relative velocity between the fluid and the wall to zero.

Solid domain boundary conditions are given for pressure p and displacement D.

Table 4-4: Solid domain boundary conditions

Patch	**Boundary condition**	
	p	D
plaque_in	tractionPressure	tractionExtrapolatedDisplacement
plaque_out	zeroGradient	fixedDisplacement

tractionPressure boundary condition transfers calculated pressure and viscous forces at the fluid side interface to the solid side interface, whereas the boundary condition *tractionExtrapolatedDisplacement* extrapolates displacement values from the center of control volume to the centers of face surfaces. *fixedDisplacement* boundary condition constrains the displacements to a fixed value.

The fluid and solid regions are solved separately. Gauss-Seidel coupling algorithm is used to enforce momentum and kinematic continuity at the fluid-to-solid interface with the Dirichlet-Neumann decomposition.
The fluid domain is solved using a Dirichlet condition for velocity at the interface, and the solid domain is solved using a Neumann condition for traction at the interface.

The coupling algorithm for all time-steps is as follows:

1. solve fluid domain
2. pass fluid interface forces to the solid interface
3. solve solid domain
4. pass solid interface velocities to the fluid interface using under-relaxation
5. update the fluid mesh
6. repeat until convergence

4.3.4. Solver control

Fluid domain calculations were performed using the *pimpleFoam* solver, while the solid domain was calculated using *stressFoam* solver. Both domains are discretized in space using the second-order accurate cell-centered finite volume method and temporal discretization is performed using the first-order accurate implicit scheme. The first order-accurate schemes are used to improve stability.
The fluid domain residuals and under-relaxation factors are the same as in the CFD simulation. The solution converged when the traction residual decreased under 10^{-5}, while the under-relaxation is achieved using the IQN-ILS procedure.

4.3.5. Fluid and solid material properties

Due to simplicity, the blood has been modeled as an incompressible and Newtonian fluid. The kinematic viscosity is set to $\nu_{\mathrm{f}} = \frac{\mu}{\rho} = 3 \cdot 10^{-6}\ \mathrm{m}^2/\mathrm{s}$, where μ is the blood dynamic viscosity and ρ_{f} is the blood density, which is set to $1000\ \mathrm{kg/m}^3$.

The plaque has been modelled as an isotropic homogenous hyperelastic and incompressible body. The homogeneous property indicates that it is made of a single material. Since the main constituents of the plaque are collagen, smooth muscle cells and lipids, an average Young's modulus, based on the [15], is $E = 8 \cdot 10^5$ Pa. An incompressible property locks Poisson's ratio to $\nu_{\mathrm{s}} = 0.5$, while the material density is set to $\rho_{\mathrm{s}} = 1200\ \mathrm{kg/m}^3$.

5. RESULTS AND DISCUSSION

The following chapter shows the effect of two different stenoses on the atherosclerotic artery. Since blood flow has a pulsating nature, the dynamical system characteristics around the plaque, such as the blood flow velocity, the pressure distribution, the wall shear stress, the wall displacement, the von Mises stress, and the traction at the plaque root will be analyzed.
The maximum velocity occurs at a time corresponding to the maximum pulsation of volume flow rate at the plaque location ($t = 0.56$ s), where the constriction of the artery is the greatest. As there is a phasic difference between the maximum volume flow rate and the maximum pressure, there are two points of interest, the maximum pressure ($t = 0.34$ s) and the maximum velocity ($t = 0.56$ s). Both of them will be compared and analyzed in the remainder of the chapter.

Calculations were done by parallel computing using the domain decomposition approach. Fluid and solid meshes and fields are divided into sub-domains that are assigned to different processors, six in this case. Solvers run in parallel on separate subdomains, and communication between processors is accomplished through the Message Passing Interface (MPI) communication protocol.

Post-processing was done in Paraview, an open-source multiple-platform application for interactive, scientific visualization, and QtiPlot, a cross-platform application for interactive scientific graphing and data analysis.

5.1. Fluid governing results

This part of the chapter will focus on the fluid-based results, which are the volume flow, the velocity, the pressure, and the WSS.

Firstly, the comparison between CFD and FSI volume flow rate is given at each artery branch as the downstream pressure conditions are the same.

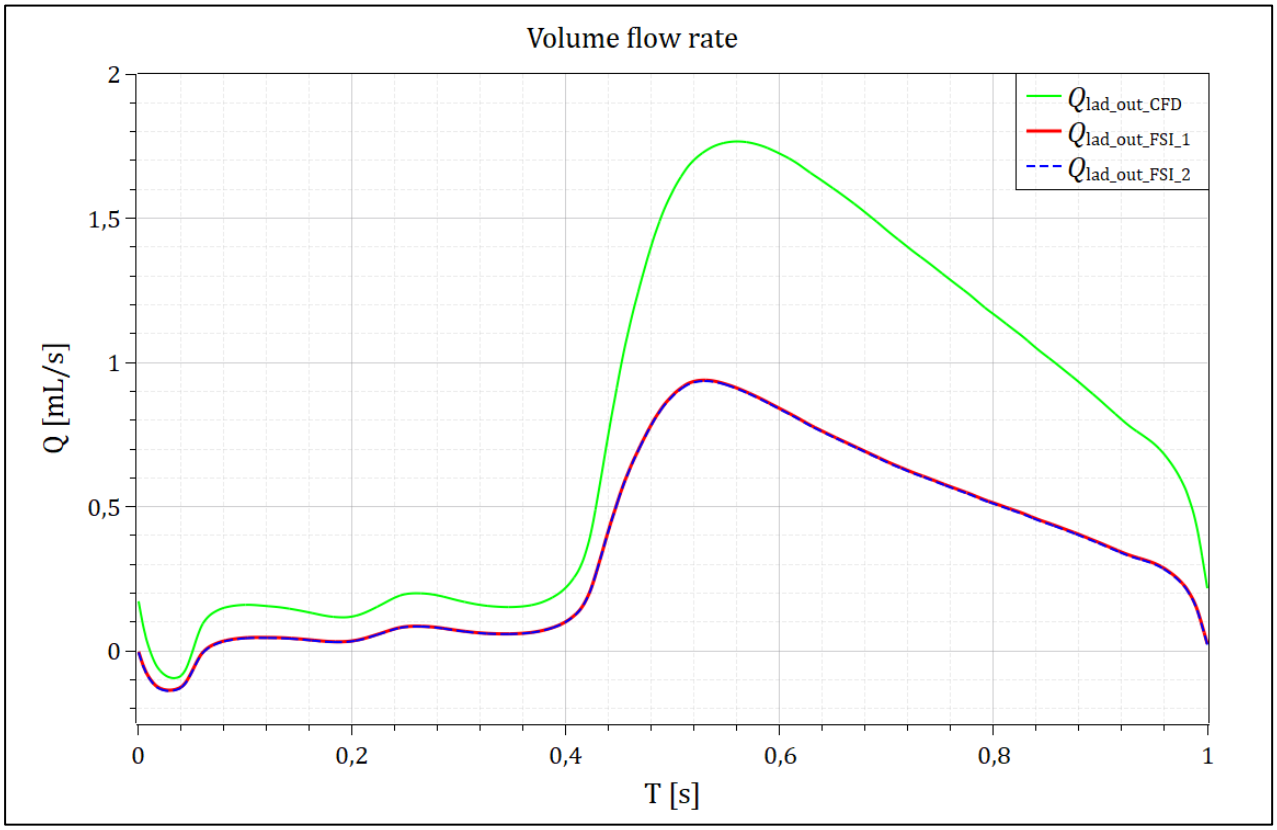

Figure 5-1. The left anterior descending volume flow rate

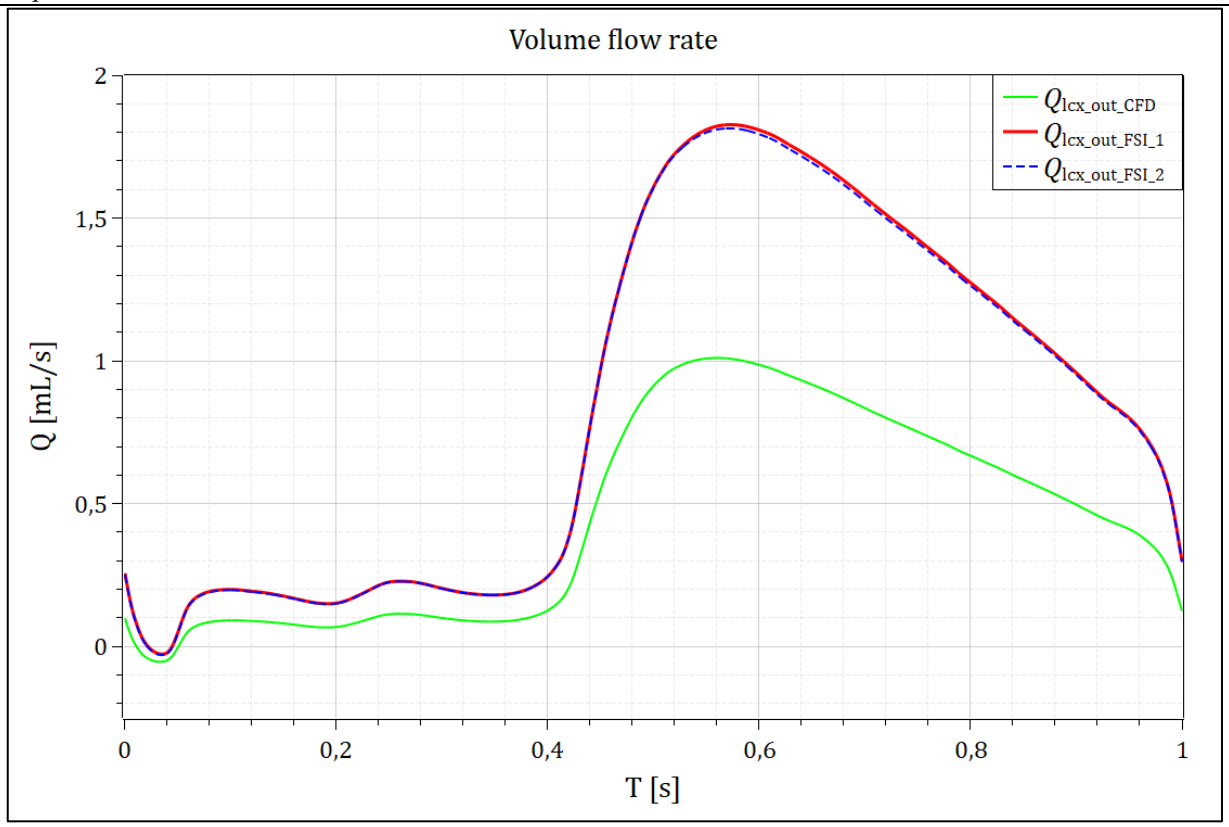

Figure 5-2. The left circumflex branch volume flow rate

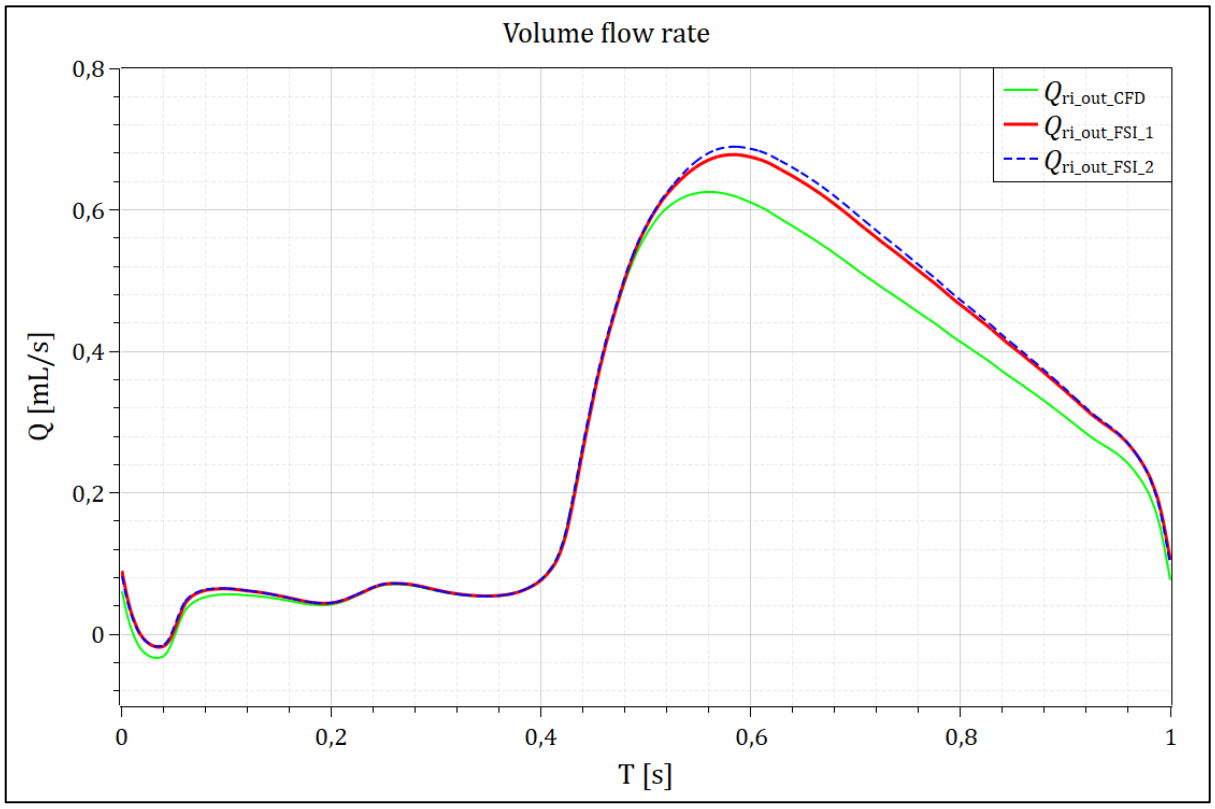

Figure 5-3. The ramus intermedius branch volume flow rate

The previous three graphs show that the volume flow changes significantly due to the plaque growth even though the downstream conditions are unchanged. The flow through the LAD branch decreases nearly twice, while the flow through the LCx and RI branches increases.

As the volume flow changes, so does the velocity. The maximum average velocity at outlets in the CFD simulation reached ~ $v_{max} = 0.15$ m/s. The average outlet velocity for both simulations can be seen in Fig 5-4.

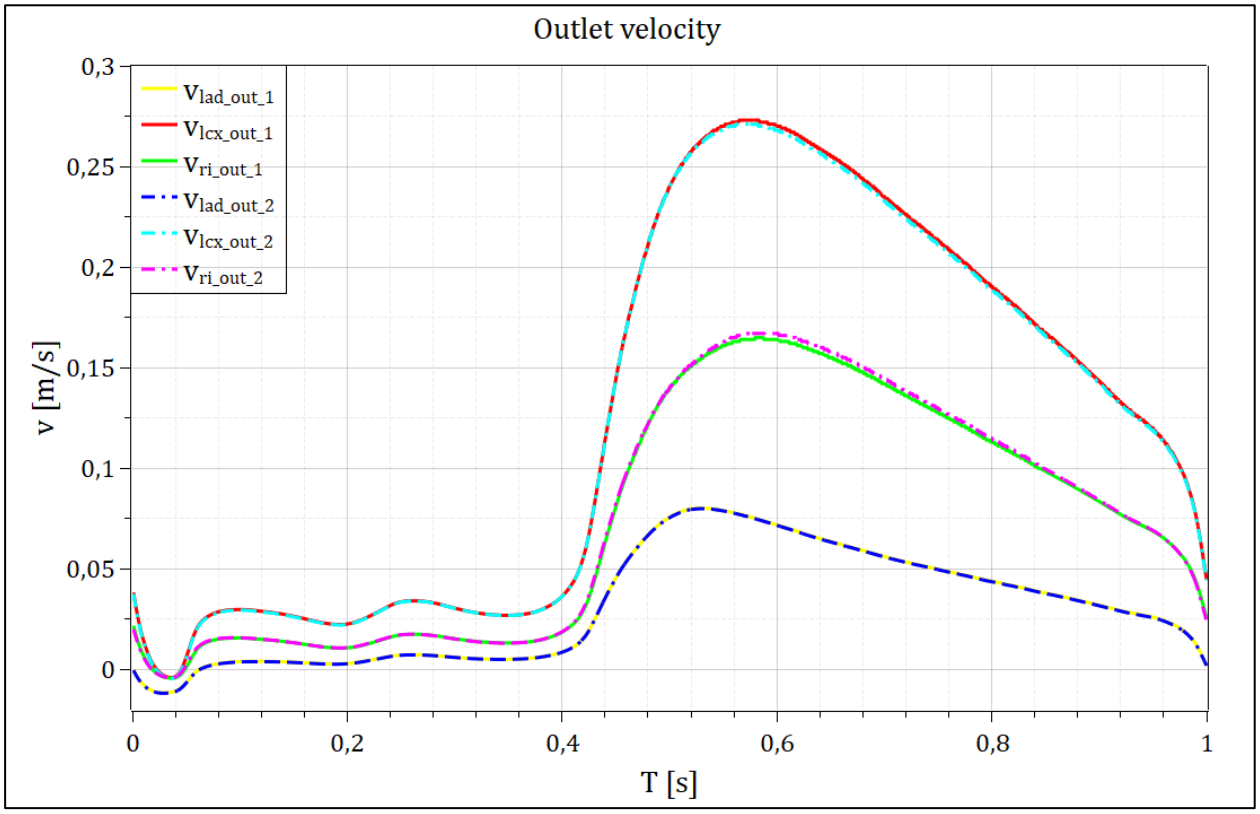

Figure 5-4. Average outlet velocity comparison

Due to the incompressible flow, the velocity is equal to $v = Q/A$, where Q represents the volume flow and A is the surface area. This means that the velocity is proportional to the volume flow. This is the reason why the LCx and RI branches have higher average velocity compared to the CFD values, while the LAD branch has a lower value.

The following figures show the velocity streamlines at $t = 0.56$ s. The vortices are generated behind the plaque and form the flow separation downstream. Flow separations represent a long-term problem as they cause low wall shear stress areas, which are favorable areas for plaque formation. Vortices also obstruct the laminar flow and they extend throughout the LM branch, up

until the beginning of the LAD. Fig 5-1 and Fig 5-4 show significantly reduced volume flow rate and the average velocity in the LAD branch, which might be due to the vortex formation.

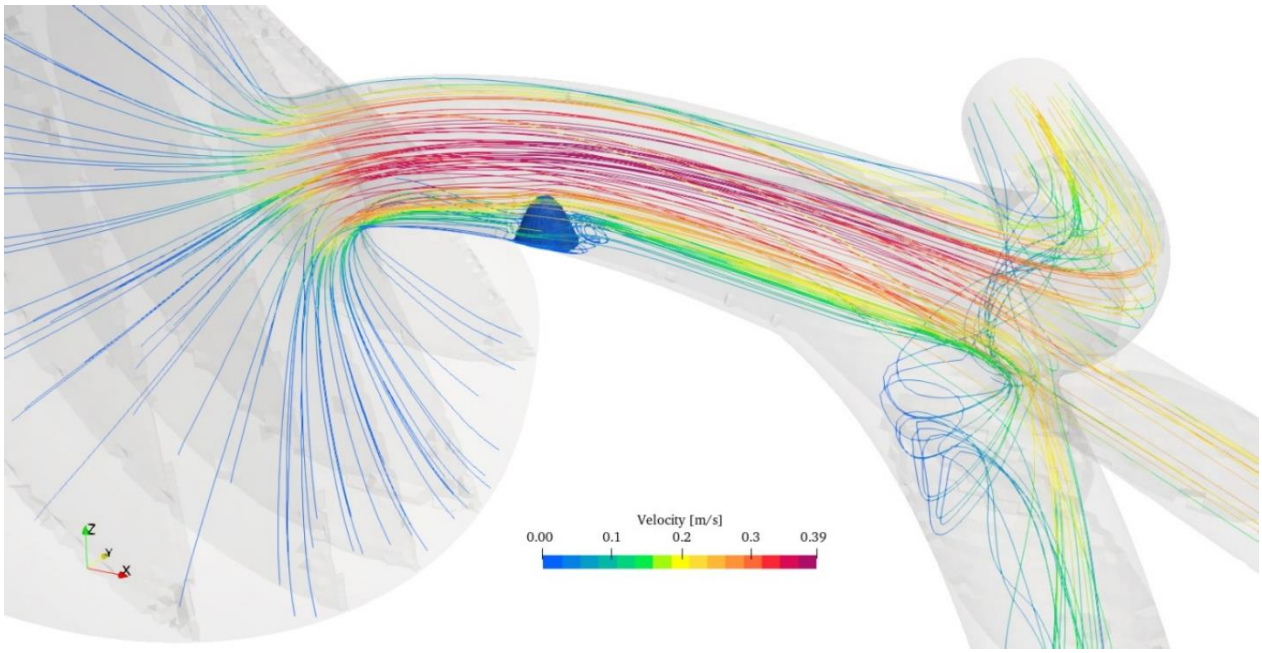

Figure 5-5. Streamlines around the plaque, model 1

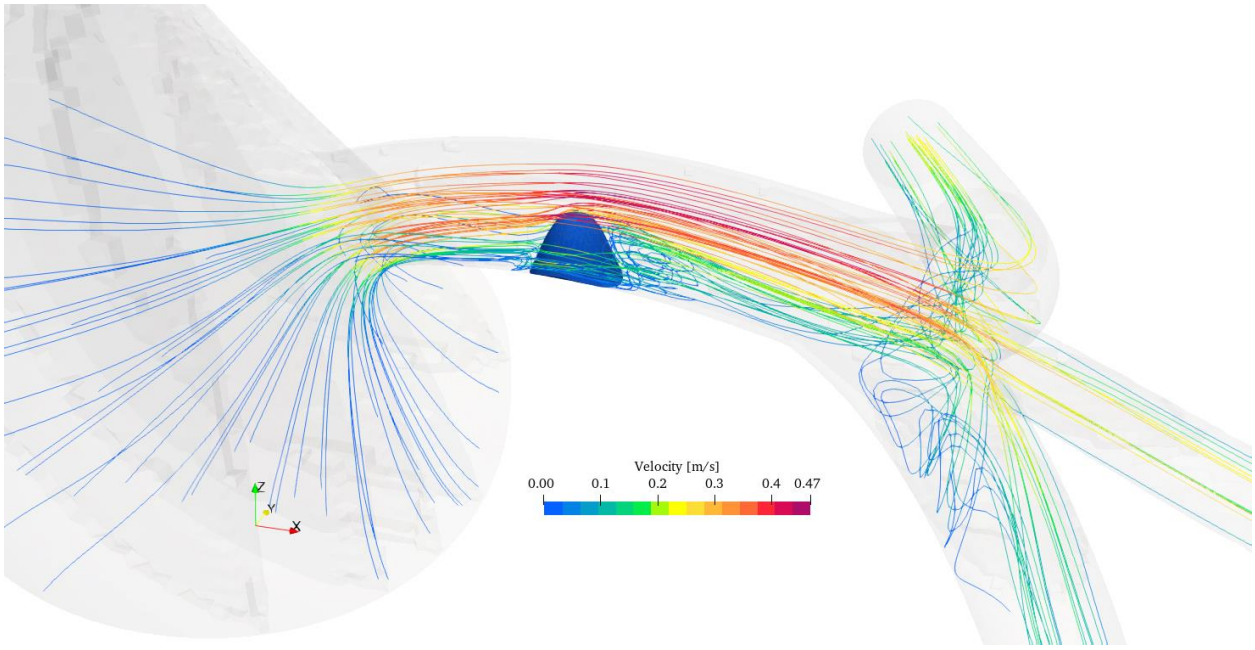

Figure 5-6. Streamlines around the plaque, model 2

Fig. 5-7 shows the pressure distribution along the artery wall. Due to the viscosity, a pressure drop is observed from upstream to downstream.

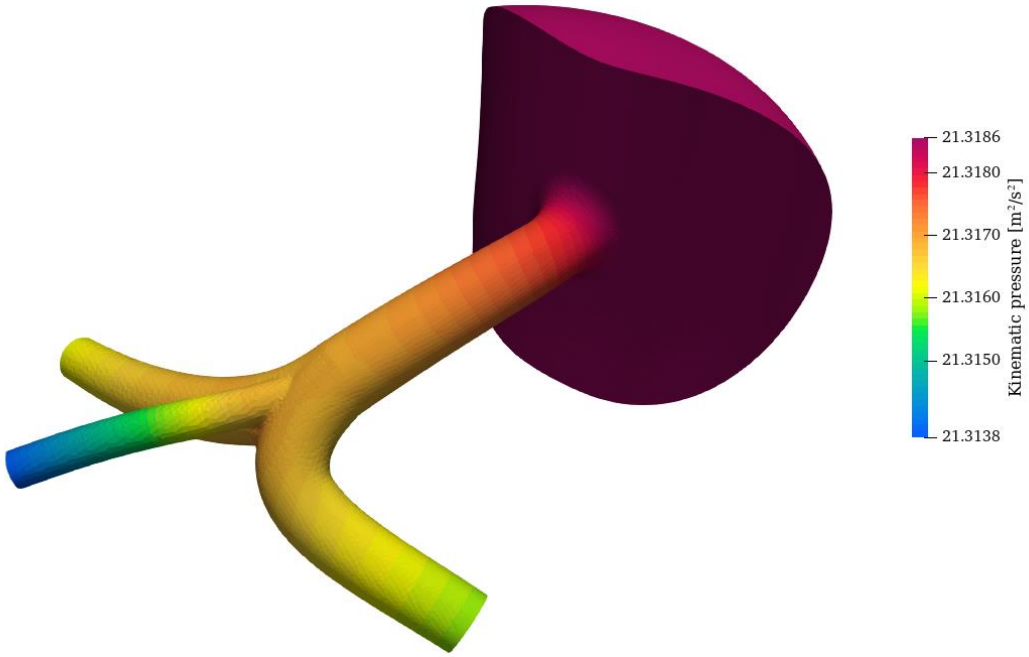

Figure 5-7. Pressure distribution, model 1

Wall shear stress along the plaque wall is illustrated in the following figures (at $t = 0.56$ s). The obtained value of WSS needs to be multiplied by the fluid density, as the current value is calculated using the kinematic viscosity, rather than the dynamic viscosity.

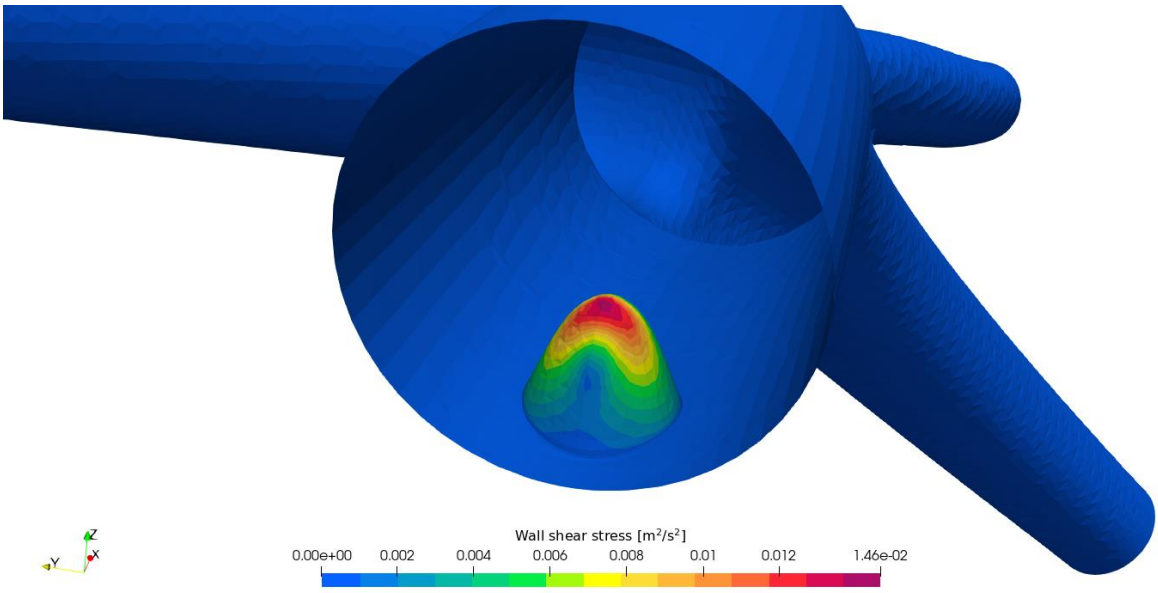

Figure 5-8. Wall shear stress distribution I, model 1

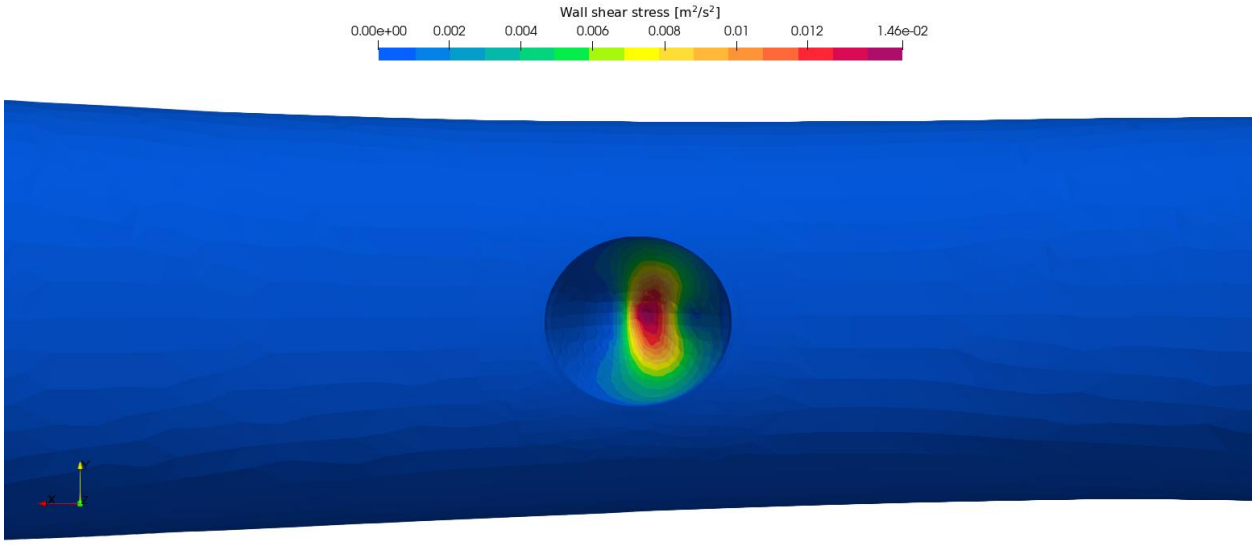

Figure 5-9. Wall shear stress distribution II, model 1

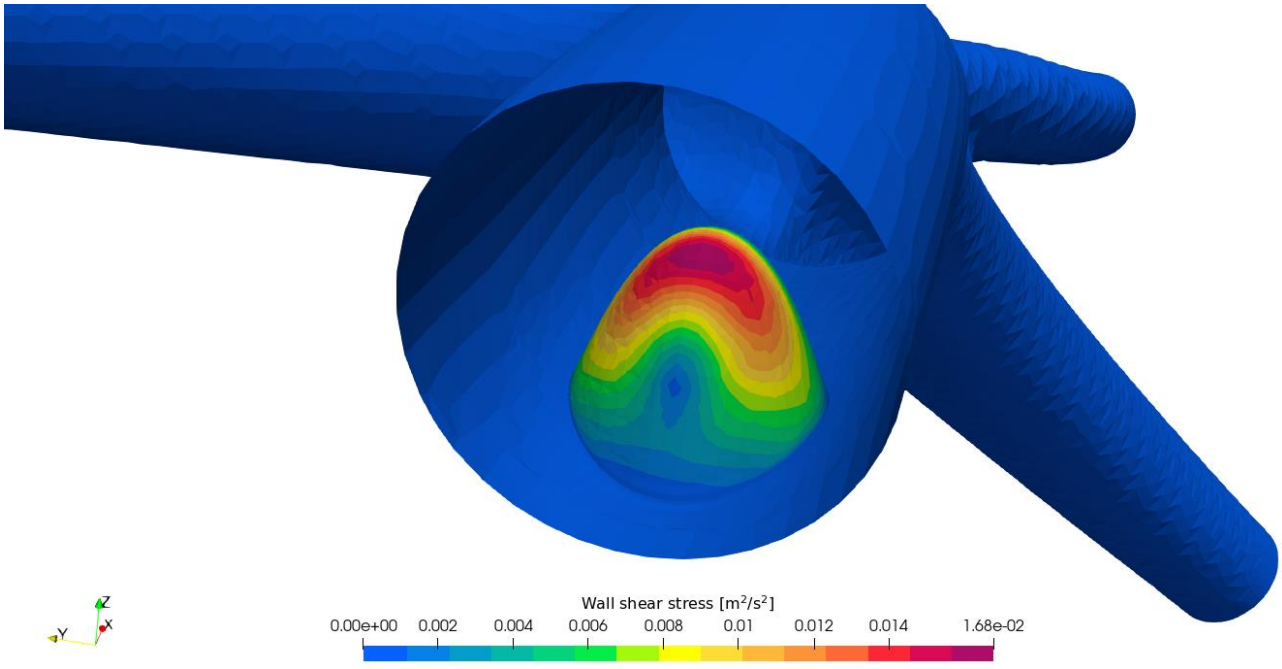

Figure 5-10. Wall shear stress distribution I, model 2

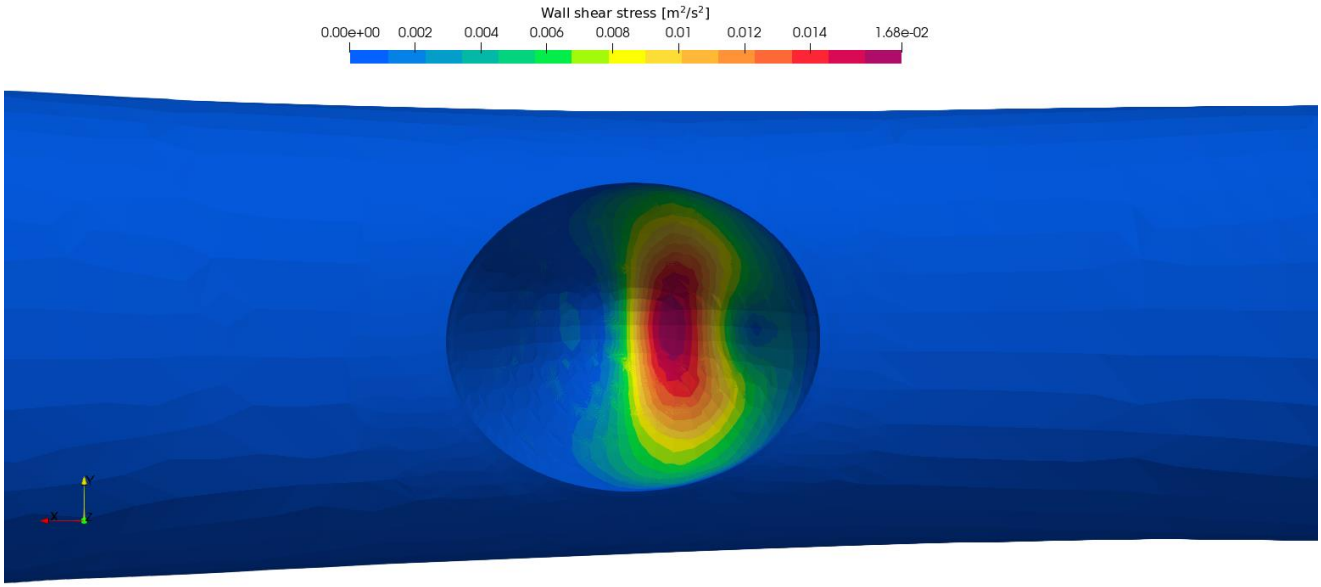

Figure 5-11. Wall shear stress distribution II, model 2

The WSS in both cases follows a similar distribution. The WSS local maximum is in the vicinity of the plaque with the 50 % stenosis model having larger values. This suggests that the higher stenoses are subjected to higher stresses. The plaque wall failure is primarily due to the WSS. The maximum values are in the middle area of the plaque shoulder (intersection of the outer surface of the plaque and the artery wall), which suggests that this area might be prone to rupture.

Fig. 5-12 shows the time-varying average WSS at the plaque wall for both geometries. Model 2 is subjected to a higher average WSS of approximately 33 %. It can be seen that the WSS waveform has a similar shape as the velocity waveform.

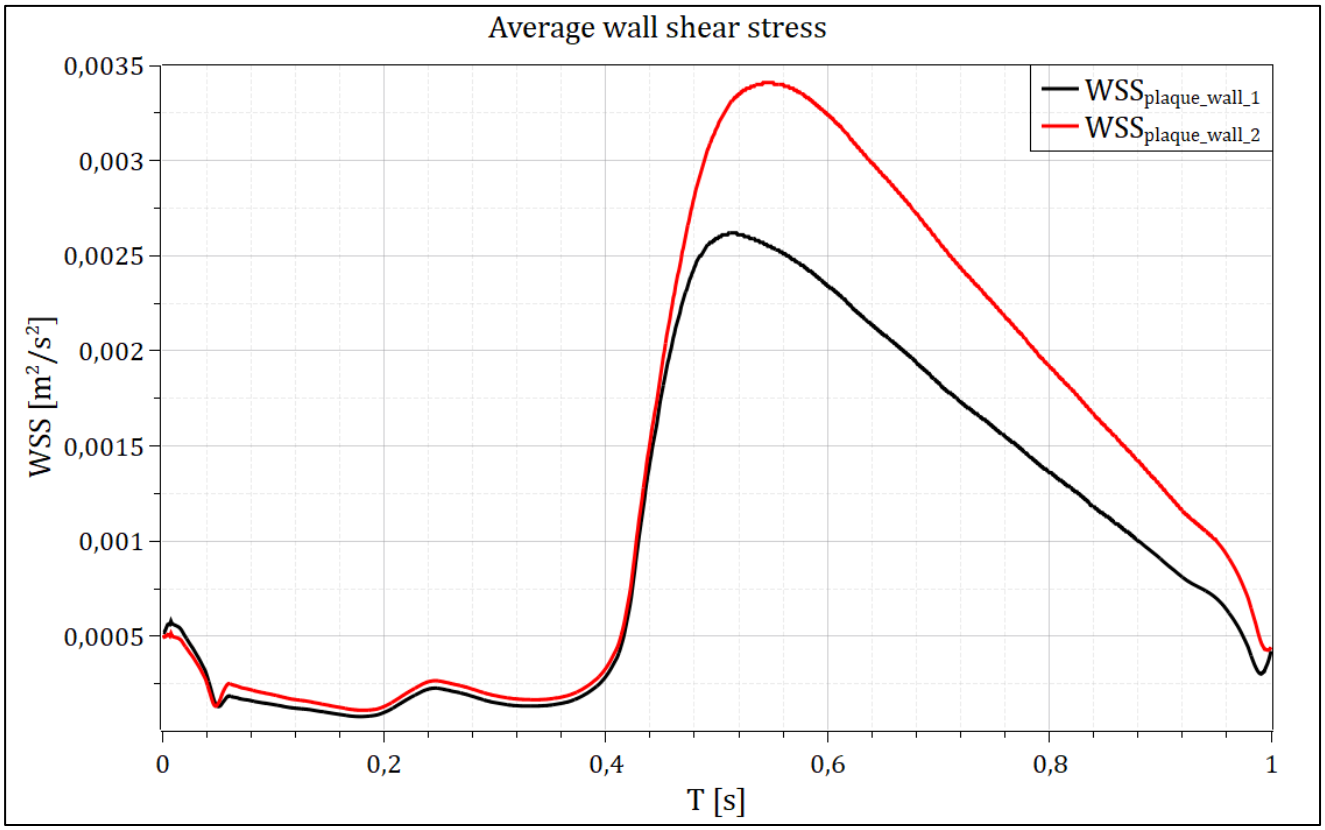

Figure 5-12. Time-varying average WSS

5.2. Solid governing results

This section of the chapter will put more emphasis on the solid-based results, such as the displacement and the von Mises stress. The material failure inside the plaque is mainly related to the maximum VMS, which represents an effective 3D stress, and is calculated as:

$$\sigma_{\mathrm{VM}} = \sqrt{\frac{1}{2}\left[\left(\sigma_{\mathrm{xx}} - \sigma_{\mathrm{yy}}\right)^2 + \left(\sigma_{\mathrm{yy}} - \sigma_{\mathrm{zz}}\right)^2 + \left(\sigma_{\mathrm{zz}} - \sigma_{\mathrm{xx}}\right)^2\right] + 3\left(\sigma_{\mathrm{xy}}^2 + \sigma_{\mathrm{yz}}^2 + \sigma_{\mathrm{zx}}^2\right)} \tag{5.1}$$

The stress components are shown in chapter 3.3 in Fig 3-4.

5.2.1. Pressure analysis

The first point of interest that will be analyzed is the maximum pressure point at $t = 0.34$ s. In the following figures, the displacement field is shown on the solid domain and the kinematic pressure field is shown on the fluid domain

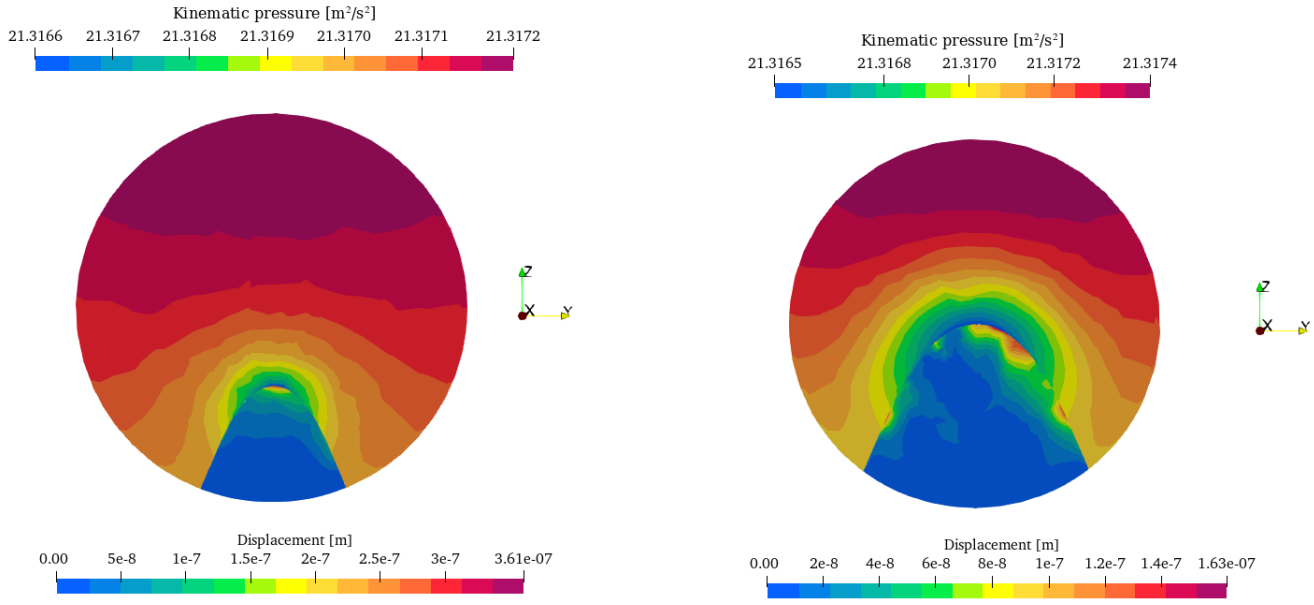

Figure 5-13. Pressure-displacement comparison I

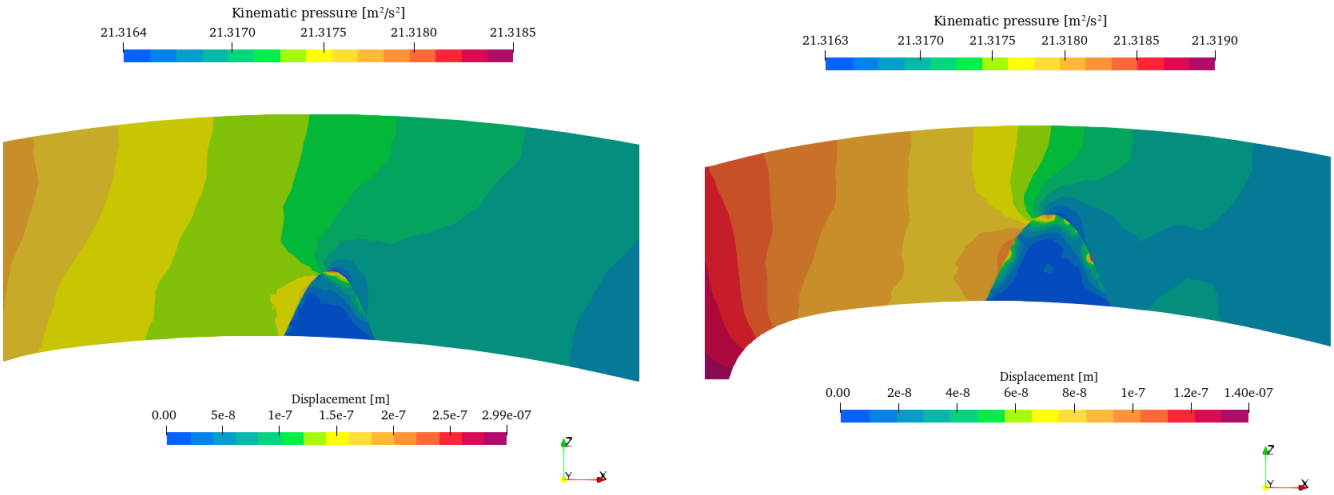

Figure 5-14. Pressure-displacement comparison II

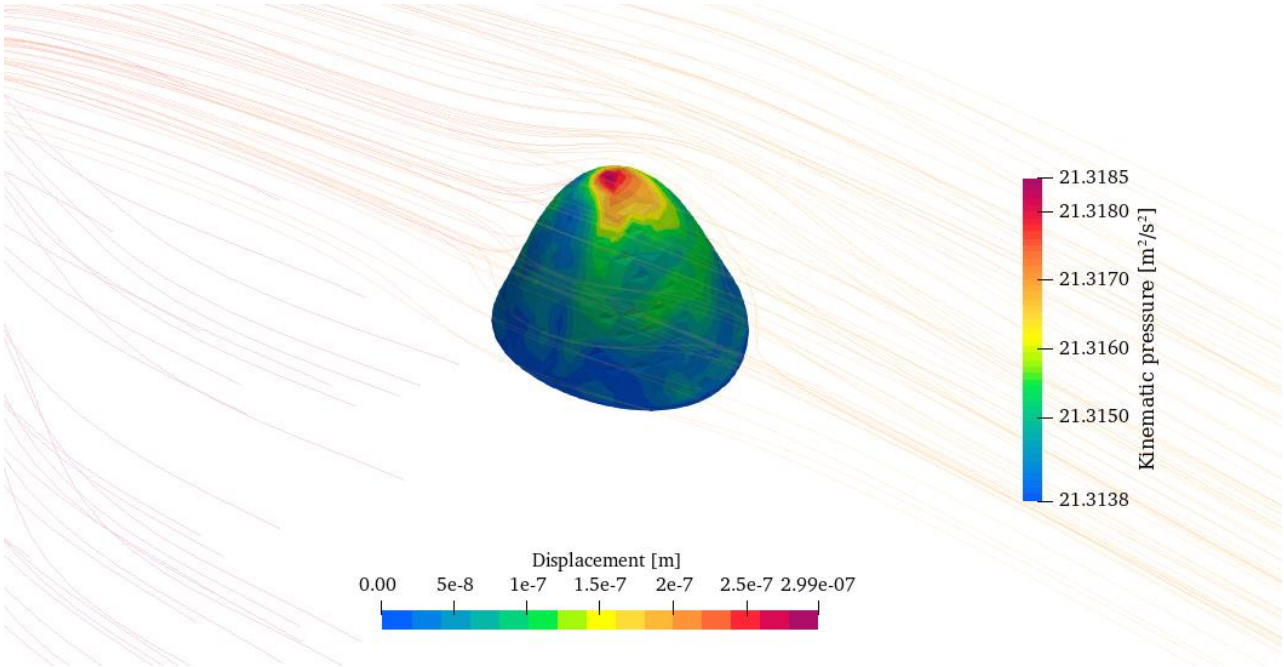

Figure 5-15. Pressure-displacement field, model 1

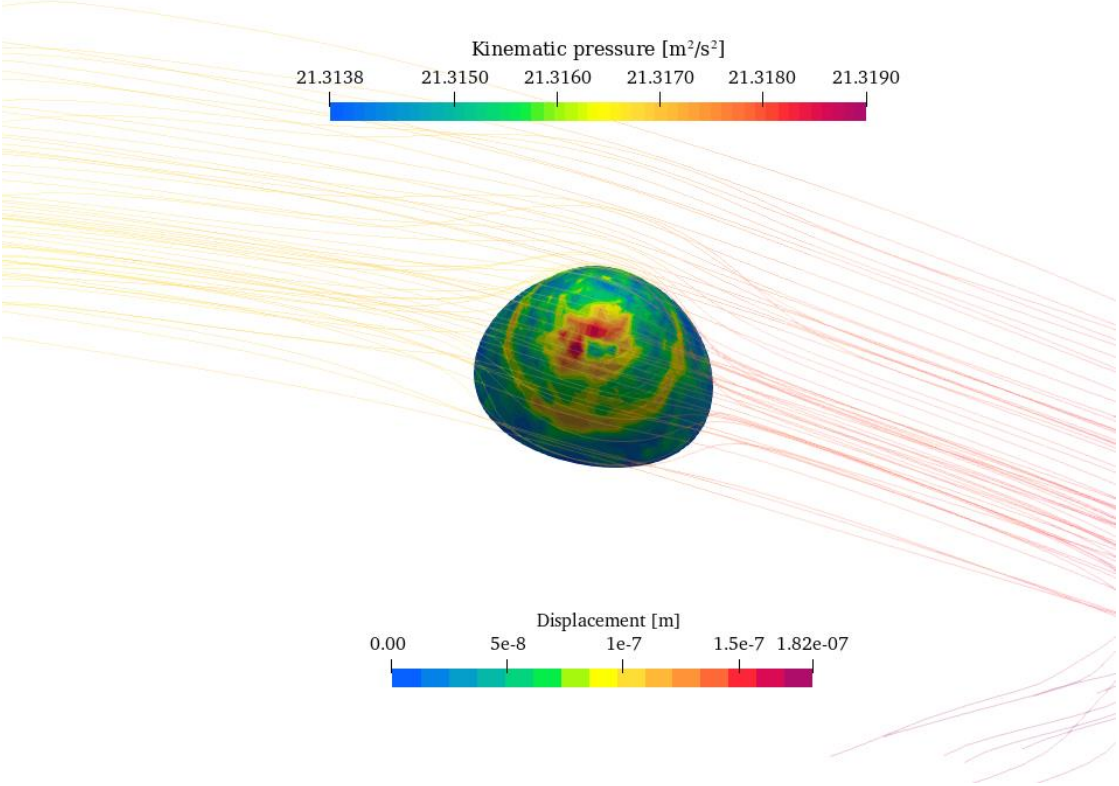

Figure 5-16. Pressure-displacement field, model 2

The comparative analysis at the maximum pressure point shows that the displacements in model 1 are twice as large as those in model 2. It is also worth noting that the largest displacements occur at the top of the plaque shoulder. The maximum displacements model 2 occur in the middle and the top region of the plaque shoulder, indicating that the load area is greater than in model 1, where they occur only in the top region. It should be noted that, given the geometry, the displacements are very small, so the stress provides a more accurate picture of the load.

In the next figures, the VMS field is shown on the solid domain and the kinematic pressure field is shown on the fluid domain.

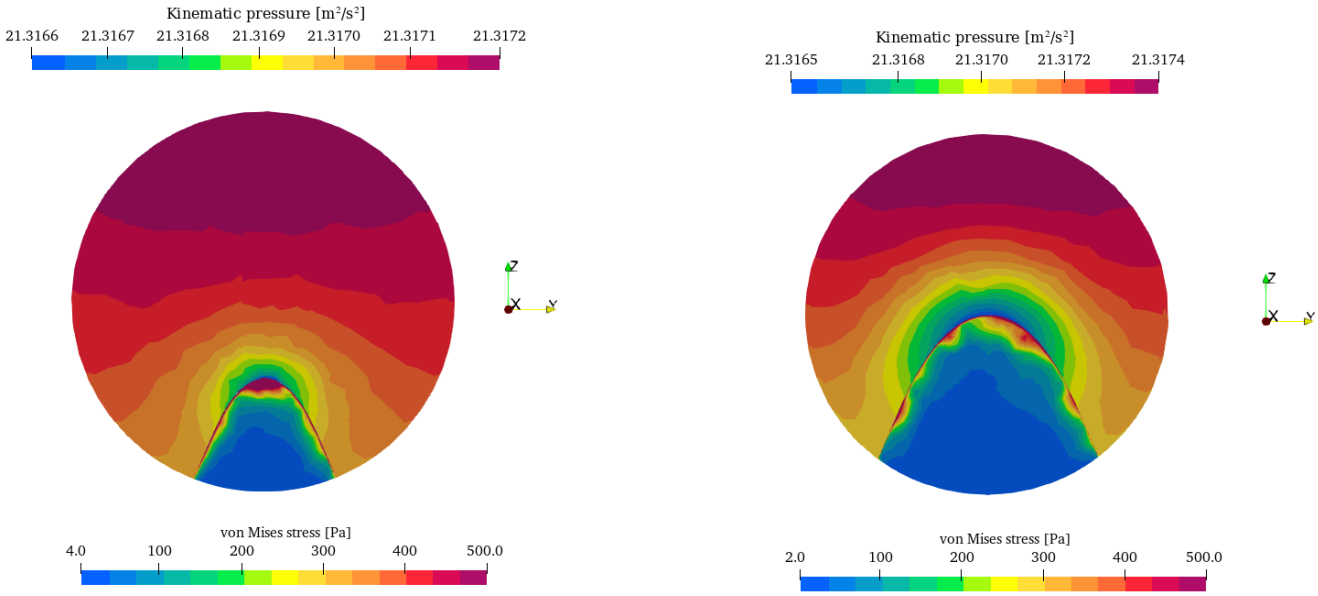

Figure 5-17. Pressure-VMS comparison I

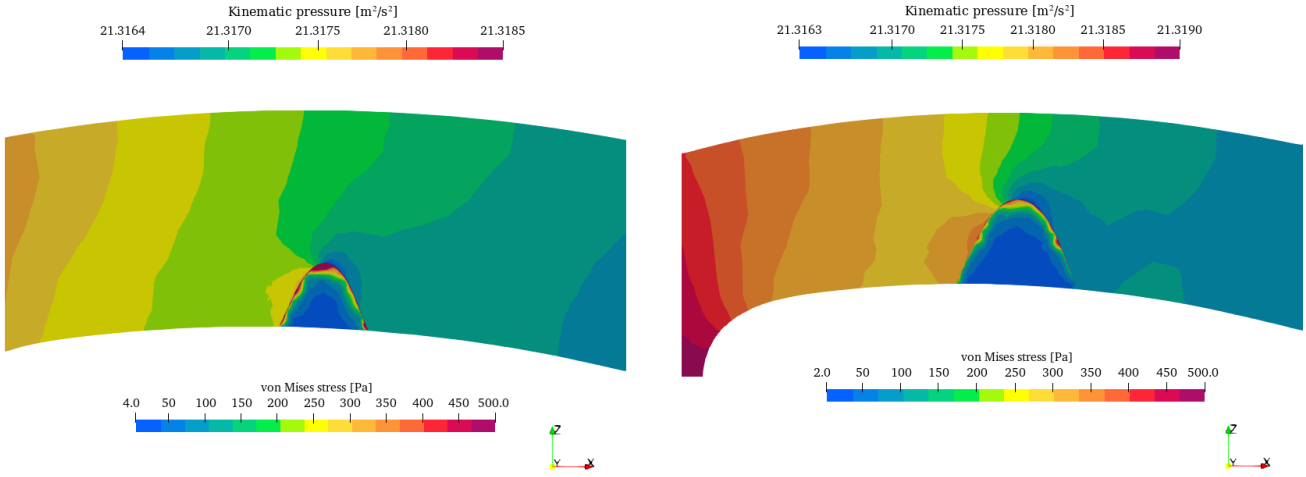

Figure 5-18. Pressure-VMS comparison II

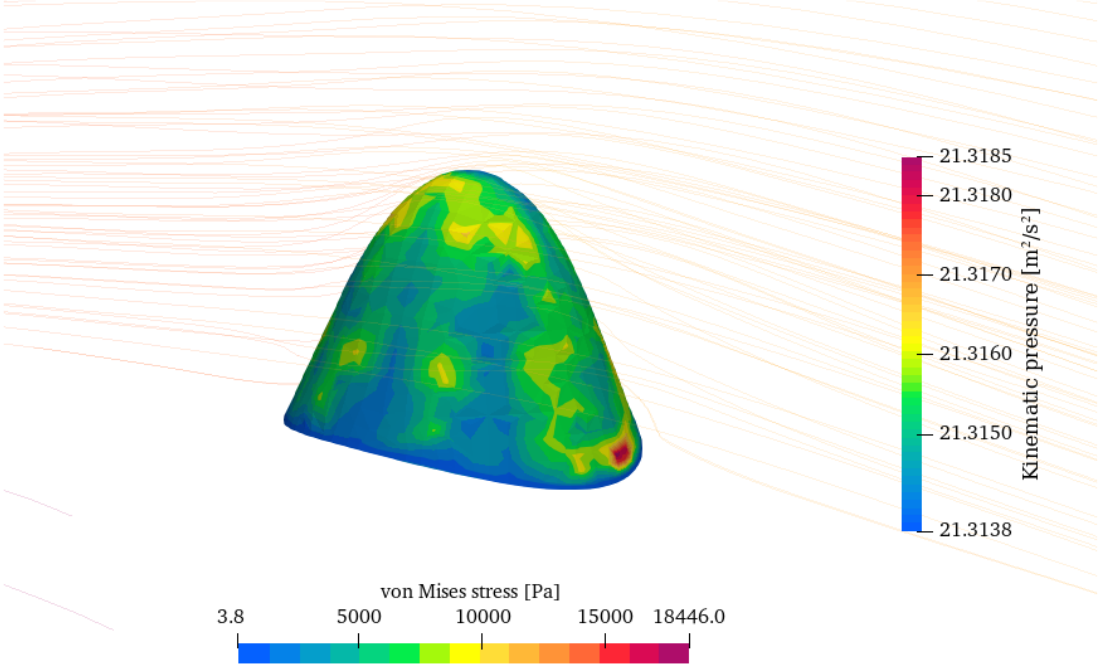

Figure 5-19. The pressure-VMS field, model 1

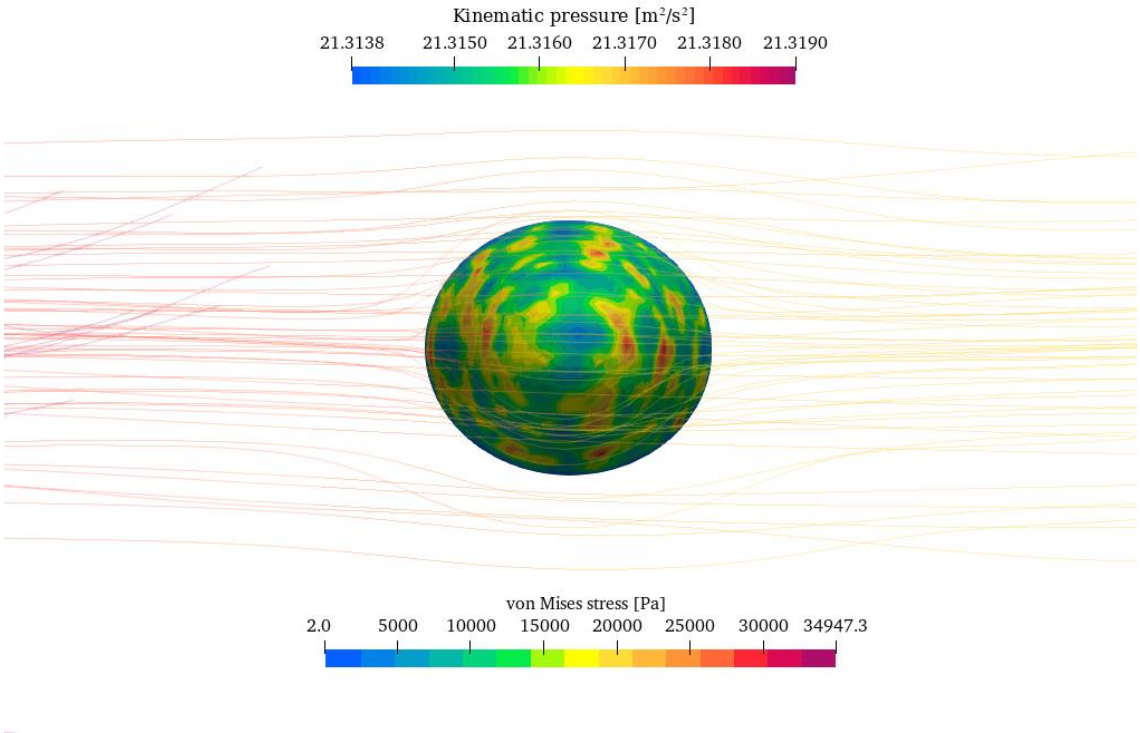

Figure 5-20. The pressure-VMS field, model 2

Figures 5-17 and 5-18 show a comparative review of stress at the same maximum stress scale to provide a more representative comparison. Both models have very low cross-sectional stresses, indicating that the rupture starts at the plaque shoulder. Surface VMS is the highest near the shoulder, which can be seen in Fig. 5-19 and Fig. 5-20. The maximum values are in the middle and the bottom region. The stress values in model 2 are nearly twice as high as in model 1, implying that a higher stenosis level is more prone to rupture.

5.2.2. Velocity analysis

The second point of interest is the maximum velocity point at $t = 0.56$ s. In the following figures, the displacement field is shown on the solid domain and the velocity field is shown on the fluid domain.

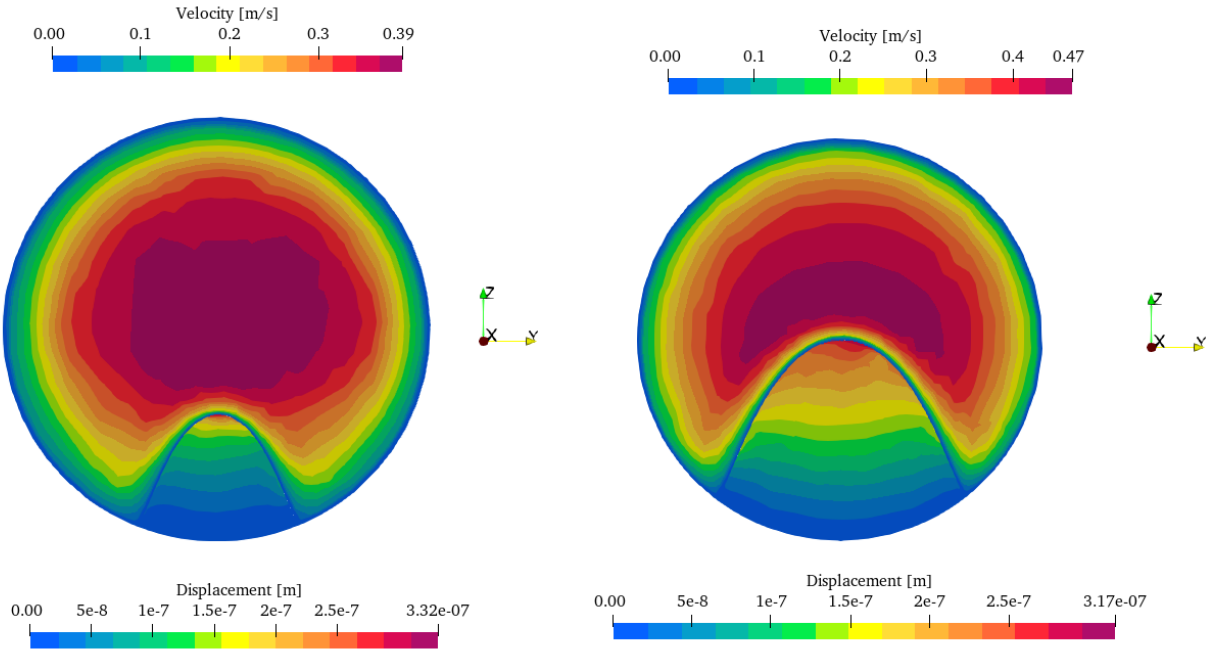

Figure 5-21. Velocity-displacement comparison I

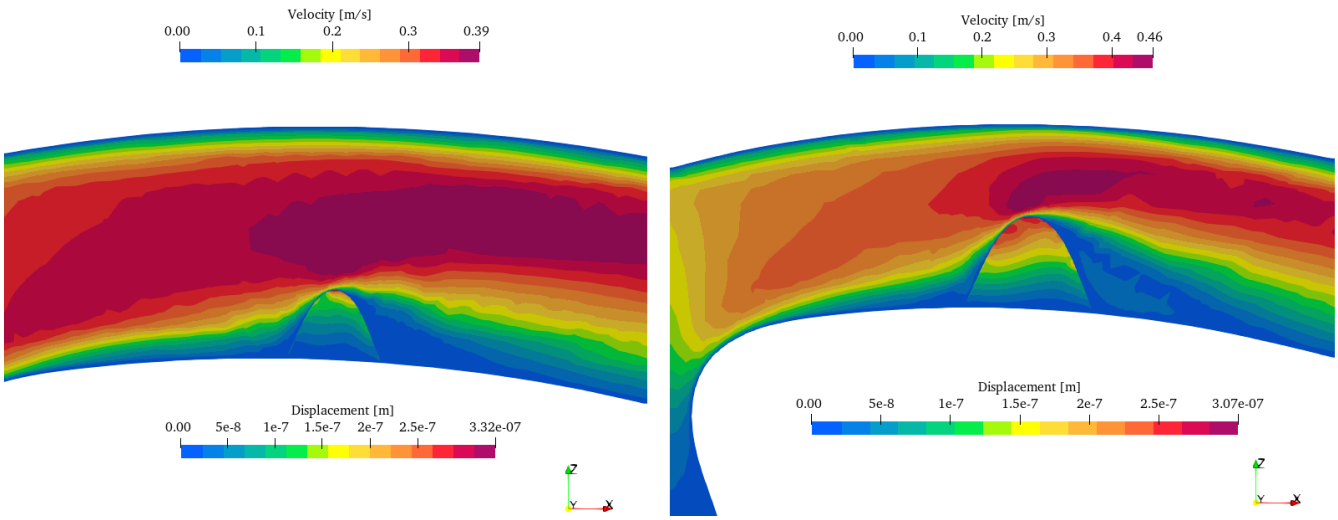

Figure 5-22. Velocity-displacement comparison II

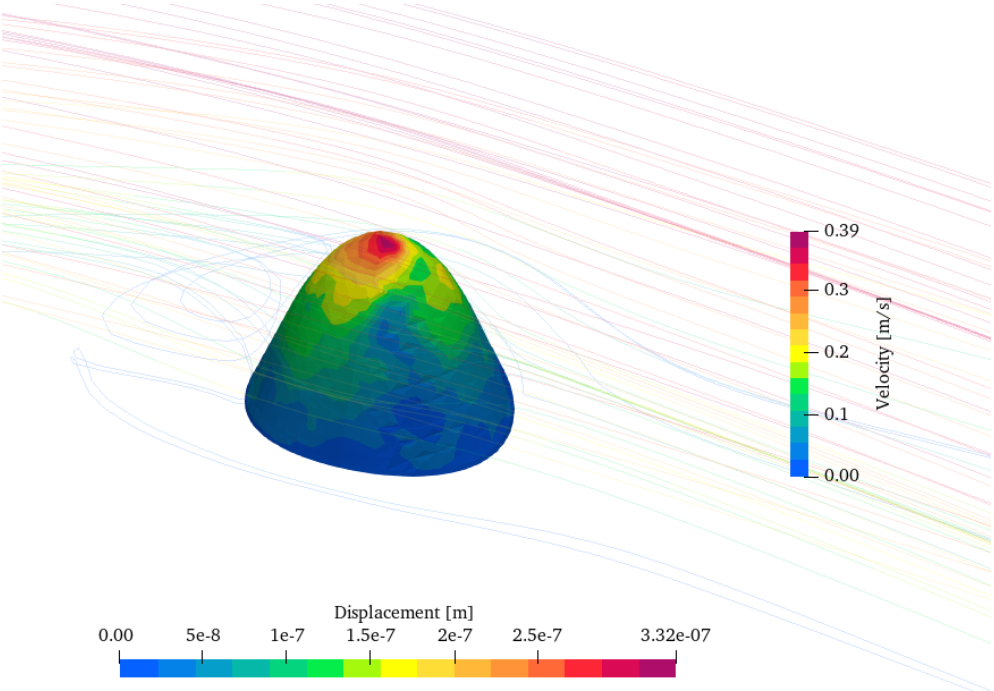

Figure 5-23. The velocity-displacement field, model 1

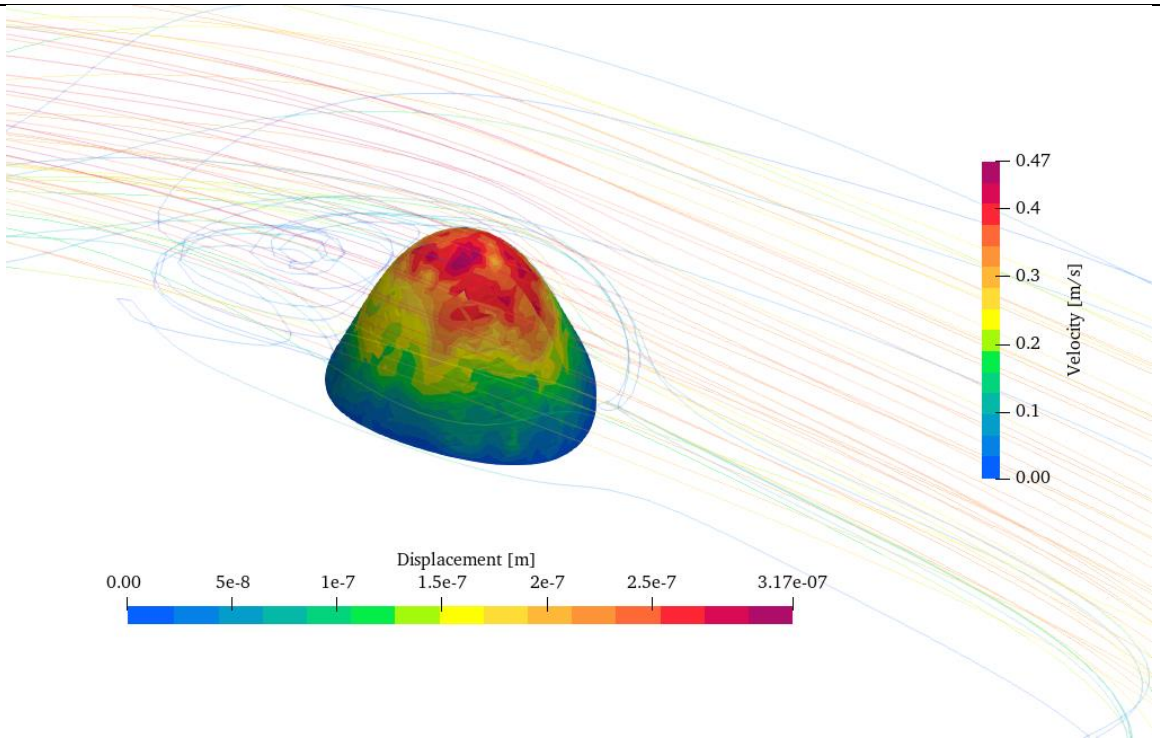

Figure 5-24. The velocity-displacement field, model 2

The displacement analysis shows that the maximum displacements in both models are nearly identical. The difference is that, in model 1, displacements occur only at the top of the shoulder, whereas, in model 2, displacements propagate from the top towards the interior, loading the plaque by the section height. This suggests that the velocity field has a significant effect on the different level stenoses, with a greater effect on the higher percentage stenoses.

As in the pressure analysis, displacements have low values, and thus stress analysis is necessary.

In the next figures, the VMS field is shown on the solid domain and the velocity field is shown on the fluid domain.

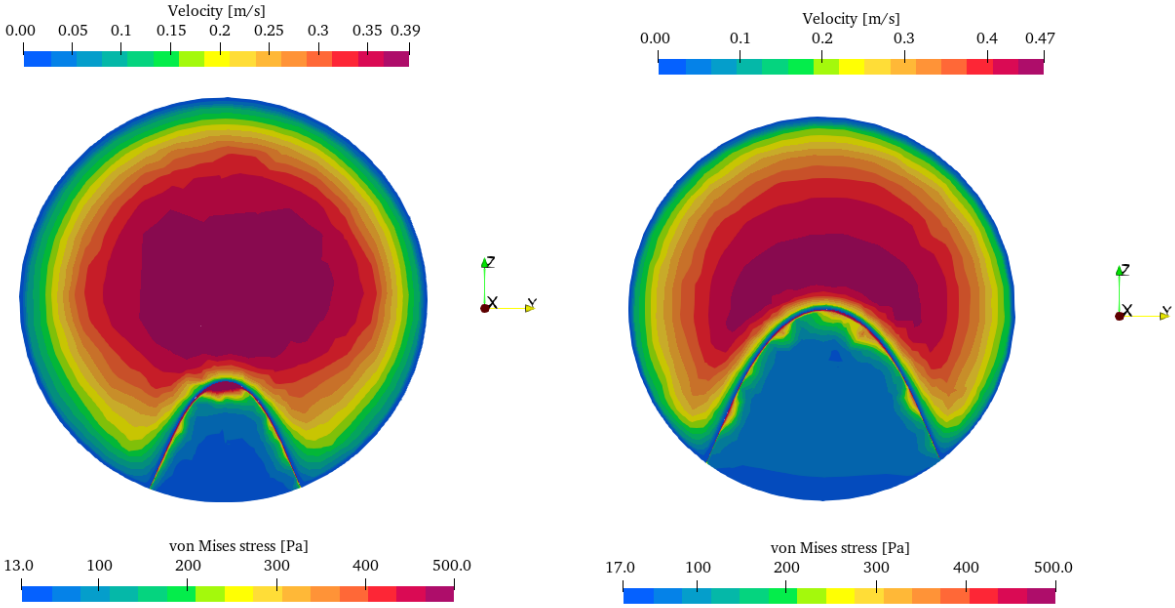

Figure 5-25. Velocity-VMS comparison I

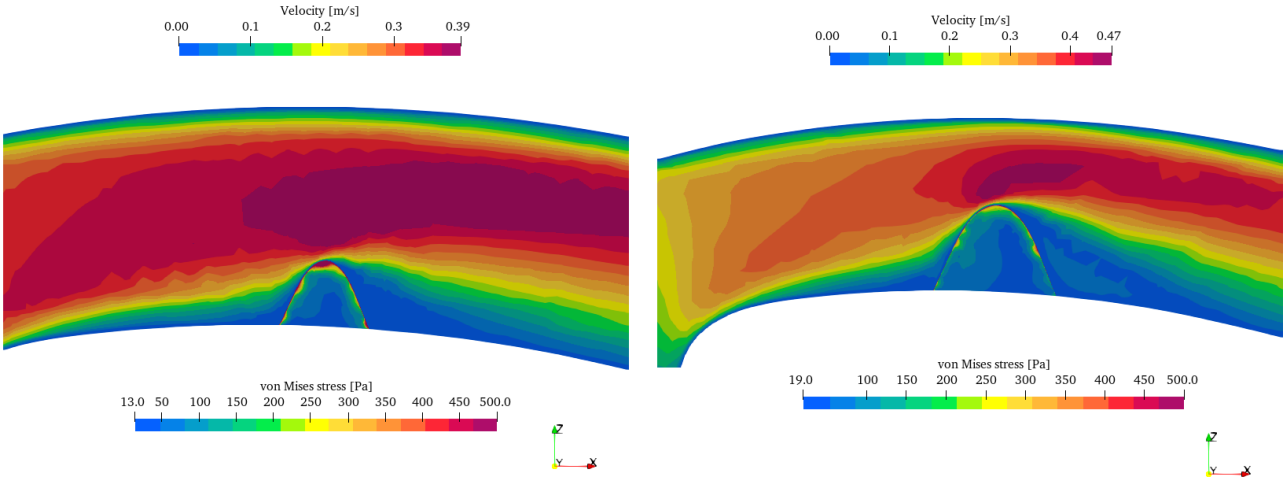

Figure 5-26. Velocity-VMS comparison II

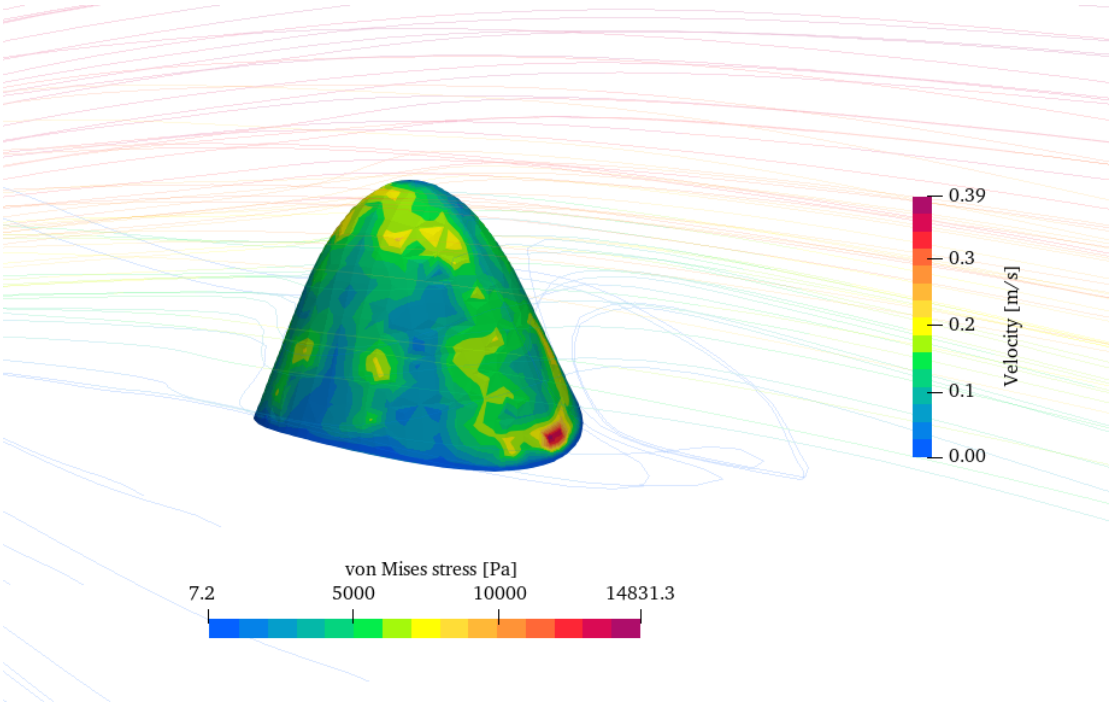

Figure 5-27. The velocity-VMS field, model 1

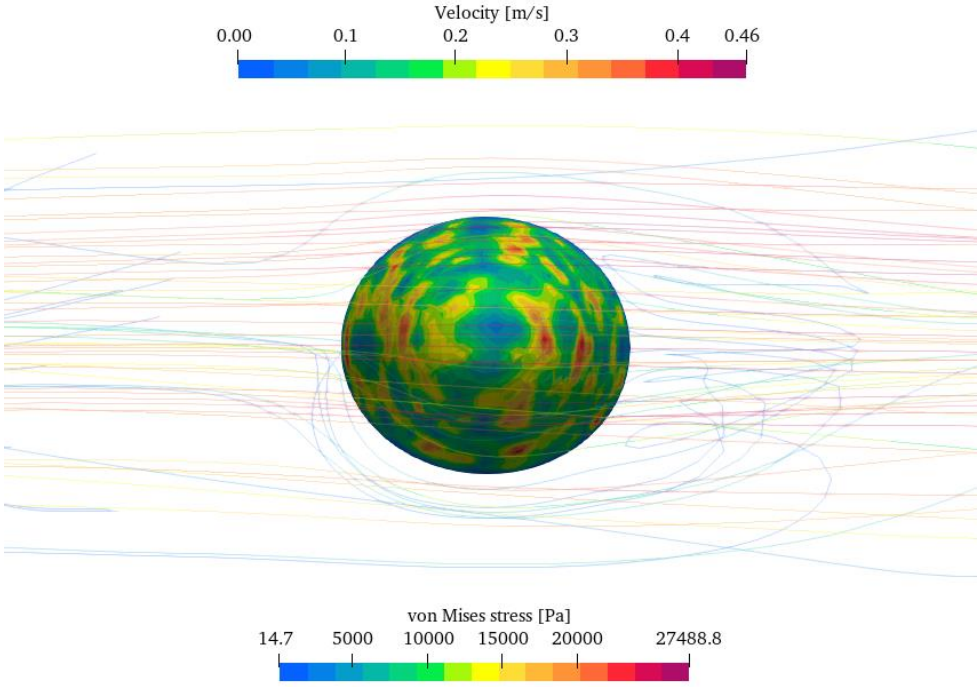

Figure 5-28. The velocity-VMS field, model 2

A similar conclusion can be made as in the pressure analysis. The cross-sectional stresses in both models are low, also suggesting the plaque rupture occurs at the shoulder rather than the plaque interior. VMSs are much higher at the surface, which implies that the shoulder is one of the most vulnerable parts. The maximum VMS is 1.85 times higher in the second model and covers a larger area than in the first model. This supports the claim made in the pressure analysis that higher-level stenoses are more vulnerable to rupture.

5.2.3. Traction force

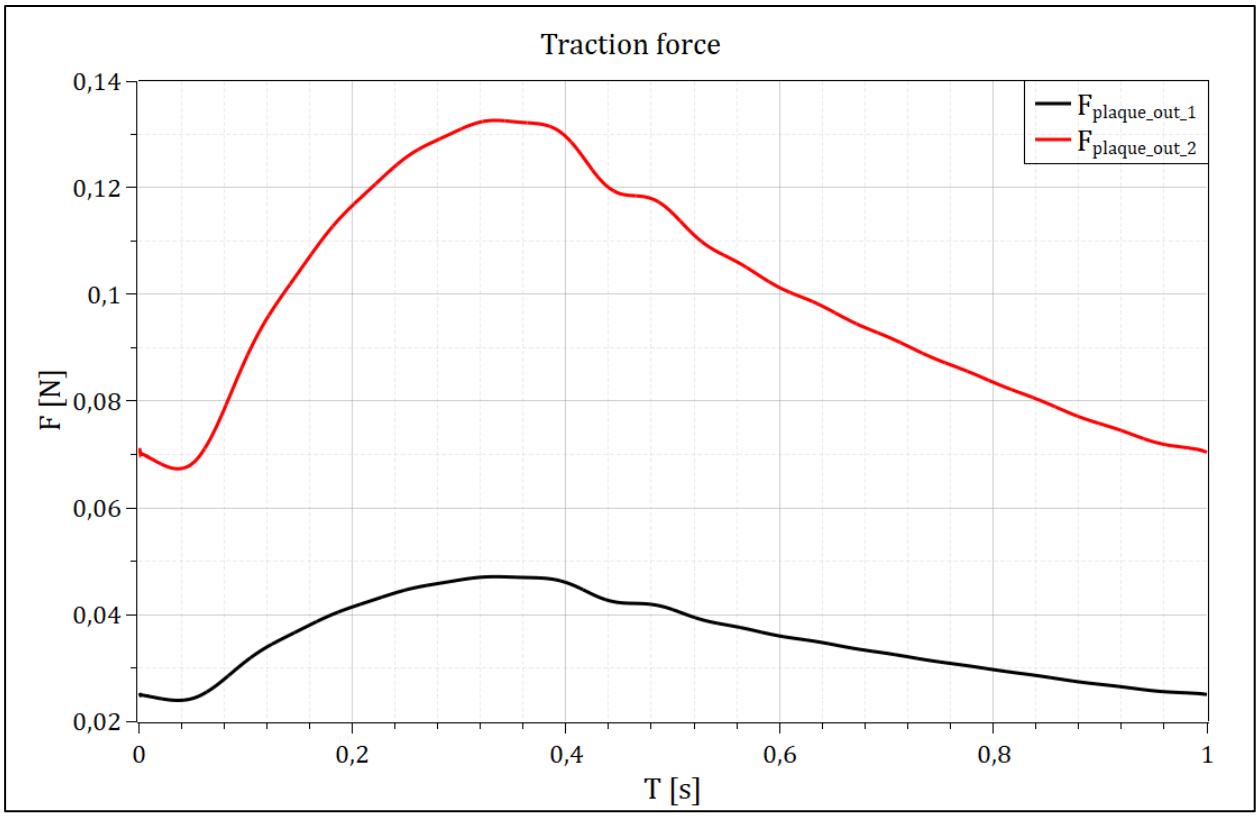

Figure 5-29. Time-varying traction force

Since the plaque root, that is, *plaque out* boundary is fixed, it is interesting to monitor the forces acting on it. Any crack at the bottom of the shoulder could lead to plaque separation and finally rupture. This information might be helpful to analyze such phenomena.

It can be seen that the traction force follows the same time-varying trend as the pressure waveform.

5.3. Results discussion

As there are two points of interest, it is important to determine which is the critical one. The evaluation of the maximum values of the WSS, the VMS, and the displacement values are given in Table 5-1, for model 1, and in Table 5-2, for model 2.

Table 5-1: Model 1 physical property comparison

Model 1	Maximum pressure (t_1=0.34s)	Maximum velocity (t_2=0.56s)	2/1
WSS	8.11e-04	1.46e-02	18.00
VMS	18446.0	14831.3	0.80
Displacement	2.99e-07	3.32e-07	1.11

Table 5-2: Model 2 physical property comparison

Model 2	Maximum pressure (t_1=0.34s)	Maximum velocity (t_2=0.56s)	2/1
WSS	8.32e-04	1.68e-02	20.19
VMS	34947.3	27488.8	0.79
Displacement	1.82e-07	3.17e-07	1.74

Table 5-1 and Table 5-2 both show a similar pattern. The last column (2/1) represents the maximum velocity value divided by the maximum pressure value.

The value of VMS at the time of max pressure differs from the value of VMS at the time of max velocity by approximately 20 % in both models, which is not that significant, due to low cross-sectional stresses. Additionally, a significant difference can be noticed between the VMS values of model 1 and model 2. VMS for model 2 is 89 % higher at the time of maximum pressure and 85 % higher at the time of maximum velocity.

Displacements at the time of max velocity are 11 % higher than the value of displacements at the time of max pressure for model 1. Regarding model 2, displacements are 74 % higher at the time of maximum velocity compared to the time of maximum pressure. It is important to mention that

the displacements obtained at the time of maximum pressure were mostly surface displacements, while the displacements at the time of maximum velocity were, both, surface and interior displacements. Even though the displacements do differ, their values are still negligible. While comparing model 1 and model 2, it can be seen that the displacements for model 2 are 4.5 % lower at the time of maximum velocity and 40 % lower at the time of maximum pressure.

The WSS is significantly higher at the moment of the maximum velocity in both cases. The value of WSS at the time of max velocity is 18 times higher than the value of WSS at the time of max pressure for model 1. Regarding model 2, WSS is 20.19 times higher at the time of maximum velocity compared to the time of maximum pressure. A comparison between the two models suggests that WSS values for model 2 are 15 % higher at the moment of the maximum velocity and 2.6 % higher at the moment of maximum pressure.

Considering the fact, that the plaque wall failure is primarily due to the WSS, the maximum velocity should be the critical point to analyze in future research.

5.4. Fatigue and plaque rupture in myocardial infarction - discussion

In this chapter, the plaque rupture will be treated as a chronic fatigue process, rather than an acute syndrome. Even though fatigue and crack propagation were not analyzed in this thesis, they should be mentioned and discussed.

5.4.1. Introduction

Plaque rupture causes the vast majority of acute myocardial infarctions. The primary mechanism is a fracture of the fibrous capsule covering the lipid core of an atheromatous plaque. According to structural analysis, rupture is associated with stress concentrations, which are affected by plaque lipid composition, fibrous cap thickness, plaque area, plaque shoulder histology, and inflammation. Plaque rupture occurs when the plaque is unable to withstand the hemodynamic blood pressure and shear stress applied to it. An excessive concentration of stress at a weak portion of the plaque surface is thought to be an important factor in the rupture process.

In mechanics, fatigue is a chronic failure process caused by repetitive loading. It is an asymptomatic but potentially progressive failure process that can result in sudden fracture at stress levels that appear to be much lower than critical stress. The cardiovascular system is a fatigue environment by nature. Each year, arterial tissues are subjected to 36,792,000 stress cycles at a heart rate of 70 beats per minute.

5.4.2. Crack initiation

The primary biomechanical measure is likely to be stress. Blood pressure, which expands and stretches an artery with each pulse, is the source of stress in an artery. Plaque is widely accepted to be most vulnerable in high-stress areas, which are thought to be the most common sites for rupture initiation. A variety of factors, including anatomy and tissue properties, influence stress concentrations.

The maximum circumferential stress along the lumen surface is typically considered the hot spot where the rupture is most likely to occur. It has been discovered that the maximum circumferential stress occurs in the plaque shoulder region. This suggests that rupture occurs at the lumen and is less likely to originate from the lipid. The failure initiation locations were found to be significantly affected by lumen shape and cap thickness. The presence of a lipid pool was also found to increase circumferential stress levels in the fibrous cap region because stress concentration is increased when materials of different stiffness are placed side by side.

5.4.3. Crack propagation

In addition to predicting rupture initiation sites, it is also important to investigate the rupture path. A propagating crack may deviate depending on the prevailing stress environment, which changes with each crack extension. The preferred rupture direction was discovered to be radial from the lumen center and was unaffected by tissue properties or anatomy. This supports the assumption that an initial stress concentration at the lumen wall is a good indication of rupture location.

The crack initially advances slowly but accelerates as it lengthens. This is due to a progressively increasing stress concentration at the tip of the emerging crack. When a critical crack length is reached, the final rupture will occur abruptly.

As previously stated, initial stress levels at the lumen surface are not high enough to explain acute plaque rupture. The dynamics of a chronic injury process or fatigue mechanism, on the other hand, may reconcile the clinical realities of relatively low-stress levels and acute rupture.

5.4.4. Fatigue

A fatigue process is an incremental failure progression caused by repetitive stresses, resulting in acute failure at pressure levels that appear to be much lower than the tissue tear strength. One of the unfortunate aspects of fatigue is that it is symptomatically silent. As a result, clinical symptoms are frequently absent until the ultimate plaque rupture and myocardial infarction. Fatigue behavior for plaque tissues is therefore still insidious. According to fatigue research, fatigue life is often divided into three phases: crack nucleation, crack propagation, and final rupture.

The nucleation phase typically represents the longest period of fatigue life. It is the most difficult period to predict. Likely, biological and biochemical factors such as inflammation, healing, and sedimentation have a greater impact on it than the two subsequent fatigue stages.

The intermediate period of stable crack propagation is probably more important because incomplete ruptures are potentially detectable. It describes a stable rupture phase, which is likely the most predictable phase before the failure mode becomes unstable (acute rupture).

The final rupture is the shortest phase and usually happens suddenly and without warning, as in myocardial infarction.

Since fatigue life is expressed in pulses, fatigue time is affected by heart rate. Mean and pulse pressure were discovered to be critical independent determinants of crack growth rate.

5.4.5. Conclusion

Anatomical variation was discovered to have a significant influence on fatigue life. A reduction in cap thickness or an increase in lipid pool size resulted in a significant reduction in fatigue life. In comparison to the previously used stress analysis, the fatigue model offers some possible explanations for plaque rupture at low-stress levels in a pulsatile cardiovascular environment, and it may be a useful tool for assessing plaque vulnerability and risk stratifying patients with luminal stenosis. Living tissues have the ability to self-recover, which can certainly influence crack growth. Future research must consider the crack closing rate to accurately describe fatigue crack growth. [16, 17]

6. CONCLUSION

The main focus of this thesis was to develop a numerical model of an atherosclerotic artery and determine the potential areas for plaque rupture, which may lead to a heart attack. An introduction was given in the first and the second chapter with a detailed medical overview of plaque formation and coronary circulation. Governing equations for the fluid-structure interaction model were concisely described in the third chapter, in which both domains were discretized with the cell-centered finite volume method. The fourth chapter gives an overview of the geometry, mesh-making process, and a detailed explanation of the boundary conditions used in the simulation and how they were obtained. The discretization of the spatial domain was performed in the open-source software cfMesh, while for conducting the numerical simulations, OpenFOAM/solids4foam was used. Firstly, the CFD simulations were conducted to determine downstream pressure conditions. Approximately 52 % of the volume flow branches into the LAD outlet, 18 % into the RI outlet, and 30 % into the LCx outlet. After obtaining the pressure values at the vessel outlets, the FSI simulations were conducted on 2 geometries: one with 50 % stenosis, and one with 30 % stenosis in order to determine differences in velocity, pressure, and wall shear stress fields on the fluid domain, but also the von Mises stress and displacement fields on the solid domain. At the end of the chapter, the simulation setup was outlined.

In chapter five, the results are shown for two points of interest, the moment of maximum pressure and the moment of maximum velocity, which were compared for the two stenosis levels. They were outlined in form of the volume flow rate, the wall shear stress, the displacements, and the von Mises stress.

Significant differences can be observed when comparing flow rates through branches obtained from the FSI simulations and flow rates through branches obtained from the CFD simulation. The flow rate in LAD is reduced in stenosis models by approximately 54 %, the flow rate in LCx is increased in stenosis models by 88 %, and the flow rate in RI is increased by 10 %. The reason for that can be the generation of the vortices behind the plaque, which form downstream flow separation. The vortices extend throughout the main branch, up until the trifurcation junction. An additional long-term problem, that flow separations cause, is the low WSS areas, in which the advancement of atherosclerosis, that is, growth of the plaque, is enabled.

Comparing WSS values of model 2 and model 1, the maximum values are 15 % higher for model 2 stenosis, whereas the average values are 33 % higher. The same thing can be noticed for the VMS values, which are 85 % higher for model 2 of the stenosis. This implies that higher percentage

stenoses are more likely to rupture. Due to the fact that maximal displacements, VMS, and WSS can be found in the middle of plaque shoulders, this area was found to be at high risk for rupture. The analysis suggested that the moment of maximum velocity was the critical point since the value of the WSS is 18 times higher in model 1 and 20 times higher in model 2, which is the main cause of the plaque wall failure, that is, the plaque rupture.

Future work, as a continuation of the thesis, would include running a simulation using a heterogeneous solid model with two materials of significantly different mechanical properties. The interior of the atherosclerotic plaque mainly consists of lipids, whereas the smooth muscle cells and collagen are closer to the wall. Their stiffness levels vary up to 20 times. Therefore, a heterogeneous solid model would enable a more accurate analysis of the plaque interior that might be crucial to the plaque rupture phenomena.

BIBLIOGRAPHY

[1] B. F. Fremgen and S. S. Frucht, *Medical Terminology: A Living Language*, 6th edition. Boston: Pearson, 2015.; pp. 148-153

[2] J. Moini, *Phlebotomy: Principles and Practice: Includes Online Access Code for Companion Website*, Illustrated edition. Burlington, MA: Jones & Bartlett Learning, 2012.; pp. 37-44

[3] J. E. Hall, *Guyton and Hall textbook of medical physiology*, 13th edition. Philadelphia, PA: Elsevier, 2016.; pp. 169-174, 262-269, 872-874

[4] F. Moukalled, L. Mangani, and M. Darwish, *The Finite Volume Method in Computational Fluid Dynamics: An Advanced Introduction with OpenFOAM® and Matlab*, vol. 113. Cham: Springer International Publishing, 2016. doi: 10.1007/978-3-319-16874-6.; pp. 48-52, 256-257, 745

[5] M. Čorak, "CFD simulacija nenominalnih radnih točaka centrifugalnog kompresora," info:eu-repo/semantics/masterThesis, University of Zagreb. Faculty of Mechanical Engineering and Naval Architecture, 2021. Accessed: Jun. 18, 2022. [Online]. Available: https://urn.nsk.hr/urn:nbn:hr:235:516890; pp. 12-13

[6] G. A. Holzapfel, *Nonlinear solid mechanics: a continuum approach for engineering*, Repr. Chichester Weinheim: Wiley, 2010.; pp. 222, 238

[7] Ž. Tuković, A. Karač, P. Cardiff, H. Jasak, and A. Ivanković, "OpenFOAM Finite Volume Solver for Fluid-Solid Interaction," *Trans. FAMENA*, vol. 42, no. 3, pp. 1–31, Oct. 2018, doi: 10.21278/TOF.42301.; pp. 3-5, 9-11

[8] P. Cardiff, *Training: Solid mechanics and fluid-solid interaction using the solids4foam toolbox*. 2020.

[9] P. Milovic and M. Eng, "UNIVERSITY OF ZAGREB FACULTY OF MECHANICAL ENGINEERING AND NAVAL ARCHITECTURE," p. 69.; p. 2

[10] S. Gamulin, M. Marusic, and Z. Kovac, *Patofiziologija. Knj. 1 Knj. 1*. Zagreb: Medicinska naklada, 2011.

[11] N. Hadjiloizou *et al.*, "Differences in cardiac microcirculatory wave patterns between the proximal left mainstem and proximal right coronary artery," *Am. J. Physiol.-Heart Circ. Physiol.*, vol. 295, no. 3, pp. H1198–H1205, Sep. 2008, doi: 10.1152/ajpheart.00510.2008.

[12] Virag, Z.: Predavanja *Mehanika bioloških* sustava, Fakultet strojarstva i brodogradnje, Zagreb

[13] "User_Guide-cfMesh_v1.1.pdf." Accessed: Jun. 25, 2022. [Online]. Available: http://cfmesh.com/wp-content/uploads/2015/09/User_Guide-cfMesh_v1.1.pdf

[14] "OpenFOAM: API Guide: src/finiteVolume/fields/fvPatchFields/derived/flowRateInletVelocity/flowRateInletVelocityFvPatchVectorField.H Source File." https://www.openfoam.com/documentation/guides/latest/api/flowRateInletVelocityFvPatchVectorField_8H_source.html (accessed Jun. 26, 2022).

[15] R. A. Baldewsing, M. G. Danilouchkine, F. Mastik, J. A. Schaar, P. W. Serruys, and A. F. W. van der Steen, "An Inverse Method for Imaging the Local Elasticity of Atherosclerotic Coronary Plaques," *IEEE Trans. Inf. Technol. Biomed.*, vol. 12, no. 3, pp. 277–289, May 2008, doi: 10.1109/TITB.2007.907980.

[16] A. C. van der Wal and A. E. Becker, "Atherosclerotic plaque rupture--pathologic basis of plaque stability and instability," *Cardiovasc. Res.*, vol. 41, no. 2, pp. 334–344, Feb. 1999, doi: 10.1016/s0008-6363(98)00276-4.

[17] A. Versluis, A. J. Bank, and W. H. Douglas, "Fatigue and plaque rupture in myocardial infarction," *J. Biomech.*, vol. 39, no. 2, pp. 339–347, Jan. 2006, doi: 10.1016/j.jbiomech.2004.10.041.